JARECKE, DENNIS W., Ph.D., May, 2005 PHYSICS

PROPERTIES OF MESONS FROM BETHE-SALPETER AMPLITUDES (103 pp.)

Director of Dissertation: Peter C. Tandy

The vector meson strong decays $\rho \to \pi\pi$, $\phi \to KK$, and $K^\star \to \pi K$ are studied within the covariant, nonperturbative, rainbow-ladder truncation of the Dyson-Schwinger equations in Quantum Chromodynamics. The model gluon propagator has gluon confinement, preserves the one-loop perturbative behavior of QCD, and contains an infrared enhancement for the dynamical generation of large constituent quark mass. The quark propagators are confined and produce a non-zero quark condensate in the chiral limit signaling dynamical chiral symmetry breaking. The analytic continuation of the Dyson-Schwinger equations are also studied. An expedient approach is used which modifies the gluon propagator in a physically insignificant way but allows for contour integration along the positive real-axis. Singularities are found that limit the Taylor expansion of quark propagators. We employ a Taylor expansion of the quark propagators and compare the resulting light scalar and vector meson masses and electroweak decay constants with solutions of the Bethe-Salpeter equation resulting from direct analytic continuation of the quark propagators. Our results show a convergence at second order in the Taylor expansion of the quark propagators and provides meson masses and electroweak decay constants within a few percent of experimental results. The 3-point decay amplitudes are studied in the impulse approximation providing vector meson strong decays within 15% of experimental results. We study a real-axis projection of the complex plane behavior of the quark propagators to obtain axial-vector and exotic meson masses 400MeV too low.

PROPERTIES OF MESONS FROM BETHE-SALPETER AMPLITUDES

A dissertation submitted to
Kent State University in partial
fulfillment of the requirements for the
degree of Doctor of Philosophy

by

Dennis W. Jarecke

May, 2005

Dissertation written by

Dennis W. Jarecke

B.S., Southwest Missouri State University, 1994

M.S., Kent State University, 2003

Ph.D., Kent State University, 2005

Approved by

_____ , Chair, Doctoral Dissertation Committee

_____ , Members, Doctoral Dissertation Committee

_____ ,

_____ ,

_____ ,

_____ ,

_____ ,

Accepted by

_____ , Chair, Department of Physics

_____ , Dean, College of Arts and Sciences

TABLE OF CONTENTS

LIST OF FIGURES

LIST OF TABLES

ACKNOWLEDGMENTS

First and foremost, I would like to thank Peter Tandy for his academic and financial support in getting me through this dissertation. Peter is a great physicist and I have been privileged to work under him for so many years. He was patient and supportive much longer than he should have been. When most advisers would have given up on me, Peter was there patiently answering my questions. Thank you, Peter.

This work closely follows that of Pieter Maris during his time at Kent State University. I am deeply grateful to Pieter for his detailed assistance on almost every aspect of this work. Thank you, Pieter.

I would also like to thank my wife Susan for her years of patience. Never once did she complain about the length of time it was taking to get through. She was always supportive of my efforts and was always willing to let me do whatever I thought I needed in regards to this program. Thank you, Susan, for being there for me during all of this. Thank you for putting up with the frustration and hopelessness that I exuded over the years.

I would like to thank the many graduate students of Kent State University who made my life there more enjoyable. I will always fondly remember the many hours spent with Elisa, Ben, and Tony playing Magic:The Gathering©; Friday night baseball with John, Tony, and Chuck; afternoon frisbee, and the many dinners. I did not always appreciate what you gave to my life, but I do now.

CHAPTER 1

Introduction

The underlying theory of quarks and gluons that make up hadrons is Quantum Chromodynamics [2, 3, 4]. Quantum Chromodynamics (QCD) is interesting because of the coupling between quarks and gluons. Their unique coupling provides the two important properties of confinement [5] and asymptotic freedom [6, 7] to quark and gluon interactions. In the large momentum transfer (small quark separation) regime the quarks are very weakly coupled to one another. This asymptotic freedom allows for the use of perturbative techniques which are essentially expansions in the quark-gluon coupling. Because the coupling is weak, perturbative Quantum Chromodynamics (pQCD) reproduces physical observables at high energies (small separation). At low momentum transfer (large separation) the coupling is so large that quarks are never free and are thus confined to hadrons. Therefore, nonperturbative techniques become essential in connecting hadron observables to QCD.

Another important feature of QCD is that of dynamical chiral symmetry breaking. In the chiral limit the current quark masses are zero and the QCD Lagrangian is globally symmetric under the $SU_L(N_f) \otimes SU_R(N_f)$ group where N_f is the number of quark flavors. However, this symmetry is not shared by the ground state. The non-zero vacuum expectation value $\langle \bar{q}q \rangle$ (also called the quark condensate) is the order parameter for the breaking of the chiral symmetry. This dynamical chiral symmetry breaking (DχSB) provides two important features of the light meson spectrum. First, the breaking of the chiral symmetry is accompanied by the appearance of massless Goldstone bosons [8]. The pions fit this description well because they have a nearly zero mass when compared to the next lightest

mesons. Second, the coupling of the quarks provides an effective dynamical quark mass that we associate with the empirical constituent quark masses of the hadron spectrum.

Since quarks and gluons are the constituents of mesons, the study of the meson spectrum and meson decays is an important tool for understanding QCD in the nonperturbative regime. The light pseudoscalar mesons are important because they are the Goldstone bosons associated with dynamical chiral symmetry breaking. The ground-state vector mesons are the next highest in mass and are the lowest spin excitations of the pseudoscalar mesons. In addition, they play an important role in the coupling of electromagnetic waves to hadrons via the vector meson dominance model. Furthermore, the strong decay of the vector mesons into two pseudoscalar mesons is through a P-wave interaction that probes the $q\bar{q}$ bound state wave functions in a way that the electroweak decays do not. In addition to the pseudoscalar and vector mesons, there are the ground-state axial-vector mesons whose masses start above 1 GeV and whose decay into two pseudoscalar mesons proceed via both S and D-wave interactions.

One approach to nonperturbative QCD is through the Dyson-Schwinger equations. The Dyson-Schwinger equations (DSE) [9, 10, 11, 12] are an exact, nonperturbative, and Poincarè invariant set of integral equations relating the various n-point functions of a theory to one another. The Dyson-Schwinger approach to QCD is consistent with quark and gluon confinement [13, 14, 15, 16] and generates DχSB [17, 18] while satisfying the one-loop renormalization group behavior of QCD [19].

The DSE's are an infinite tower of coupled integral equations in the sense that a given n-point function is dependent upon at least one m>n-point function. This dependency on higher and higher n-point functions requires some truncation scheme of the Dyson-Schwinger approach in order to obtain a tractable set of equations. One such truncation scheme is the weak coupling expansion where the Dyson-Schwinger equations generate

all the Feynman diagrams obtainable in perturbation theory. Another commonly used truncation scheme is the rainbow-ladder truncation of the Dyson-Schwinger quark self-energy equation and the Bethe-Salpeter equation. The rainbow-ladder truncation scheme is important both for its tractability as well as its preservation of the Ward identities [20]. In particular, the satisfaction of the axial-vector Ward-Takahashi identity is crucial in providing a model of QCD that respects dynamical chiral symmetry breaking [21].

The current approach follows after the tradition of modeling the form of the gluon propagator and then solving the DSE's for the quark propagator and the Bethe-Salpeter amplitudes in the rainbow-ladder truncation. Because the propagators are directly related by the DSEs, we are guaranteed that the Ward identities are preserved. This insures both electromagnetic and axial current conservation. The development of modeling the gluon propagator using the Dyson-Schwinger approach started with identifying a $1/q^4$ dependence in the low momentum regime of the gluon propagator [22, 23]. It was believed that this dependence was the main cause of confinement and DχSB [5]. With this in mind, the first model used an integrable singularity in the form of a delta function [24]. This model showed that an effective gluon with a simple infrared enhancement was capable of successfully reproducing both the light meson spectrum and some heavier meson masses. This work was followed up by [25, 26, 27] where three different infrared enhancements were used in addition to some sort of $1/\ln[q^2/\Lambda^2_{QCD}]$ tail. In [25] two different gluons were used both with the same asymptotic behavior consistent with the gluon at the 1-loop level. It used a delta function as one of its enhancements and Ce^{-ak^2} as the other. The work in [26] used one gluon with a delta function plus $C_1e^{-a_1k^2} + C_2k^2e^{-a_2k^2}$ plus a gluon consistent with the renormalization group at the 2-loop level. Finally, [27] used only a $Ck^2e^{-ak^2}$ plus a tail at the 2-loop level. More work was done by [28] who used a delta function for its infrared enhancement and a $(1 - e^{-ak^2})/k^2$ term for its asymptotic behavior. This model

was quickly followed by [19] which is very similar to the model used in this work.

The focus of this work is twofold. First, the Euclidean metric used in this work and in the literature requires knowledge of the quark propagators in the complex plane. In particular, the on-mass-shell bound-state wave functions used to calculate meson masses, electroweak decays, and strong decays requires an analytic continuation of the Euclidean momentum. The domain in the complex plane in which information about the quark propagators is needed increases with increasing meson mass. For light mesons such as the pion and kaon, the domain of the complex plane needed is small and the required analytic continuation of the Dyson-Schwinger equations is tractable. However, for heavier mesons such as the vector and axial-vector mesons, the domain of the complex plane is very large and the required analytic continuation of the Dyson-Schwinger equations becomes computationally cumbersome. In addition, models of this genre can contain complex conjugate singularities in the quark propagator that are encompassed by the domain of integration of the BSE for meson masses above 1 GeV [28]. A more tractable approach is to Taylor expand the quark propagators into the complex plane [27]. This momentum expansion method is advantageous because it requires knowledge of the quark propagators only along the real spacelike p^2 axis. However, comparisons of this method with direct analytic continuation of the DSE's have been missing in the literature. This work was done in parallel with that of [1] where a direct analytic continuation of the quark DSE was used for the solution of the Bethe-Salpeter equations of the light pseudoscalar and vector mesons. The purpose of this work is to provide a justification of the momentum expansion approach in order to use the Taylor-expanded quark propagators in a region of the complex plane where direct analytic continuations of the DSE's are impractical for the calculation of the axial vector and exotic mesons.

The main focus of this work is to calculate the strong decays of the light vector mesons

into two pseudoscalar mesons. The idea of vector meson dominance in the Dyson-Schwinger approach is that the quark-photon vertex is dominated by the propagation of an intermediate state ρ meson in the vicinity of the ρ mass shell. Thus, a nonperturbative approach to calculating pion and kaon electromagnetic form factors should naively be expected to generate the $g_{\rho\pi\pi}$, $g_{\phi KK}$, and $g_{K^*K\pi}$ coupling constants of the same quality. The impulse approximation has been used in the Dyson-Schwinger approach to calculate the quark-photon vertex [29] and pion and kaon electromagnetic form factors [30, 31]. The success of these techniques is a clear indication that the impulse approximation should reproduce the strong decays of light vector mesons without fine tuning of the model in [1].

In Chapter 2 we review the field theory of QCD and renormalization group behavior at the one-loop level. We then review the Dyson-Schwinger equation for the quark self-energy and the two-body bound-state Bethe-Salpeter equation. Next, we briefly discuss how dynamical chiral symmetry breaking is observed in this approach. In Chapter 3 we calculate the quark propagators along the real spacelike axis and show that an analytic continuation into the complex plane requires a numerically cumbersome contour of integration in the complex plane. We discuss a physically insignificant change to the model that allows for an analytic continuation of the quark momentum into the complex plane while keeping the contour integration along the real axis and calculate the position of complex conjugate singularities in the second and third quadrants of the complex plane that limit the usefulness of the momentum expansion method. In Chapter 4 we calculate the masses and electroweak decays of light pseudoscalar and vector mesons using the momentum expansion method. These results are compared with an exact analytic continuation of the quark DSE. In Chapter 5 we calculate the $\rho \to \pi\pi$, $\phi \to KK$, and $K^* \to K\pi$ strong decays using the impulse approximation. In Chapter 6 we examine a new approach to calculating the quark propagators in the complex plane using only the real argument of the quark

propagators and compare this with previous calculations. Finally, we calculate the mass of the a_1 and b_1 axial-vector mesons and $\hat{\pi}$ and $\hat{\rho}$ exotic mesons. In Chapter 7 conclusions are discussed.

CHAPTER 2

The Dyson-Schwinger Approach to QCD

2.1 Quantum Field Theory

The Minkowski space QCD Lagrangian density [32]

$$\mathcal{L}_{QCD} = \bar{q}\left(i\gamma^{\mu}\partial_{\mu} - m\right)q + g\bar{q}\gamma^{\mu}\frac{\lambda^{a}}{2}qA^{a}_{\mu} - \frac{1}{4}F^{a}_{\mu\nu}F^{a\mu\nu} \tag{2.1}$$

is our starting point for QCD. The first term in Eq. 2.1 is the non-interacting term for quark field $q(x)$ where the quark flavor index is suppressed and the current quark mass, m, is a diagonal 3x3 matrix for the up, down, and strange quark flavors. The second term is the interaction Lagrangian between the quarks and gluon, $A^{a}_{\mu}(x)$. The superscript a represents one of eight gluon color indices. The third term is the non-interacting gluon Lagrangian where

$$F^{a\mu\nu} = \partial^{\mu}A^{a\nu} - \partial^{\nu}A^{a\mu} + gf^{abc}A^{b\mu}A^{c\nu}. \tag{2.2}$$

The λ^{a} matrices are the hermitian generators of the SU(3) Lie Algebra [33] where the trace of the product of two of the generators of given by

$$Tr\left[\lambda^{a}\lambda^{b}\right] = 2\delta_{ab} \tag{2.3}$$

and their commutation relation is given by

$$\left[\lambda^{a}, \lambda^{b}\right] = 2if^{abc}\lambda^{c}. \tag{2.4}$$

The QCD Lagrangian comes from demanding the invariance of the free quark Lagrangian density

$$\mathcal{L}_{0} = \bar{q}\left(i\gamma_{\mu}\partial^{\mu} - m\right)q \tag{2.5}$$

under the non-Abelian SU(3) local gauge transformations

$$q(x) \to e^{-ig\theta^a(x)\lambda^a/2} q(x) \tag{2.6}$$

and

$$\bar{q}(x) \to \bar{q}(x) e^{ig\theta^a(x)\lambda^a/2} \tag{2.7}$$

of the quark fields and

$$A^a_\mu(x) \to A^a_\mu(x) - \partial_\mu \theta^a(x) + g f^{abc} \theta^b(x) A^c_\mu(x) \tag{2.8}$$

of the gluon field. See Chapter 3, pages 18-20 of [34] for more details.

The QCD action

$$S[q, \bar{q}, A^a_\mu] = \int d^4x \left[\bar{q} \left(i\gamma^\mu \partial_\mu - m \right) q + g \bar{q} \gamma^\mu \frac{\lambda^a}{2} q A^a_\mu - \frac{1}{4} F^a_{\mu\nu} F^{a\mu\nu} \right] \tag{2.9}$$

needs to be fixed to a specific gauge to avoid functional integrations over equivalent gauge configurations. See Chapter 3, pages 32-36 of [34] for more details. The gauge fixing action

$$\begin{aligned} S_\xi[q, \bar{q}, A^a_\mu, w, \bar{w}] &= S[q, \bar{q}, A^a_\mu] \\ &+ \int d^4x \left[(\partial^\mu \bar{w}^a)(\delta_{ab} \partial_\mu w^b - g f^{abc} w^b A^c_\mu) - \frac{1}{2\xi} (\partial^\mu \frac{\lambda^a}{2} A^a_\mu)^2 \right] \end{aligned} \tag{2.10}$$

along with the generating functional

$$\begin{aligned} Z[\eta, \bar{\eta}, J^{a\mu}, \Omega^a, \bar{\Omega}^a] &= \int Dq\, D\bar{q}\, DA^a_\mu\, Dw\, D\bar{w}\, \exp\Big\{ iS_\xi[q, \bar{q}, A^a_\mu, w, \bar{w}] \\ &+ i \int d^4x \left[\bar{\eta} q + \eta \bar{q} + A^a_\mu J^{a\mu} + \bar{\Omega}^a w^a + \Omega^a \bar{w}^a \right] \Big\} \end{aligned} \tag{2.11}$$

define the quantum field theory for QCD [34]. ξ is the bare or unrenormalized gauge fixing parameter. In this work we use the Landau or transverse gauge where $\xi = 1$ [35]. Eq. 2.10 contains the gauge fixing w and $\bar{w}$ Fadeyev-Popov ghost fields. To generate the Green's functions of the theory, the anticommuting sources η, $\bar{\eta}$, Ω^a, and $\bar{\Omega}^a$ and commuting source $J^{a\mu}$ are added to the Lagrangian. The physical theory is defined when the sources are set to zero.

Z is a moment-generating functional because various functional derivatives of it give the Green's functions of the theory. The nth derivative of Z is referred to as the n-point function of the theory. The gluon propagator $D^{ab}_{\mu\nu}(x-y)$ is a Green's function of the theory and is also referred to as the gluon 2-point function. The gluon propagator gives the probability amplitude for the gluon to go from one space-time point to another and is related to the generating functional by

$$D^{ab}_{\mu\nu}(x-y) = (-i)^2 \frac{\delta^2 \ln(Z)}{\delta J^{a\mu}(x) \delta J^{b\nu}(y)}\bigg|_{J^{a\mu}=J^{b\nu}=0}. \tag{2.12}$$

In a similar manner the quark propagator or quark 2-point function, $S(x-y)$, gives the probability amplitude of the quark to go from one space-time point to another and is related to the generating functional by

$$S(x-y) = (-i)^2 \frac{\delta^2 \ln(Z)}{\delta \eta(x) \delta \bar{\eta}(y)}\bigg|_{\eta=\bar{\eta}=0}. \tag{2.13}$$

2.2 Euclidean Metric

This work uses a Euclidean formulation of QCD [12, 36, 37, 38] where

$$a \cdot b = a_\mu \delta_{\mu\nu} b_\nu. \tag{2.14}$$

Lattice QCD and most nonperturbative quantum field theory calculations are performed in the Euclidean metric for practical reasons. The Euclidean 4-vectors can be obtained from the Minkowski 4-vectors by an analytic continuation to imaginary time. In particular, the space-time and momentum-energy 4-vectors are related by

$$t^E = it^M, \tag{2.15}$$

$$\vec{x}^E = \vec{x}^M, \tag{2.16}$$

$$E^E = iE^M, \tag{2.17}$$

and

$$\vec{p}^E = \vec{p}^M. \tag{2.18}$$

The gamma matrices are related by

$$\gamma^{0E} = \gamma^{0M} \tag{2.19}$$

and

$$\vec{\gamma}^{\,E} = -i\vec{\gamma}^{\,M}. \tag{2.20}$$

These rules for going from Minkowski space to Euclidean space make the following changes in the Dyson-Schwinger equations,

$$\int_{-\infty}^{\infty} d^4k^M = -i \int_{-\infty}^{\infty} d^4k^E, \tag{2.21}$$

$$\gamma^M \cdot p^M = -i\gamma^E \cdot p^E, \tag{2.22}$$

$$q^M \cdot p^M = -q^E \cdot p^E, \tag{2.23}$$

and

$$p^M \cdot x^M = -p^E \cdot x^E. \tag{2.24}$$

Finally, from Eq. 2.23 we see that the invariant mass of a free particle in the Euclidean metric is defined as $P^2 = -m^2$. See Appendix A.

2.3 The Running Coupling Constant of QCD

The renormalized dressed gluon propagator is

$$D^{ab}_{\mu\nu}(k) = \delta_{ab}\left(\delta_{\mu\nu} - \frac{k_\mu k_\nu}{k^2}\right)\frac{d(k^2,\mu^2)}{k^2} + \delta_{ab}\xi\frac{k_\mu k_\nu}{k^4} \tag{2.25}$$

where ξ is the gauge parameter,

$$d(k^2,\mu^2) = \frac{1}{1+\Pi(k^2,\mu^2)}, \tag{2.26}$$

and $\Pi(k^2,\mu^2)$ is the renormalized gluon vacuum polarization. The Slavnov-Taylor identity [39, 40] in QCD insures that the longitudinal part of $D^{ab}_{\mu\nu}(k^2)$ is not affected by interactions. See chapter three, pages 32-36 of [34].

The renormalization group equation [41, 42] for the gluon propagator allows for the study of the large momentum sector of QCD where the quark-gluon coupling, α_s, becomes weak and perturbation theory can be used [6, 43, 7]. To lowest order in the β-function [32], the renormalization scale dependence of α_s comes from

$$\mu\frac{\partial\alpha_s}{\partial\mu} = -\frac{\beta_0}{2\pi}\alpha_s^2 \tag{2.27}$$

where

$$\beta_0 = 11 - \frac{2}{3}N_f. \tag{2.28}$$

Eq. 2.27 can be solved [34] to give

$$\alpha_s(Q) = \frac{4\pi}{\beta_0 ln(Q^2/\Lambda_{QCD}^2)} \tag{2.29}$$

for $Q^2 > \Lambda_{QCD}^2$. The parameter Λ_{QCD} sets the momentum scale below which α_s becomes large and perturbation theory diverges. In position space, α_s becomes large for quark separations larger than $1/\Lambda_{QCD}$ [44].

2.4 Dyson-Schwinger Equation for the Quark Propagator

The Dyson-Schwinger equation for the quark propagator is a relationship between the quark propagator, the gluon propagator, and the quark-gluon vertex. The renormalized form of the equation is

$$S(p)^{-1} = Z_2(i\gamma\cdot p + m_{bm}) + \Sigma'(p) \tag{2.30}$$

where

$$\Sigma'(p) = Z_1\int^{\Lambda}\frac{d^4q}{(2\pi)^4}g^2D_{\mu\nu}(p-q)\frac{\lambda^a}{2}\gamma_\mu S(q)\Gamma^a_\nu(q,p) \tag{2.31}$$

is the unrenormalized quark self-energy, $D_{\mu\nu}(p-q)$ is the renormalized dressed-gluon propagator, and $\Gamma^a_\nu(q,p)$ is the renormalized dressed quark-gluon vertex [45, 46]. See Figure 2.1. Λ is the regularization mass scale which is removed at the end of a calculation by taking the limit $\Lambda\to\infty$. Z_1, Z_2, and m_{bm} are the quark-gluon vertex renormalization constant,

the quark wave function renormalization constant, and the quark bare mass, respectively. Z_1, Z_2, and m_{bm} are all dependent on the renormalization point, μ, and the regularization mass scale, Λ. Furthermore S, Γ^a_ν, and m_{bm} are dependent on the quark flavor.

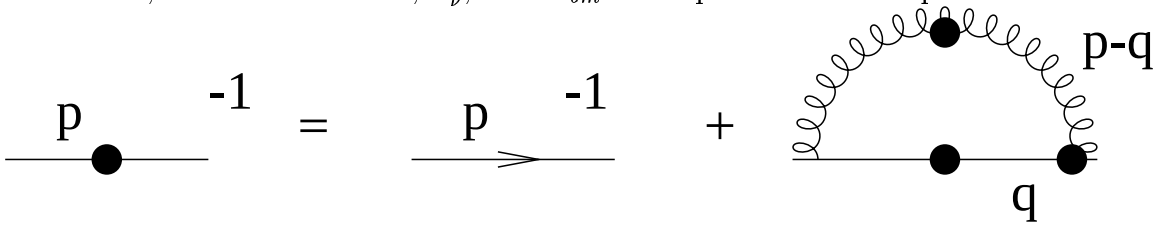

Figure 2.1: Dyson-Schwinger Equation for the Quark Self Energy.

Eq. 2.30 is renormalized such that at the renormalization point

$$S(p)^{-1}|_{p^2=\mu^2} = i\gamma \cdot p + m_R(\mu^2), \tag{2.32}$$

where $m_R(\mu^2)$ is the renormalized current-quark mass. Away from the renormalization point

$$S(p)^{-1} = i\gamma \cdot pA(p^2, \mu^2) + B(p^2, \mu^2), \tag{2.33}$$

where A and B are the vector and scalar amplitudes of the quark propagator, respectively.

2.5 Bethe-Salpeter Equation

The Bethe-Salpeter equation [47, 48] is the fully relativistic description of two-particle bound states in quantum field theory and is, therefore, to be used in describing meson $q\bar{q}$ bound states [49, 12]. Bound states are identified as poles in the $q\bar{q}$ scattering matrix [50]. More specifically, the bound states are poles in the scattering amplitude at specific values of the invariant masses depending on the quantum numbers of the $q\bar{q}$ pair [51].

The Bethe-Salpeter equation,

$$\Gamma^{ab}_M(p;P) = \int^\Lambda \frac{d^4q}{(2\pi)^4} K(p,q;P) S^a(q+\eta P) \Gamma^{ab}_M(q;P) S^b(q-\beta P), \tag{2.34}$$

gives the Bethe-Salpeter amplitude (BSA) or amputated, one-particle-irreducible quark-meson vertex, $\Gamma_M^{ab}(p;P)$, where the quark has flavor a and the antiquark has flavor b. Here $P^2 = -m^2$, where m is the bound state mass, p is the relative $q\bar{q}$ momentum, and Λ is the regularization mass scale as previously defined. For scalar and pseudoscalar mesons, M is only a label specifying the type of meson but, for vector and axial-vector mesons, the Bethe-Salpeter amplitude carries a Lorentz index and ,therefore, M will contain a mathematically significant index representing some component in space-time. In particular, we can write Γ_5 for pseudoscalars, Γ_μ for vectors and $\Gamma_{5\mu}$ for axial-vectors where $\mu = 1, \cdots, 4$. The parameters η and $\beta = 1 - \eta$ specify the amount of momentum sharing between the quark and antiquark. For nonrelativistic motion $\eta = \frac{m_a}{m_a+m_b}$ and $\beta = \frac{m_b}{m_a+m_b}$ [52], where m_a and m_b refer to the mass of quarks a and b, respectively. We choose the convention $\eta = \beta = 1/2$ for all meson calculations in this work. The kernel K is the renormalized, amputated $q\bar{q}$ scattering kernel that is irreducible with respect to cutting a pair of $q\bar{q}$ lines. K operates in the direct product space of color and Dirac spin.

The Bethe-Salpeter wave function,

$$\chi_M^{ab}(q;P) = S^a(q+\eta P)\Gamma_M^{ab}(q;P)S^b(q-\beta P), \tag{2.35}$$

allows Eq. 2.34 to be written as

$$\left[\Gamma_M^{ab}(p;P)\right]_{tu} = \int^\Lambda \frac{d^4q}{(2\pi)^4} K_{tu}^{rs}(p,q;P)\left[\chi_M^{ab}(q;P)\right]_{sr}, \tag{2.36}$$

where r, s, t, and u represent the combined color-Dirac matrix indices.

The Bethe-Salpeter amplitude, $\Gamma^{ab}(q;P)$, has a corresponding anti-meson solution, $\bar{\Gamma}^{ba}(q;P)$, that gives the amplitude of an anti-meson separating into two quarks. They are related by $\bar{\Gamma}_M^{ba}(q;P) = \left[C^{-1}\Gamma_M^{ab}(-q;P)C\right]^T$ where $C = \gamma_2\gamma_4$ is the charge conjugation operator and T denotes the transpose. (See Appendix A.)

The normalization condition,

$$2P_\mu = \frac{\partial}{\partial P_\mu}\Bigg\{ \int^\Lambda \frac{d^4q}{(2\pi)^4} Tr_{CD}\left[\bar{\Gamma}^{ba}_M(q;-K)S^a(q+\eta P)\Gamma^{ab}_M(q;K)S^b(q-\beta P)\right] + \int^\Lambda \frac{d^4q}{(2\pi)^4}\int^\Lambda \frac{d^4k}{(2\pi)^4}\left[\bar{\chi}^{ba}_M(k;-K)\right]_{ut} K^{rs}_{tu}(k,q;P)\left[\chi^{ab}_M(q;K)\right]_{sr}\Bigg\}\Bigg|_{P^2=K^2=-m^2}, \tag{2.37}$$

insures that the Bethe-Salpeter amplitude describes one meson with unit probability [49]. In the ladder-rainbow truncation the kernel is independent of the meson momentum and thus the second term is zero. In general, a properly normalized BSA will result in a conserved electromagnetic current of the meson [29, 30].

2.6 Dynamical Chiral Symmetry Breaking

The appearance of nearly massless pions in the meson spectrum and a nonzero quark condensate [53] is a clear signal of dynamical chiral symmetry breaking in QCD where the pions are identified as the Goldstone Bosons of the dynamical broken chiral symmetry. The satisfaction of the axial-vector Ward-Takahashi identity provides the proper description of this phenomenon in the Dyson-Schwinger approach [21]. Furthermore, truncations of the Dyson-Schwinger equations, such as the rainbow-ladder truncation, that satisfy the axial-vector Ward-Takahashi identity can also properly describe pions as the Goldstone Bosons of dynamical chiral symmetry breaking.

The renormalized axial-vector Ward-Takahashi identity in the chiral limit is

$$-iP_\mu\Gamma^j_{5\mu}(k;P) = S^{-1}(k_+)\gamma_5\frac{\tau^j}{2} + \gamma_5\frac{\tau^j}{2}S^{-1}(k_-) \tag{2.38}$$

where

$$\begin{aligned}\Gamma^j_{5\mu}(k;P) &= \frac{\tau^j}{2}\gamma_5[\,\gamma_\mu F(k;P) + \gamma\cdot k k_\mu G(k;P) - \sigma_{\mu\nu}k_\nu H(k;P)\,] \\ &+ \tilde{\Gamma}^j_{5\mu}(k;P) + f_\pi\frac{P_\mu}{P^2}\Gamma^j_\pi(k;P)\end{aligned} \tag{2.39}$$

is the axial-vector vertex, f_π is the pion electroweak decay constant given in Eq. 4.54, Γ_π is the most general decomposition of a pseudoscalar Bethe-Salpeter amplitude, and F, G,

H, and $\tilde{\Gamma}_{5\mu}$ are regular as $P^2 \to 0$. By assuming that $m_\pi^2 = 0$, substituting Eq. 2.33 and Eq. 2.38 into Eq. 2.39 one obtains the chiral limit relations

$$f_\pi E_\pi(k;0) = B(k^2), \tag{2.40}$$

$$F(k;0) + 2f\pi F_\pi(k;0) = A(k^2), \tag{2.41}$$

$$G(k;0) + 2f_\pi G_\pi(k;0) = 2A'(k^2) \tag{2.42}$$

and

$$H(k;0) + 2f_\pi H_\pi(k;0) = 0 \tag{2.43}$$

where E_π, F_π, G_π, and H_π are the Lorentz invariant terms of the pion Bethe-Salpeter amplitude given in Eq. 4.27.

In perturbation theory $B(p^2) = 0$ in the chiral limit. However, Eq. 2.40 shows that the Dyson-Schwinger approach also allows for a nonzero $B(p^2)$ in the chiral limit. A nonzero $B(p^2)$ signals dynamical mass generation given by

$$M(p^2) = \frac{B(p^2)}{A(p^2)} \tag{2.44}$$

and leads to massless Goldstone bosons. Furthermore, the quark condensate,

$$-\langle \bar{q}q \rangle_\mu^0 = \lim_{\Lambda\to\infty} Z_4(\mu,\Lambda) N_c \int^\Lambda \frac{d^4q}{(2\pi)^4} Tr_D[S_{\hat{m}=0}(q)] \tag{2.45}$$

$$= \lim_{\Lambda\to\infty} Z_4(\mu,\Lambda) N_c \int^\Lambda \frac{d^4q}{(2\pi)^4} \frac{B(q^2)}{q^2 A(q^2) + B(q^2)}, \tag{2.46}$$

which is the order parameter of dynamical chiral symmetry breaking is now nonzero by virtue of a nonzero $B(p^2)$.

CHAPTER 3

Numerical Solutions to the DSE

3.1 Model Gluon Propagator

From Eq. 2.30 we use the *ansatz* [19]

$$Z_1 g^2 D_{\mu\nu}(p-q)\frac{\lambda^a}{2}\gamma_\mu S(q)\Gamma^a_\nu(q,p) \tag{3.1}$$
$$\rightarrow \quad \frac{\mathcal{G}(k^2)}{k^2}T_{\mu\nu}(k)\frac{\lambda^a}{2}\gamma_\mu S(q)\frac{\lambda^a}{2}\gamma_\nu$$

where $k = p - q$ is the gluon 4-momentum and $T_{\mu\nu}(k) = \delta_{\mu\nu} - k_\mu k_\nu/k^2$ is the transverse operator in the Landau gauge that picks out components of a 4-vector that are perpendicular to k. The quantity $T_{\mu\nu}(k)/k^2$ is the gluon propagator in the absence of the vacuum polarization. This *ansatz*, commonly known as the rainbow approximation, includes the replacement of $\Gamma^a_\nu(q,p)$ by the bare quark-gluon vertex. The effective running coupling in this work is modeled in the form [1]

$$\frac{\mathcal{G}(k^2)}{k^2} = \frac{4\pi^2 D}{\omega^6}k^2 e^{-k^2/\omega^2} + \frac{4\pi^2\gamma_m\mathcal{F}(k^2)}{(1/2)\ln[\tau + (1 + k^2/\Lambda^2_{QCD})^2]}. \tag{3.2}$$

The first term is an infrared enhancement that is needed to give us an appropriate amount of dynamically generated constituent quark mass by setting the quark condensate to a value consistent with experimental observations [54]. The second term is used to reproduce the 1-loop perturbative result of QCD by going to $\alpha(k^2)/k^2$ in the limit of large spacelike k. See Figure 3.2. The function $\mathcal{F}(k^2)$ is given by

$$\mathcal{F}(k^2) = \frac{1 - e^{-k^2/(4m_t^2)}}{k^2} \tag{3.3}$$

where $m_t = 0.5$ GeV sets the scale between the perturbative and nonperturbative pieces of Eq. 3.2.

Figure 3.1: The infrared behavior of $\mathcal{G}(k^2)/k^2$.

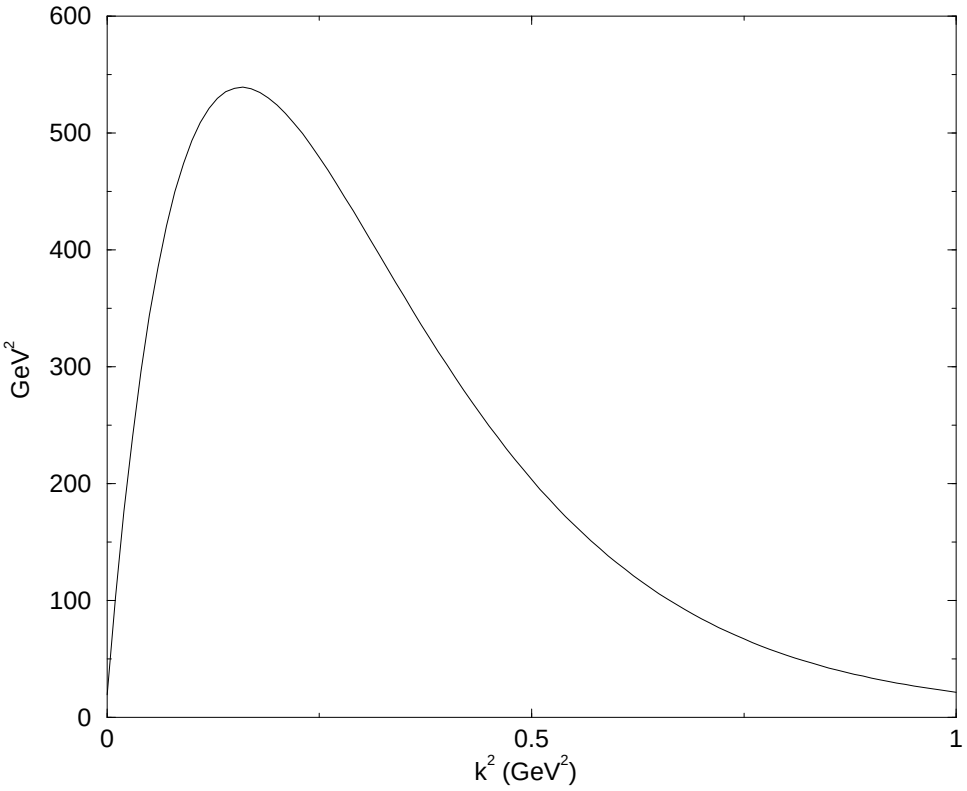

Figure 3.2: Comparison between the 1-loop $\alpha(k^2)$ and $\mathcal{G}(k^2)/k^2$.

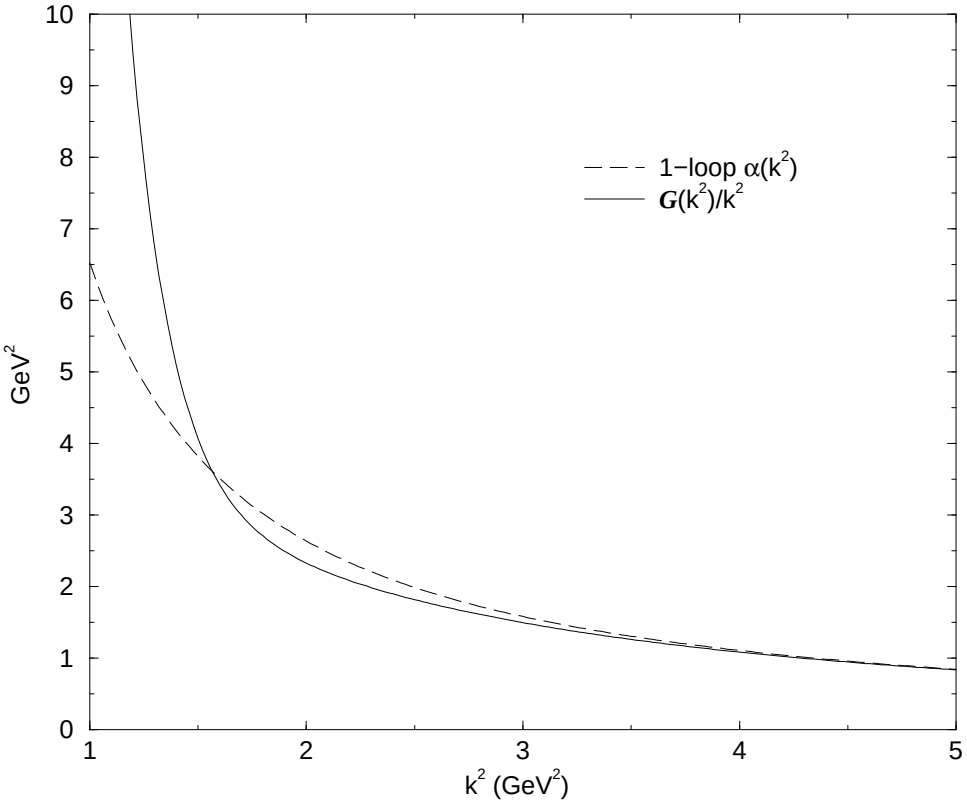

The parameters $N_f = 4$ and $\gamma_m = 12/(33 - 2N_f)$ are the number of quark flavors and the 1-loop anomalous dimension of mass, respectively. The parameter $\Lambda_{QCD} = 0.234$ GeV sets the scale between the perturbative and nonperturbative regions in QCD. The parameter $\tau = e^2 - 1$ is used to create gluon confinement by ensuring that the log term in Eq. 3.2 is not singular on the real axis. From [1], three parameter sets were defined by three different values of ω while D, the up quark mass, and the strange quark mass were fitted to the pion decay constant (f_π), the pion mass, and the kaon mass. Table 3.1 gives the parameter set out of the three in [1] that is used in this work.

Table 3.1: Model Parameters

ω	D	$m^{u=d}_{\mu=1\,GeV}$	$m^{s}_{\mu=1\,GeV}$
0.4 GeV	0.93 GeV^2	5.54 MeV	124 MeV

3.2 Spacelike Calculation of the Quark Propagator

We now want to solve Eq. 2.30 for the vector and scalar amplitudes $A(p^2)$ and $B(p^2)$, respectively. As given in the previous chapter the renormalized quark propagator has the form

$$S(p)^{-1} = i\gamma \cdot pA(p^2) + B(p^2). \tag{3.4}$$

The quark propagator can also be written as

$$S(p) = -i\gamma \cdot p\sigma_v(p^2) + \sigma_s(p^2) \tag{3.5}$$

where A, B, σ_v, and σ_s are related by

$$\sigma_v(p^2) = \frac{A(p^2)}{p^2A^2(p^2) + B^2(p^2)} \tag{3.6}$$

and

$$\sigma_s(p^2) = \frac{B(p^2)}{p^2A^2(p^2) + B^2(p^2)}. \tag{3.7}$$

Before we find $A(p^2)$ and $B(p^2)$ we need to find $A'(p^2)$ and $B'(p^2)$ which are the regularized but unrenormalized vector and scalar amplitudes, respectively. $A'(p^2)$ and $B'(p^2)$ come from the unrenormalized quark self-energy,

$$\Sigma'(p) = i\gamma\cdot p\{A'(p^2)-1\} + B'(p^2) = \frac{4}{3}\int^{\Lambda}\frac{d^4q}{(2\pi)^4}\frac{\mathcal{G}(k^2)}{k^2}T_{\mu\nu}(k)\gamma_\mu S(q)\gamma_\nu, \tag{3.8}$$

which is related to the renormalized quark propagator by

$$S(p)^{-1} = Z_2(i\gamma\cdot p + m_{bm}) + \Sigma'(p). \tag{3.9}$$

We can multiply Eq. 3.8 by $\gamma\cdot p$ and take the trace to obtain

$$4p^2(A'(p^2)-1) = -i\frac{4}{3}\int^{\Lambda}\frac{d^4q}{(2\pi)^4}\frac{\mathcal{G}(k^2)}{k^2}T_{\mu\nu}(k)\mathrm{Tr}(\gamma\cdot p\gamma_\mu S(q)\gamma_\nu) \tag{3.10}$$

and take the trace of Eq. 3.8 to get

$$4B'(p^2) = \frac{4}{3}\int^{\Lambda}\frac{d^4q}{(2\pi)^4}\frac{\mathcal{G}(k^2)}{k^2}T_{\mu\nu}(k)\mathrm{Tr}(\gamma_\mu S(q)\gamma_\nu). \tag{3.11}$$

The factor of $4/3$ comes from the trace of the contraction between $\lambda^a/2$ and $\lambda^a/2$.

To simplify A' and B' we will use Eq. 3.5 and recall that the trace of any odd number of gamma matrices is zero. For A' we have:

$$p^2(A'(p^2)-1) = -i\frac{4}{3}\int^{\Lambda}\frac{d^4q}{(2\pi)^4}\frac{\mathcal{G}(k^2)}{k^2}T_{\mu\nu}(k)\frac{1}{4}\mathrm{Tr}(\gamma\cdot p\gamma_\mu S(q)\gamma_\nu) \tag{3.12}$$

$$= -\frac{4}{3}\int^{\Lambda}\frac{d^4q}{(2\pi)^4}\frac{\mathcal{G}(k^2)}{k^2}T_{\mu\nu}(k)\frac{1}{4}\mathrm{Tr}(\gamma\cdot p\gamma_\mu\gamma\cdot q\gamma_\nu)\sigma_v(q^2) \tag{3.13}$$

$$= -\frac{4}{3}\int^{\Lambda}\frac{d^4q}{(2\pi)^4}\frac{\mathcal{G}(k^2)}{k^2}T_{\mu\nu}(k)\frac{1}{4}\mathrm{Tr}(\gamma_\lambda\gamma_\mu\gamma_\rho\gamma_\nu)p_\lambda q_\rho\sigma_v(q^2). \tag{3.14}$$

From Appendix A we know that

$$\mathrm{Tr}(\gamma_\lambda\gamma_\mu\gamma_\rho\gamma_\nu) = 4(\delta_{\lambda\mu}\delta_{\rho\nu} - \delta_{\lambda\rho}\delta_{\mu\nu} + \delta_{\lambda\nu}\delta_{\mu\rho}). \tag{3.15}$$

Therefore,

$$T_{\mu\nu}(k)\frac{1}{4}\mathrm{Tr}(\gamma_\lambda\gamma_\mu\gamma_\rho\gamma_\nu) = -\left\{\delta_{\lambda\rho} + 2\frac{k_\lambda k_\rho}{k^2}\right\} \tag{3.16}$$

and

$$p^2(A'(p^2)-1) = \frac{4}{3}\int^{\Lambda}\frac{d^4q}{(2\pi)^4}\frac{\mathcal{G}(k^2)}{k^2}\left\{\delta_{\lambda\rho}+2\frac{k_\lambda k_\rho}{k^2}\right\}p_\lambda q_\rho\sigma_v(q^2) \tag{3.17}$$

$$= \frac{4}{3}\int^{\Lambda}\frac{d^4q}{(2\pi)^4}\frac{\mathcal{G}(k^2)}{k^2}\sigma_v(q^2)\left\{p\cdot q+2\frac{k\cdot p\,k\cdot q}{k^2}\right\} \tag{3.18}$$

Now for B' we have:

$$B'(p^2) = \frac{4}{3}\int^{\Lambda}\frac{d^4q}{(2\pi)^4}\frac{\mathcal{G}(k^2)}{k^2}T_{\mu\nu}(k)\sigma_s(q^2)\frac{1}{4}\mathrm{Tr}(\gamma_\mu\gamma_\nu) \tag{3.19}$$

$$= \frac{4}{3}\int^{\Lambda}\frac{d^4q}{(2\pi)^4}\frac{\mathcal{G}(k^2)}{k^2}T_{\mu\nu}(k)\sigma_s(q^2)\delta_{\mu\nu} \tag{3.20}$$

since

$$T_{\mu\nu}(k)\delta_{\mu\nu} = \left\{\delta_{\mu\nu}-\frac{k_\mu k_\nu}{k^2}\right\}\delta_{\mu\nu} = 3. \tag{3.21}$$

B' becomes

$$B'(p^2) = 4\int^{\Lambda}\frac{d^4q}{(2\pi)^4}\frac{\mathcal{G}(k^2)}{k^2}\sigma_s(q^2). \tag{3.22}$$

We can accomplish the integration $\int d^4q$ by observing that the integrands in Eq. 3.18 and Eq. 3.22 are functions of p^2, q^2, and $p\cdot q$. Our momentum 4-vector is

$$q = |q|\,(\cos\phi\sin\theta\sin\beta, \sin\phi\sin\theta\sin\beta, \cos\theta\sin\beta, \cos\beta) \tag{3.23}$$

and the integration over momentum 4-space is

$$\int^{\Lambda} d^4q = \int_0^{\Lambda} q^3dq\int_0^{2\pi}d\phi\int_0^{\pi}\sin\theta d\theta\int_0^{\pi}\sin^2\beta d\beta. \tag{3.24}$$

If we take the direction of p_μ to be along the 4th axis, the integrands will be independent of θ and ϕ and the integration over θ and ϕ can be done analytically reducing Eq. 3.24 to

$$\int^{\Lambda} d^4q = 4\pi\int_0^{\Lambda} q^3dq\int_0^{\pi}\sin^2\beta d\beta \tag{3.25}$$

and with the substitution $u=\cos\beta$ it becomes

$$\int^{\Lambda} d^4q = 4\pi\int_0^{\Lambda} q^3dq\int_{-1}^{1}\sqrt{1-u^2}du. \tag{3.26}$$

Equations 3.18 and 3.22 then become

$$p^2(A'(p^2)-1) = \frac{4}{3(2\pi)^4}4\pi \int_0^\Lambda q^3 dq \int_{-1}^{1} \sqrt{1-u^2}du \qquad (3.27)$$
$$\frac{\mathcal{G}((p-q)^2)}{p^2-2pqu+q^2}\sigma_v(q^2)\cdot\left\{pqu+2\frac{(p^2-pqu)\,(pqu-q^2)}{p^2-2pqu+q^2}\right\}$$

and

$$B'(p^2) = \frac{4}{(2\pi)^4}4\pi \int_0^\Lambda q^3 dq \int_{-1}^{1} \sqrt{1-u^2}du\, \frac{\mathcal{G}((p-q)^2)}{p^2-2pqu+q^2}\,\sigma_s(q^2). \qquad (3.28)$$

Now that we have $A'(p^2)$ and $B'(p^2)$ we can determine Z_2, m_R, $A(p^2)$, and $B(p^2)$. Eq. 2.32 requires that

$$Z_2(\mu^2,\Lambda^2) = 2 - A'(\mu^2,\Lambda^2) \qquad (3.29)$$

and

$$m_R(\mu^2) = Z_2(\mu^2,\Lambda^2)m_{bm} + B'(\mu^2,\Lambda^2). \qquad (3.30)$$

The renormalization of $A(p^2)$ and $B(p^2)$ are given by

$$A(p^2,\mu^2) = 1 + A'(p^2,\Lambda^2) - A'(\mu^2,\Lambda^2) \qquad (3.31)$$

and

$$B(p^2,\mu^2) = m_R(\mu^2) + B'(p^2,\Lambda^2) - B'(\mu^2,\Lambda^2). \qquad (3.32)$$

The exception to this is in the chiral limit where $Z_2(\mu^2,\Lambda^2)m_{bm} = 0$ [19] and Eq. 3.32 reduces to $B(p^2,\mu^2) = B'(p^2,\Lambda^2)$.

Solving for $A(p^2)$ and $B(p^2)$ is now a problem of solving two coupled, nonlinear integral equations. The procedure used is to make a guess for $\sigma_v(p^2)$ and $\sigma_s(p^2)$, numerically solve Eqs. 3.27 and 3.28, apply the renormalization condition in Eqs. 3.31 and 3.32 to obtain $A(p^2)$ and $B(p^2)$, use Eqs. 3.6 and 3.7 to obtain a new guess for $\sigma_v(p^2)$ and $\sigma_s(p^2)$, and repeat until $\sigma_v(p^2)$ and $\sigma_s(p^2)$ are known to some accuracy. Our accuracy criterion is a calculation of the average relative error of $\sigma_v(p^2)$ and $\sigma_s(p^2)$ between two adjacent iterations. Our iteration procedure terminates itself when we reach an average relative

error less than 10^{-8}. We also watch the maximum relative error to make sure no point in either $\sigma_v(p^2)$ or $\sigma_s(p^2)$ deviates too far from the average relative error. Figures 3.3 and 3.4 are our numerical calculations of $A(p^2)$ and $B(p^2)$, respectively. Figures 3.5 and 3.6 show our numerical calculation $\sigma_v(p^2)$ and $\sigma_s(p^2)$, respectively. Our renormalized quark mass function, $M(p^2) = B(p^2)/A(p^2)$, is shown in Figure 3.7.

To compare this model to lattice calculations [55] we fit the renormalized current quark mass to lattice data. From Figure 3.8 we see that our chiral limit quark mass function is in good agreement with the chiral extrapolation of the lattice calculations. In the presence of explicit chiral symmetry breaking, we fit the current quark mass at our renormalization point with $M(p^2)$ and $Z(p^2)$, separately. We then obtained the two current quark masses at 1 GeV using

$$m(\mu)\langle\bar{q}q\rangle^{\circ}_{\mu} = \hat{m}\langle\bar{q}q\rangle^{\circ} \tag{3.33}$$

where $\langle\bar{q}q\rangle^{\circ}$ is the renormalization-point-independent vacuum quark condensate [19]. The renormalization-point-independent vacuum quark condensate is obtained by fitting $M(p^2)$ to

$$M(p^2) = \frac{2\pi^2\gamma_m}{3}\frac{(-\langle\bar{q}q\rangle^{\circ})}{p^2(\frac{1}{2}\ln[p^2/\Lambda^2_{QCD}])^{1-\gamma_m}} \tag{3.34}$$

in the chiral limit at large p^2. The results shown in Figure 3.9 indicate good agreement with $M(p^2)$ due to our implementation of DχSB, but also shows differences in the calculation of $Z(p^2)$. Lattice calculations produce a regulated but un-renormalized $Z(p^2)$. For this reason the scale of the field renormalization function $Z(p^2)$ is arbitrary and only comparisons to its shape are meaningful. The bare quark-gluon vertex typically causes $Z(p^2)$ to saturate slower than lattice calculations. This discrepancy in $Z(p^2)$ signals a deficiency in the bare quark-gluon vertex [56, 57] and in our model gluon propagator.

Figure 3.3: Up and Strange Quark $A(p^2)$

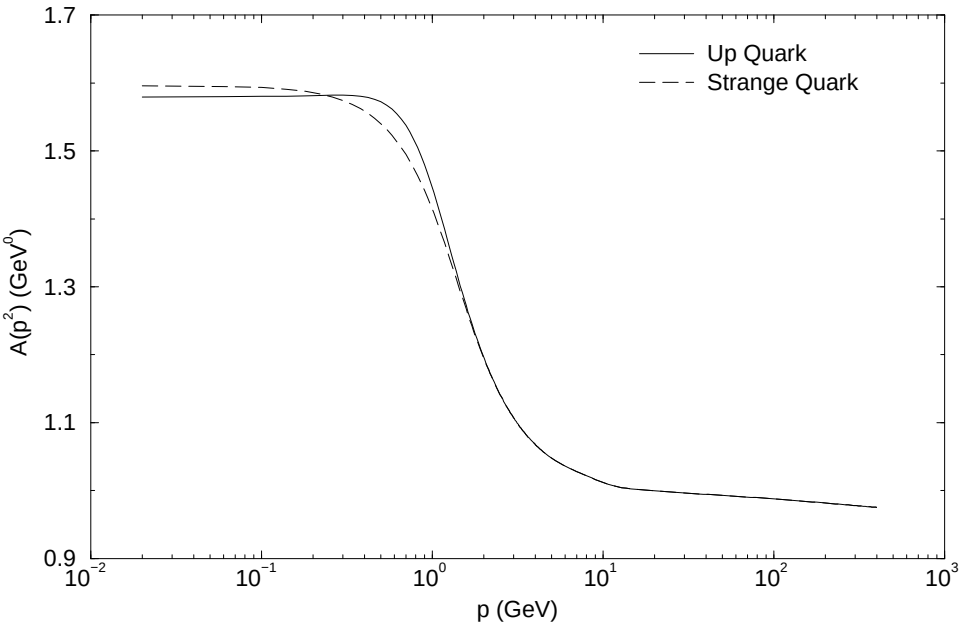

Figure 3.4: Up and Strange Quark $B(p^2)$

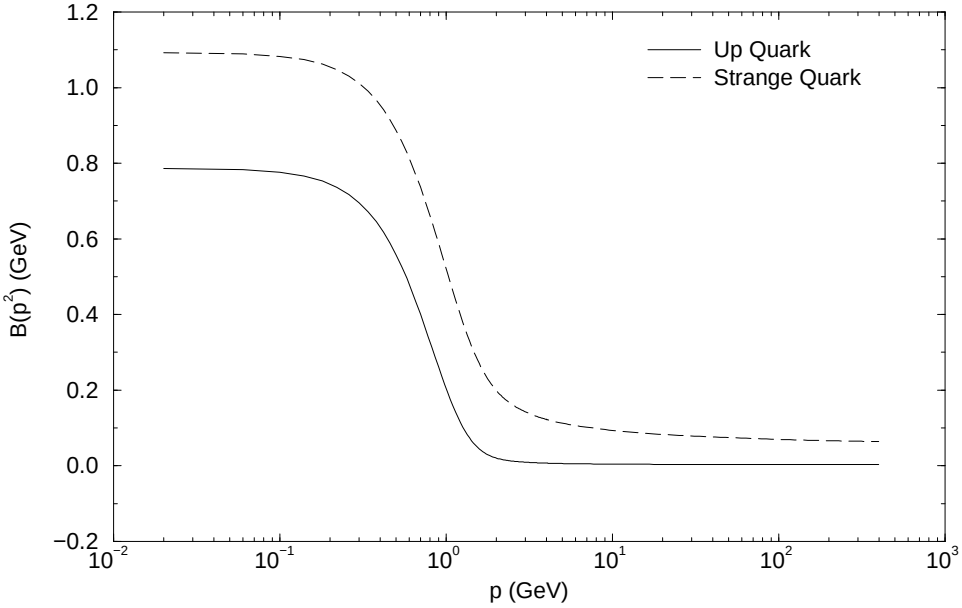

Figure 3.5: Up and Strange Quark $\sigma_v(p^2)$

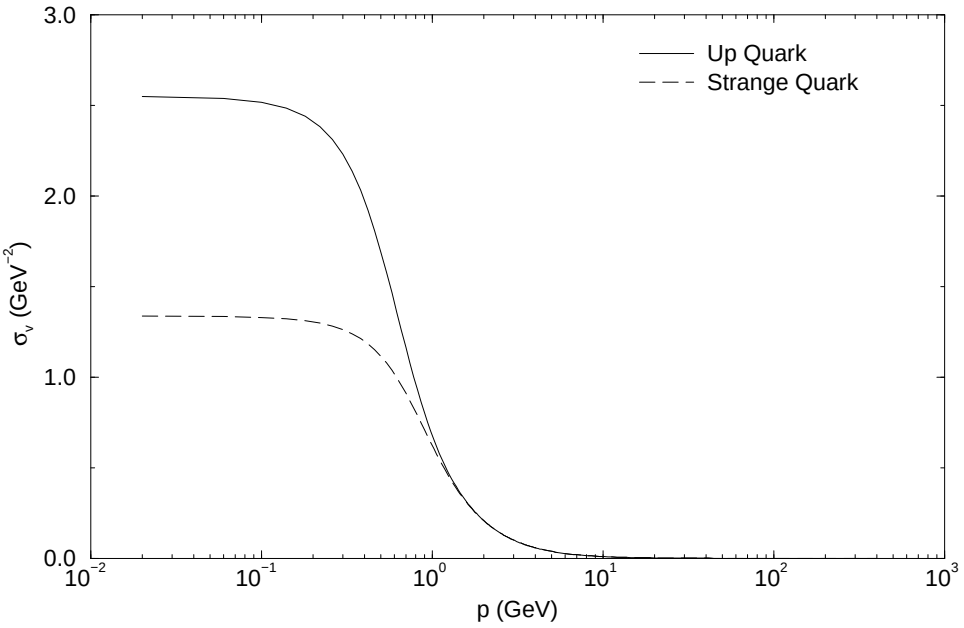

Figure 3.6: Up and Strange Quark $\sigma_s(p^2)$

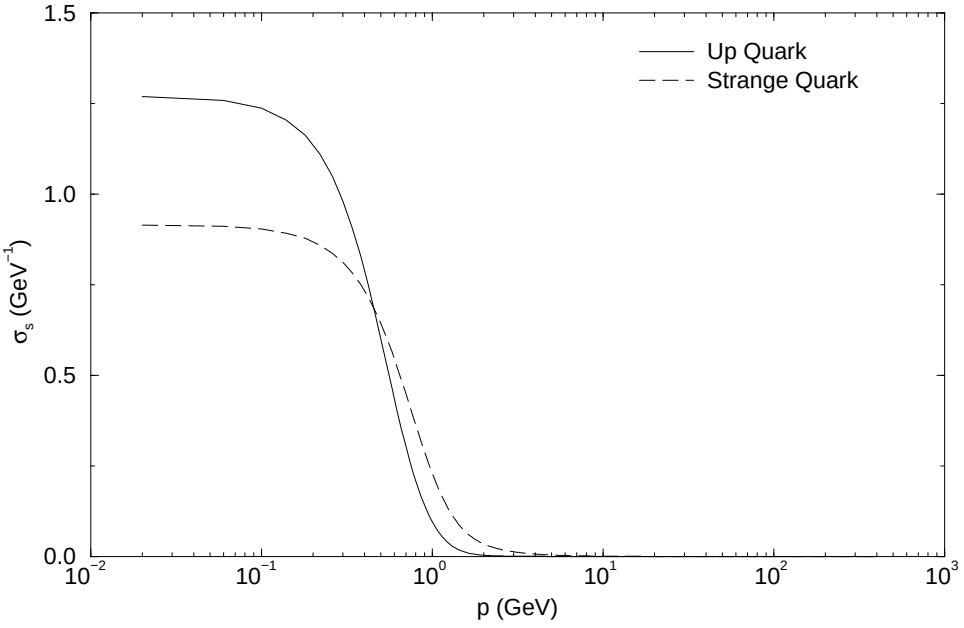

Figure 3.7: Up and Strange Quark Mass Functions

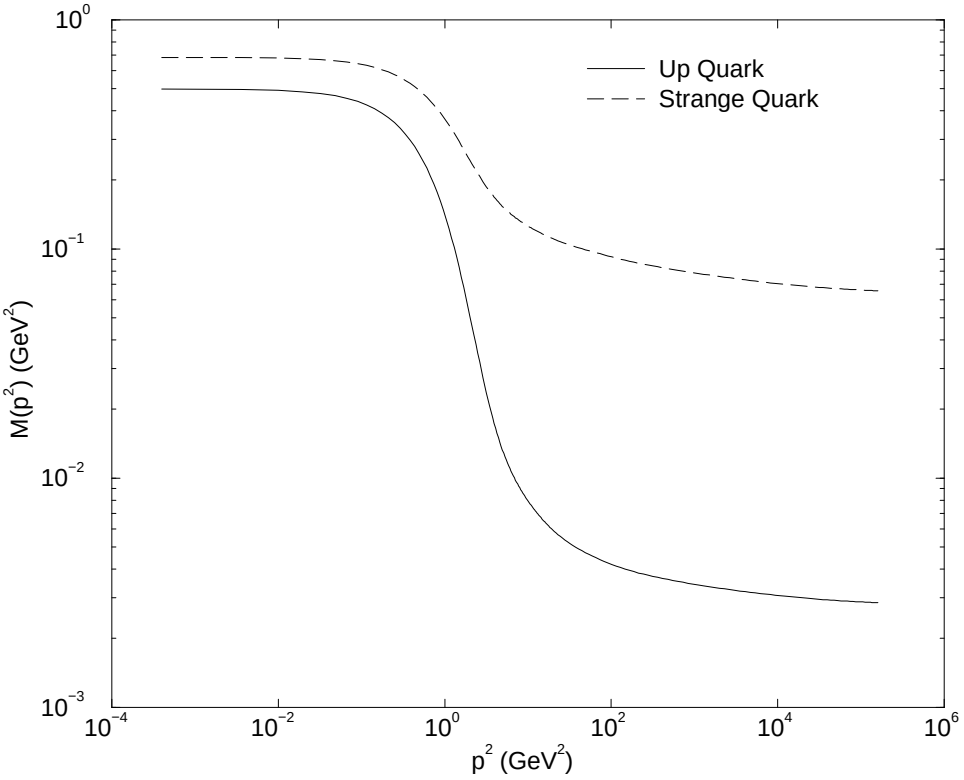

Figure 3.8: DSE comparison to Lattice QCD calculations in the chiral limit.

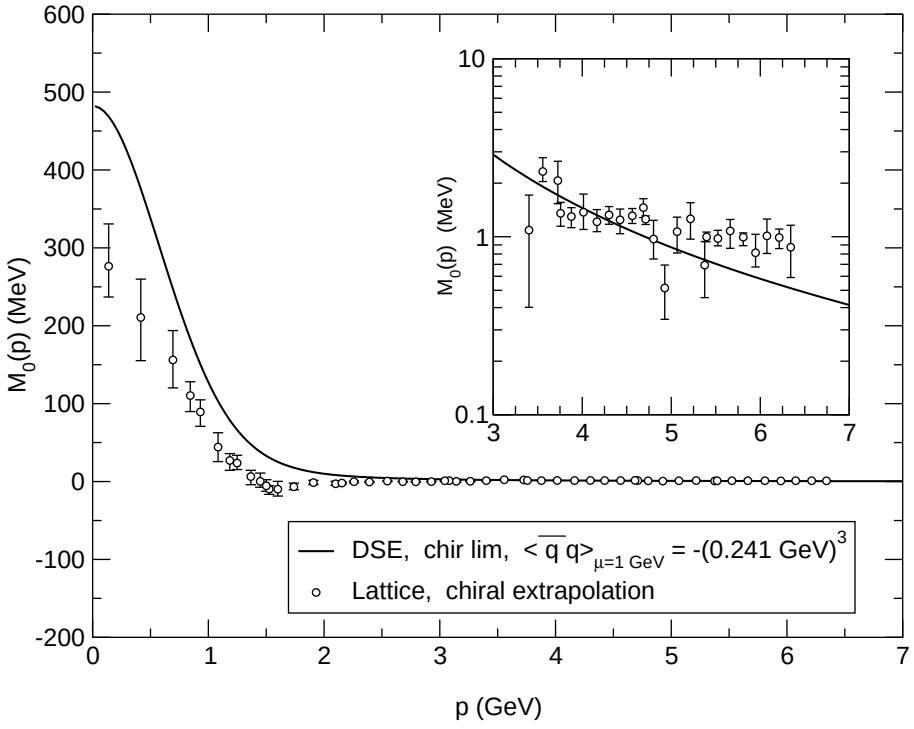

Figure 3.9: DSE comparison to Lattice QCD.

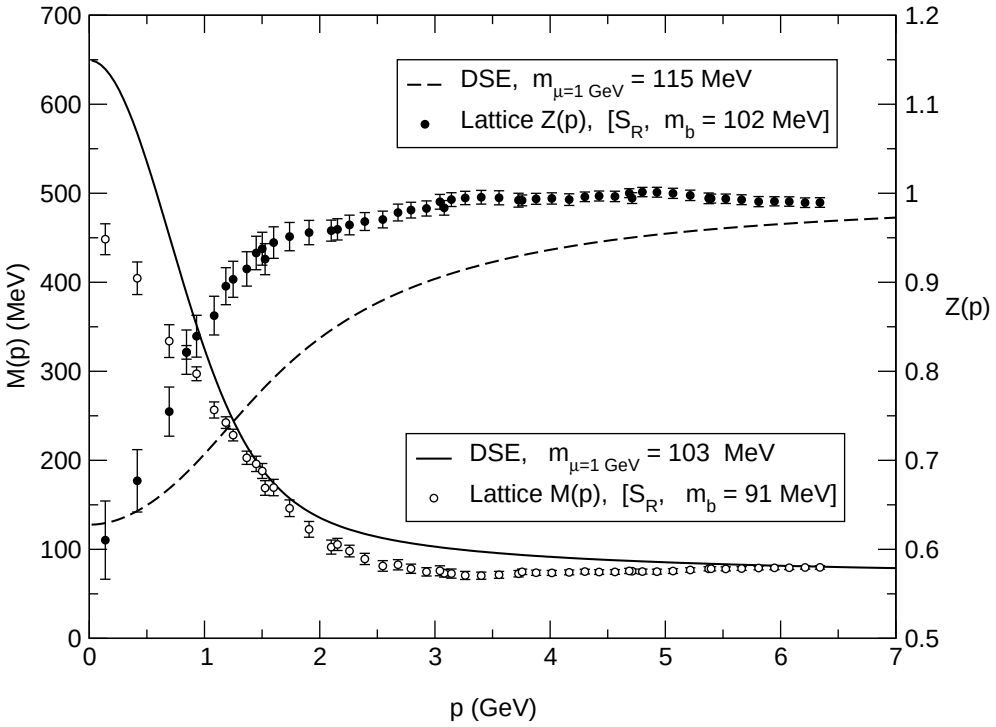

3.3 Analytic Angular Solution to the DSE

Here we show an analytic solution to the angular part of the quark propagators without the 1-loop perturbative tail. The angular part of Eq. 3.27 without the tail piece is

$$\Theta[p^2(A'(p^2)-1)] = \frac{4\pi^2 D}{\omega^6}\int_{-1}^{1}\sqrt{1-u^2}du\left\{pqk^2u+2(p^2-pqu)(pqu-q^2)\right\}e^{-k^2/\omega^2} \tag{3.35}$$

and Eq. 3.28 without the tail piece is

$$\Theta[B'(p^2)] = \frac{4\pi^2 D}{\omega^6}\int_{-1}^{1}\sqrt{1-u^2}du\left\{k^2e^{-k^2/\omega^2}\right\}. \tag{3.36}$$

With $k^2 = p^2 - 2pqu + q^2$ our above integrals reduce to finding

$$\psi_1(z) = \int_{-1}^{1}\sqrt{1-u^2}e^{zu}du, \tag{3.37}$$

$$\psi_2(z) = \int_{-1}^{1}\sqrt{1-u^2}ue^{zu}du., \tag{3.38}$$

and

$$\psi_3(z) = \int_{-1}^{1}\sqrt{1-u^2}u^2e^{zu}du. \tag{3.39}$$

The integral representation of the modified Bessel functions of integer order[58],

$$I_\nu(z) = \frac{(z/2)^\nu}{\sqrt{\pi}\,\Gamma(\nu+1/2)}\int_0^\pi e^{\pm z\cos(\theta)}\sin^{2\nu}(\theta)d\theta, \tag{3.40}$$

immediately solves the integrals $\psi_1(z) = \pi I_1(z)/z$, $\psi_2(z) = \pi I_2(z)/z$, and $\psi_3(z) = \pi I_2(z)/z^2 + \pi I_3(z)/z$ with the substitution $u = \cos(\theta)$ and with an integration by parts in the case of ψ_2 and ψ_3. Eqs. 3.35 and 3.36 are now

$$\Theta[p^2(A'(p^2)-1)] = \frac{2\pi^3 D}{\omega^4}e^{-(p^2+q^2)/\omega^2}\Big\{-2pq\,I_1(2pq/\omega^2) + [\,3(p^2+q^2)-2\omega^2\,]\,I_2(2pq/\omega^2) - 4pq\,I_3(2pq/\omega^2)\Big\} \tag{3.41}$$

and

$$\Theta[B'(p^2)] = \frac{2\pi^3 D}{pq\omega^4}e^{-(p^2+q^2)/\omega^2}\left\{(p^2+q^2)I_1(2pq/\omega^2) - 2pqI_2(2pq/\omega^2)\right\}. \tag{3.42}$$

3.4 Complex Plane Calculation of the Quark Propagator

In this section we show that a a non-trivial contour integration is required to calculate the values of the quark propagator in the complex plane. We also show that a physically unobservable change to the model can allow for trivial contour integration along the real axis.

We analytically continue our DSE into the complex plane by making the substitution

$$p^2 \to re^{i\theta}. \tag{3.43}$$

Equations 3.27 and 3.28 are easily solved because we now have a converged solution for the spacelike $\sigma_v(q^2)$ and $\sigma_s(q^2)$ where q is purely real and we fix r and θ, calculate $A'(p^2)$ and $B'(p^2)$ from Eqs. 3.27 and 3.28, apply the renormalization conditions from Eqs. 3.31 and 3.32, and solve for $\sigma_v(p^2)$ and $\sigma_s(p^2)$ using Eqs. 3.6 and 3.7.

Our technique is to choose an angle in the second quadrant and plot the propagator along the ray. See Figures 3.10 and 3.11 for up quark $\sigma_v(p^2)$. There are two significant features of these graphs. The first is the possibility of singularities in σ_v and σ_s. (Corresponding graphs in A and B do not show the possibility of singularities.) The second is the numerical instability of the graphs. Before we can confidently identify a true singularity we need to find the origin of this numerical instability. (Corresponding graphs in A and B show the same numerical instability.)

The instabilities occur as a regular, equally spaced pattern as a function of p^2 and the frequency of the instabilities doubled when we doubled the number of quadrature points in the spacelike grid. The location of the numerical instabilities are independent of the number of angle quadrature points. The numerical instabilities are not caused by crossing a branch cut in the square root function. The numerical instabilities are present only when the 1-loop pQCD tail term in Eq. 3.2 is included. Furthermore, the instabilities are not correlated with singularities of the explicit log function in Eq. 3.2.

Figure 3.10: Real part of σ_v in the complex plane.

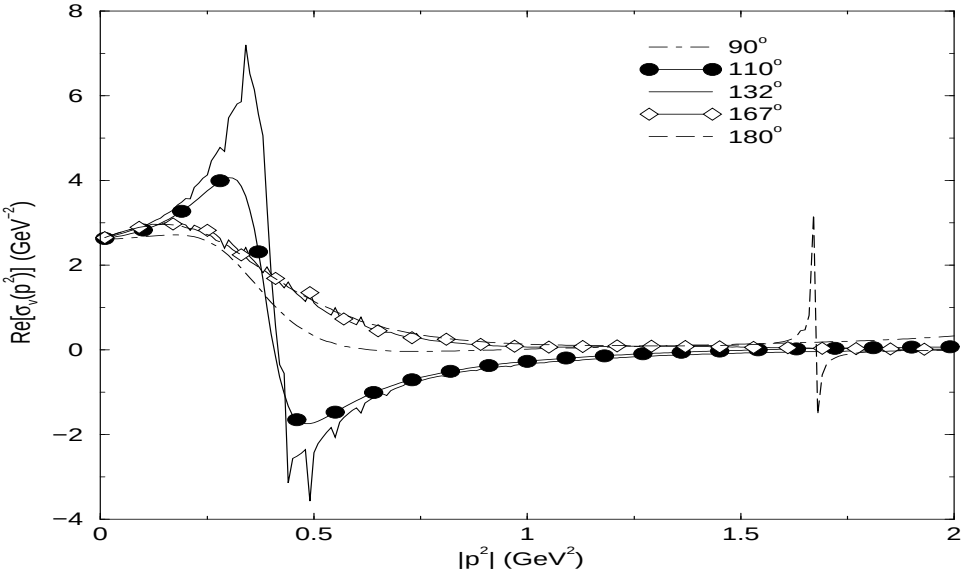

Figure 3.11: Imaginary part of σ_v in the complex plane.

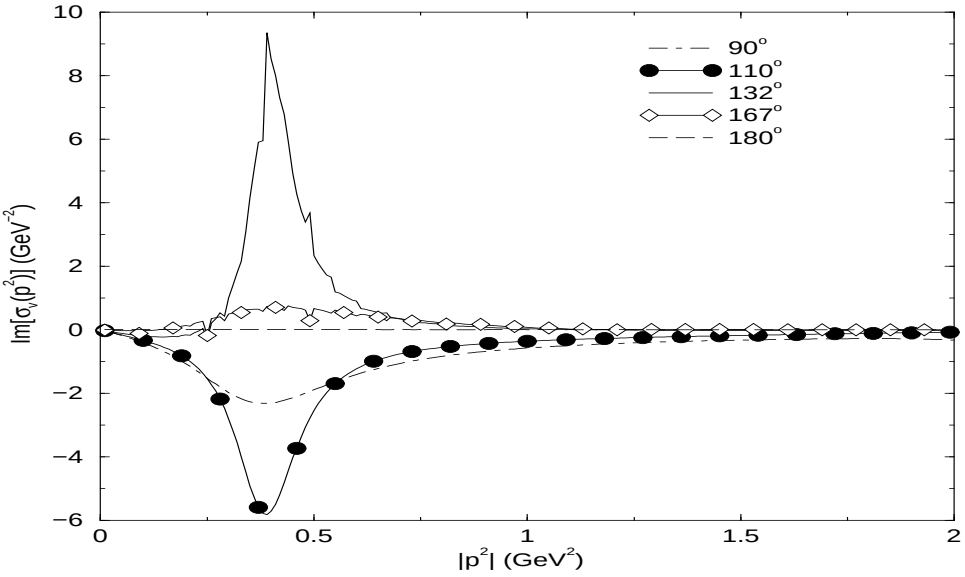

Figure 3.12: $K(p,q)$ at $|p^2| = 0.25$ GeV^2.

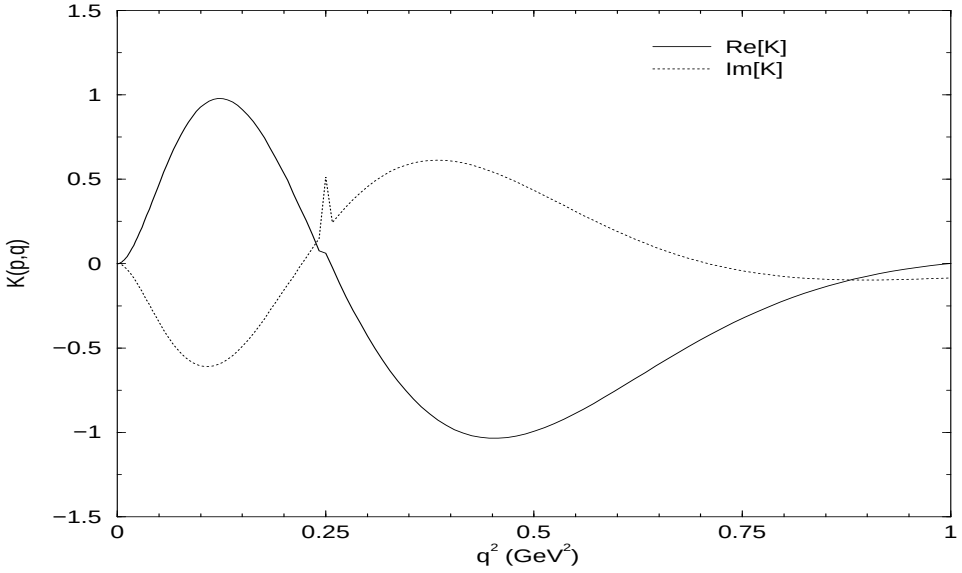

Figure 3.13: $K(p,q)$ at $|p^2| = 0.5 GeV^2$.

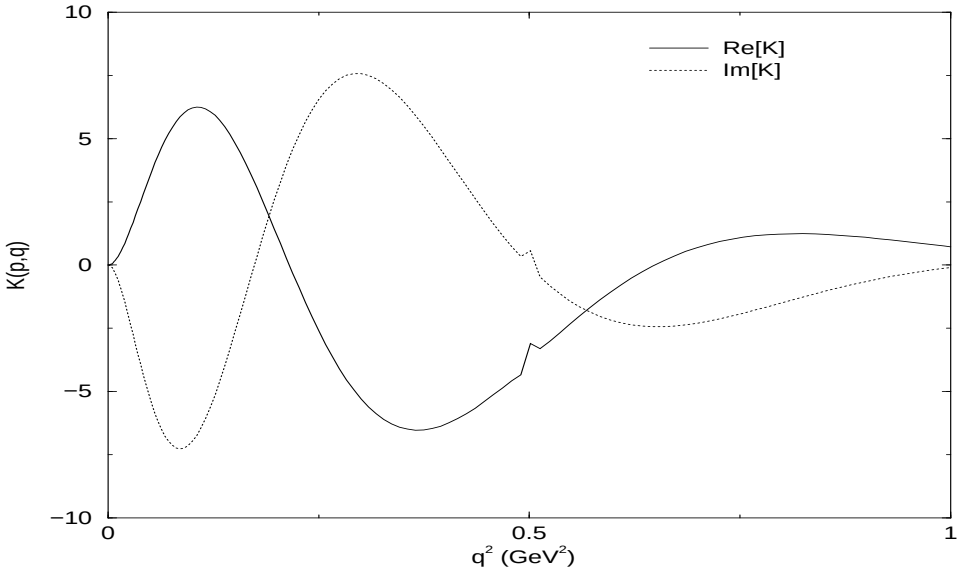

To analyse the numerical instability, we write Eq. 3.27 for $A(p^2)$ in the form

$$p^2(A'(p^2)-1) = \int_0^{\Lambda^2} K(p,q)\,\sigma_v(q^2)\,d(q^2) \tag{3.44}$$

where

$$\begin{aligned} K(p,q) &= \frac{4(4\pi)}{3(2\pi)^4}\frac{q^2}{2}\int_{-1}^{1}\sqrt{1-u^2}du\frac{\mathcal{G}((p-q)^2)}{p^2-2pqu+q^2} \\ &\times \left\{pqu+2\frac{(p^2-pqu)\,(pqu-q^2)}{p^2-2pqu+q^2}\right\} \end{aligned} \tag{3.45}$$

and the integration variable has changed from q to q^2. (Our actual calculations integrate over q^2.) From Eq. 3.44 and Figure 3.5 we know that any numerical instability that comes into $A(p^2)$ must enter through $K(p,q)$ and not $\sigma_v(q^2)$. Figures 3.12 and 3.13 are graphs of the real and imaginary parts of $K(p,q)$ at set values of $|p^2|$. We see that our instabilities come from $K(p,q)$ when $|p^2| = q^2$.

Specifically, we assumed that the analytic function $k\cdot p\,k\cdot q/k^2$, which is nonsingular for real p^2 when $k^2=(p-q)^2=0$, was also non-singular when p^2 was continued into the complex plane. This assumption is not true. When both p^2 and q^2 are real,

$$u = \frac{1}{2}\left\{\frac{p}{q}+\frac{q}{p}\right\} \tag{3.46}$$

will give the value of u so that $k^2=0$. If $p\neq q$ then $u>1$ for k^2 to be equal to zero. When $p=q$ then $u=1$ and the integrand has a singularity at the right limit of integration. However, when $p=q$ then

$$\frac{k\cdot p\,k\cdot q}{k^2} = \frac{q^4(1-u)(u-1)}{2q^2(1-u)} = \frac{1}{2}q^2(u-1) \tag{3.47}$$

and the singularity is canceled by $k\cdot p\,k\cdot q$. Now when $p^2=re^{i\theta}$ and $q^2=Re^{i\phi}$ are both complex we find that $k^2=0$ when

$$u = \frac{1}{2}\left\{\left(\sqrt{\frac{r}{R}}+\sqrt{\frac{R}{r}}\right)\cos\left(\frac{\theta-\phi}{2}\right)+i\left(\sqrt{\frac{r}{R}}-\sqrt{\frac{R}{r}}\right)\sin\left(\frac{\theta-\phi}{2}\right)\right\}. \tag{3.48}$$

Since the integration in Eq. 3.45 is over real u we see that $k^2 \neq 0$ when $r \neq R$ and $\theta \neq \phi$. When either $r = R$ or $\theta = \phi$ then the imaginary part of Eq. 3.48 is zero and the integration over u may encompass a singularity. In particular, when $\theta = \phi$ and $r \neq R$ then $k^2 \neq 0$ for u along the limits of integration by the same arguments as when p^2 and q^2 are real. However, when $r = R$ and $\theta \neq \phi$ then $k^2 = 0$ when $u = \cos((\theta - \phi)/2)$, which is guaranteed to be within the limits of integration. Furthermore, when $|p^2| = |q^2|$ and $\theta \neq \phi$ then $k \cdot p\, k \cdot q/k^2$ is a multivalued function of p^2 and q^2. Finally, when $r = R$ and $\theta = \phi$,

$$\frac{k \cdot p\, k \cdot q}{k^2} = \frac{1}{2} p^2 (u - 1) \tag{3.49}$$

is analytic for u along the limits of integration in Eq. 3.45 and is single valued.

$K(p, q)$ results from integrating over a nonintegrable singularity when p^2 is continued to the complex plane and q^2 is not. This occurs only at the point when $|p^2| = q^2$. For $K(p, q)$ to be properly defined the integration over q^2 in Eq. 3.44 must be along any contour that includes $q^2 = p^2$. However, this numerically intractable problem can be circumvented with a physically insignificant change to $\mathcal{G}(k^2)/k^2$ while keeping the integration over q^2 along the real axis.

The singularity in $k \cdot p\, k \cdot q/k^2$ in the equation for $A(p^2)$ is canceled by the k^2 factor in the infrared enhancement of Eq. 3.2. There is no corrsponding k^2 factor in the 1-loop perturbative tail term of the kernel. To see this, we perform a Taylor series expansion of Eq. 3.3 in the low k^2 limit to obtain

$$\mathcal{F}(k^2) = \frac{1}{4m_t^2} - \frac{1}{2} \frac{k^2}{(4m_t^2)^2} + \cdots. \tag{3.50}$$

If we change $\mathcal{F}(k^2)$ to

$$\mathcal{F}(k^2) = \frac{1 - e^{-k^4/(4m_t^2)^2}}{k^2} \tag{3.51}$$

and look at its Taylor series expansion we find that

$$\mathcal{F}(k^2) = \frac{k^2}{(4m_t^2)^2} - \frac{1}{2} \frac{k^6}{(4m_t^2)^4} + \cdots \tag{3.52}$$

Figure 3.14: Real part of σ_v in the complex plane with modified $\mathcal{F}(k^2)$.

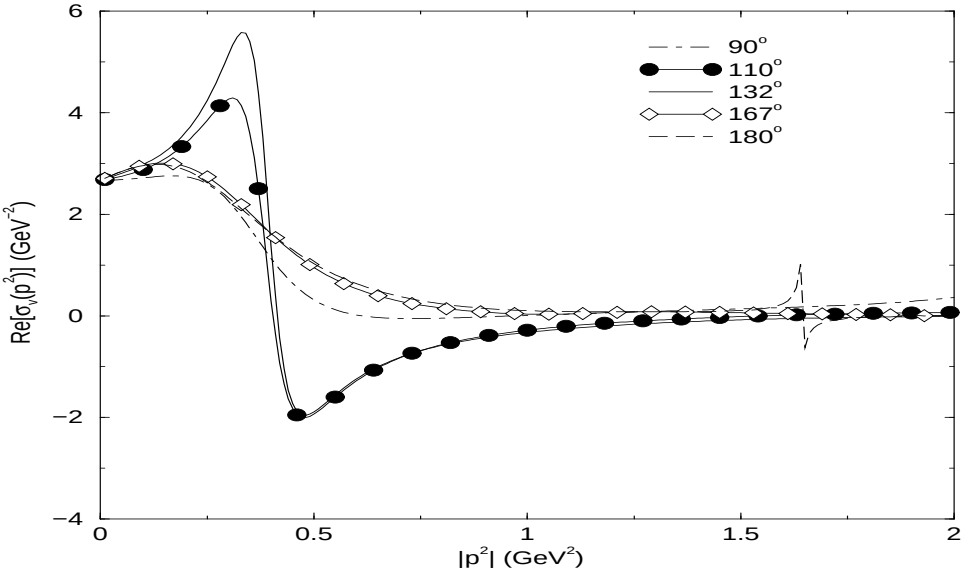

and the factors of k^2 in Eq. 3.52 will now cancel the $1/k^2$ in $k \cdot p\, k \cdot q/k^2$ to give us a finite expression everywhere in the complex plane. Figures 3.14 and 3.15 are the same as 3.10 and 3.11 but with the modified $\mathcal{F}(k^2)$ as given in Eq. 3.51.

The model characterized by Eq. 3.2 with $\mathcal{F}(k^2)$ replaced by Eq. 3.51 produces changes of less than one percent in the meson observables calculated in this work. Since the infrared behavior of the gluon is unknown we are free to model its behavior with either a zero or nonzero value at $k^2 = 0$. The role of $\mathcal{F}(k^2)$ is to dictate at what momentum the 1-loop pQCD tail term turns on. In the infrared, $\mathcal{F}(k^2)$ causes the 1-loop pQCD tail term to be some very small value compared to the infrared enhancement given by the first term in Eq. 3.2. In the ultraviolet, $\mathcal{F}(k^2)$ causes the 1-loop pQCD tail term to go to $1/[k^2 \ln(k^2/\Lambda^2_{QCD})]$. Both $\mathcal{F}(k^2)$s given by Eqs. 3.3 and 3.51 accomplish this task. Figure 3.16 suggests that replacing Eq. 3.3 by Eq. 3.51 trivially modifies the infrared behavior of the gluon while allowing for contour integration along the real axis. Furthermore, the integrated strength of the gluon is modeled to produce the empirical value of the quark

Figure 3.15: Imaginary part of σ_v in the complex plane with modified $\mathcal{F}(k^2)$.

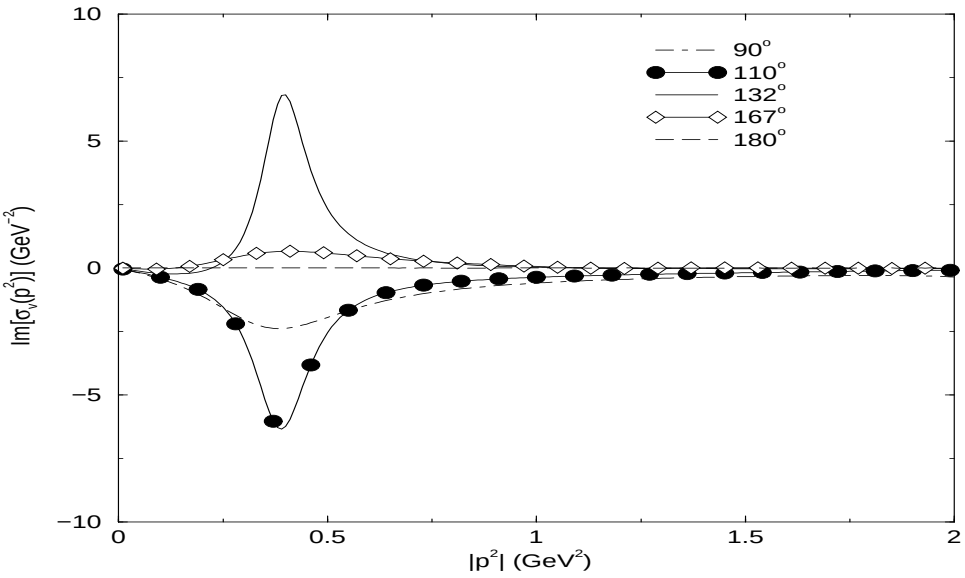

condensate. The modification to $\mathcal{F}(k^2)$ is such that the value of the quark condensate changes by less than 0.3%. The parameters in Table 3.1 can be readjusted to fit the quark condensate but the changes are so small that we do not do so.

Having modified the model to allow for contour integration along the real axis, we can now positively identify singularities in σ_v and σ_s in the complex plane. In the chiral limit we find singularities at an (r, θ) of $(0.375 \pm 0.01$ GeV^2,$122 \pm 1°)$, $(1.18 \pm 0.03$ GeV^2,$161 \pm 1°)$, and $(1.66 \pm 0.02$ GeV^2,$180°)$. Figure 3.17 shows that the singularities at 122° and 161° are mirrored by corresponding singularities in the third quadrant according to the Schwarz Reflection Principle [59]. The up quark singularities are at an (r, θ) of $(0.39 \pm 0.02$ GeV^2,$122 \pm 1°)$, $(1.1 \pm 0.04$ GeV^2,$155 \pm 1°)$, and $(1.64 \pm 0.04$ GeV^2,$180°)$. The strange quark singularities are at an (r, θ) of $(0.71 \pm 0.01$ GeV^2,$122 \pm 1°)$, $(1.60 \pm 0.01$ GeV^2,$142 \pm 1°)$, and $(1.30 \pm 0.02$ GeV^2,$180°)$. The strange quark shows an area of numerical instability between 158°-169° and 1.4 GeV^2-1.8 GeV^2. We did not investigate this area any further. When the perturbative tail piece in Eq. 3.2 is removed from the model, the positions of

Figure 3.16: Comparison of different $\mathcal{F}(k^2)$'s in $\mathcal{G}(k^2)/k^2$. The solid line with circles represents the original model with $\mathcal{F}(k^2)$ given in Eq. 3.3 and the diamonds represent $\mathcal{G}(k^2)/k^2$ with $\mathcal{F}(k^2)$ given in Eq. 3.51.

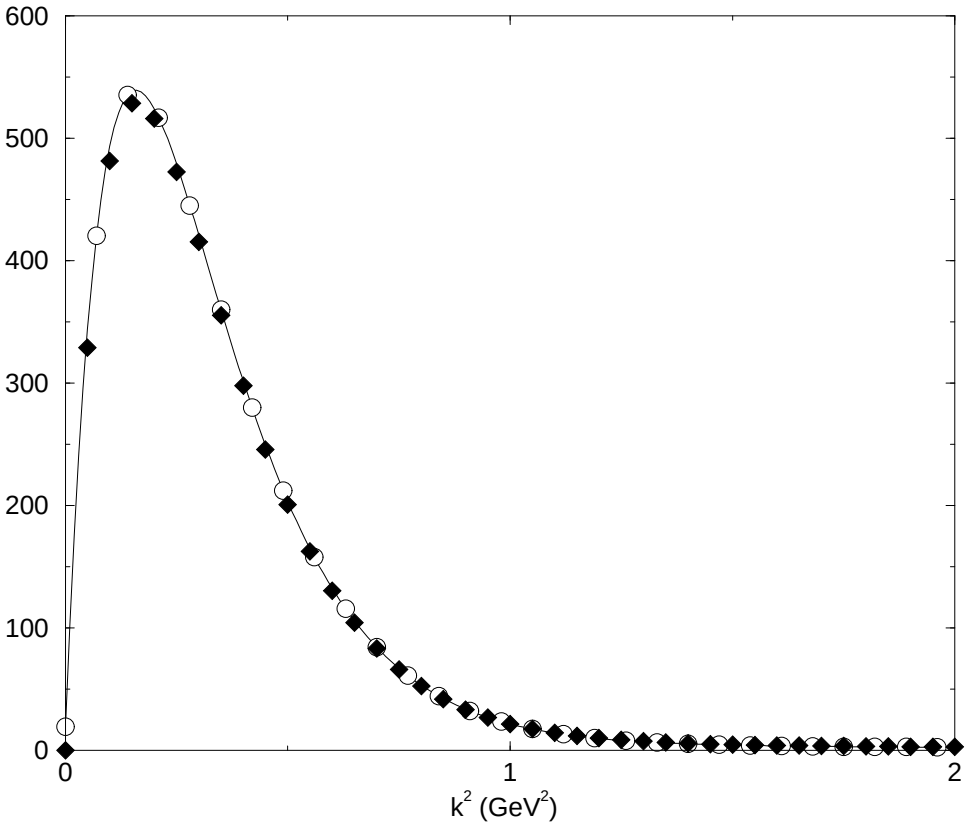

Figure 3.17: Singularities in the real part of the chiral limit $\sigma_v(p^2)$. The singularities shown are at an (r, θ) of $(0.375 \pm 0.01$ GeV^2,$122 \pm 1^\circ)$.

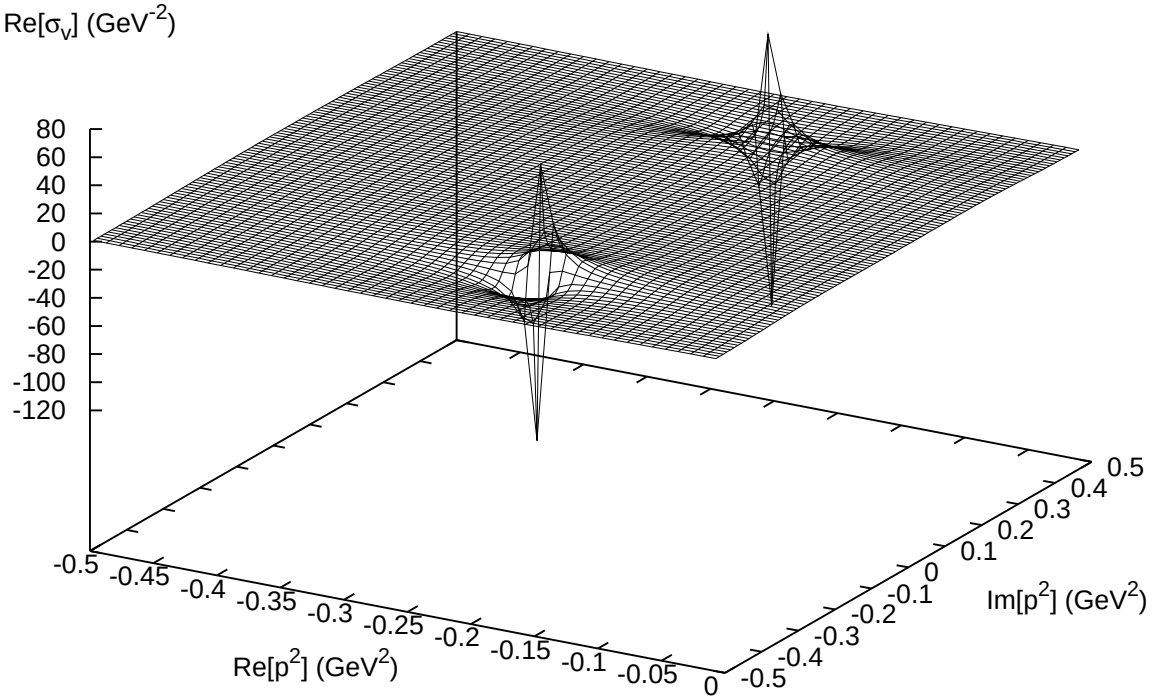

the singularities change only slightly except for the one at (1.1 GeV^2,155°) which no longer exists or has moved out of our search area that has a maximum radius of 2 GeV^2. For our meson calculations in the next chapter, only the singularities at $122 \pm 1^\circ$ will affect our calculations. Its effect will be to limit how high we go in the meson spectrum by limiting our calculations to the ϕ meson and below.

CHAPTER 4

Properties of Pseudoscalar and Vector Mesons

4.1 General Technique

To solve the Bethe-Salpeter amplitude in Eq. 2.34,

$$\left[\Gamma_M^{ab}(p;P_i)\right]_{tu} = \int^{\Lambda} \frac{d^4q}{(2\pi)^4} K_{tu}^{rs}(p,q;P_i)\left[S^a(q+\eta P_i)\Gamma_M^{ab}(q;P_i)S^b(q-\beta P_i)\right]_{sr}, \tag{4.1}$$

we use the ladder truncation,

$$K_{tu}^{rs}(p,q;P_i) \to -\frac{\mathcal{G}(k^2)}{k^2}T_{\mu\nu}(k)\left[\frac{\lambda^c}{2}\gamma_\mu\right]^{ru} \otimes \left[\frac{\lambda^c}{2}\gamma_\nu\right]^{ts}, \tag{4.2}$$

where $\mathcal{G}(k^2)$ is the effective running coupling constant and $k = p-q$ is the gluon momentum. See Fig. 4.1. The Bethe-Salpeter Equation now takes on the form

$$\begin{aligned} \Gamma_M^{ab}(p;P_i) &= -\int^{\Lambda} \frac{d^4q}{(2\pi)^4}\frac{\mathcal{G}(k^2)}{k^2}T_{\mu\nu}(k)\frac{\lambda^c}{2}\gamma_\mu\, S^a(q+\eta P_i) \\ &\times \Gamma_M^{ab}(q;P_i)S^b(q-\beta P_i)\frac{\lambda^c}{2}\gamma_\nu \end{aligned} \tag{4.3}$$

where mesons of different quantum numbers have different forms of $\Gamma_M^{ab}(q;P_i)$. In general $\Gamma_M^{ab}(q;P_i)$ is created by taking all possible combinations of q, P, and γ matrices that have the appropriate transformations under charge conjugation (C), spatial inversion (P), and time reversal (T) [49].

Equation 4.3 is valid only for discrete momenta P_i satisfying $P_i^2 = -m_i^2$ where m_i is the mass of the meson in state i. However, the equation can be generalized to continuous momenta by changing Eq. 4.3 to

$$\begin{aligned} \lambda(P^2)\Gamma_M^{ab}(p;P) &= -\int^{\Lambda} \frac{d^4q}{(2\pi)^4}\frac{\mathcal{G}(k^2)}{k^2}T_{\mu\nu}(k)\frac{\lambda^c}{2}\gamma_\mu\, S^a(q+\eta P) \\ &\times \Gamma_M^{ab}(q;P)S^b(q-\beta P)\frac{\lambda^c}{2}\gamma_\nu. \end{aligned} \tag{4.4}$$

Figure 4.1: Ladder BSE Feynman Diagram.

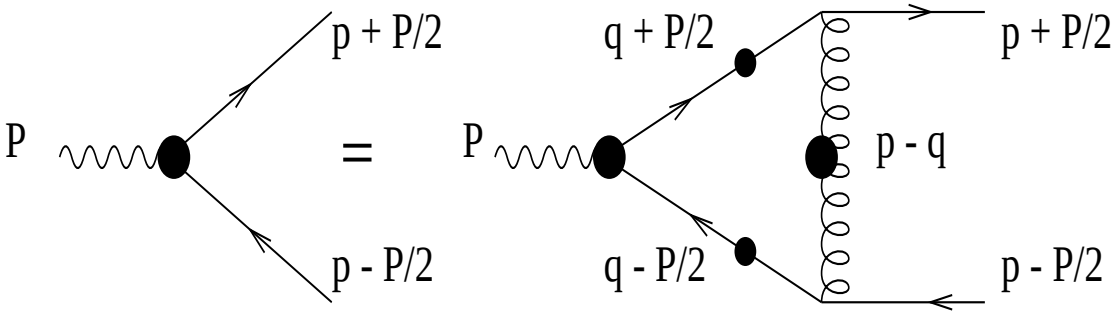

The discrete values of P^2 that produce $\lambda(P^2 = -m_i^2) = 1$ signify Bethe-Salpeter solutions with mass m_i [60]. The smallest value of m_i satisfying this is the ground state mass.

The general form of

$$\Gamma_M^{ab}(q;P) = \sum_{i=1}^{N} C_M^i(q;P) A^i(q;P) \tag{4.5}$$

is a sum over the different covariants, $C_M^i(q;P)$, times a Lorentz invariant amplitude, $A^i(q;P)$. The transformation properties of $\Gamma_M^{ab}(q;P)$ under C, P, and T are contained in $C_M^i(q;P)$ only. The label M on $\Gamma_M^{ab}(q;P)$ and $C_M^i(q;P)$ can be a meson label, Lorentz index, or both as discussed below Eq. 2.34. Since $A^i(q;P)$ is a Lorentz invariant and a function of q and P it can only be a function of q^2, P^2, and $q \cdot P$. The number of covariants is denoted by N and are different for different mesons. Mesons that transform as a scalar or pseudoscalar have four covariants and mesons that transform as a vector or axial-vector have twelve covariants [49].

The covariants with the proper transformations under C, P, and T are not unique because one covariant basis can be converted to another by a linear transformation. If an ortho-normal basis of covariants is chosen such that the trace over Dirac space is

$$Tr_D\left[C_M^i(q;P) C_M^j(q;P)\right] = \delta_{ij} \tag{4.6}$$

then Eq. 4.3 may be projected onto that basis to give a set of linear equations for the

invariant amplitude A^i,

$$\lambda(P^2)A^i(p;P) = -\sum_{j=1}^{N}\int^{\Lambda}\frac{d^4q}{(2\pi)^4}\frac{\mathcal{G}(k^2)}{k^2}T_{\mu\nu}(k)R^{ij}_{\mu\nu}(p,q;P)A^j(q;P), \tag{4.7}$$

where

$$R^{ij}_{\mu\nu}(p,q;P) = Tr_{DC}\left[C^i_M(p;P)\frac{\lambda^c}{2}\gamma_\mu S^a(q+\eta P)C^j_M(q;P)S^b(q-\beta P)\frac{\lambda^c}{2}\gamma_\nu\right] \tag{4.8}$$

and the original integral equation has now changed to a set of coupled, linear-integral equations. If the meson is a vector or axial-vector then $\Gamma^{ab}_M(q;P)$ and $C^i_M(q;P)$ carry a Lorentz index, which is summed over in Eqs. 4.6 and 4.8.

We solve Eq. 4.7 numerically in a manner similar to our DSE solution in Chapter 3. With

$$\int^{\Lambda} d^4q = \int_0^{\Lambda} q^3dq\int_0^{2\pi}d\phi\int_0^{\pi}\sin\theta d\theta\int_0^{\pi}\sin^2\beta d\beta \tag{4.9}$$

and

$$q = |q|\,(\cos\phi\sin\theta\sin\beta, \sin\phi\sin\theta\sin\beta, \cos\theta\sin\beta, \cos\beta) \tag{4.10}$$

we are free to choose P_μ to be in the 4th direction only and reduce all occurrences of $q\cdot P$ to $q\cdot P = |q|P_4\cos\beta$. Also, we are free to choose which plane p_μ is in to further simplify. We choose p_μ to be in the 3-4 plane. The ϕ integration in Eq. 4.9 can then be done analytically and Eq. 4.7 becomes

$$\begin{aligned}\lambda(P^2)A^i(p;P) &= -\frac{2\pi}{(2\pi)^4}\sum_{j=1}^{N}\int_0^{\Lambda}q^3dq\int_0^{\pi}\sin\theta d\theta\int_0^{\pi}\sin^2\beta\,d\beta \\ &\times \frac{\mathcal{G}(k^2)}{k^2}T_{\mu\nu}(k)R^{ij}_{\mu\nu}(p,q;P)A^j(q;P).\end{aligned} \tag{4.11}$$

In practice we make the substitutions $u=\cos\beta$ and $v=\cos\theta$ so that

$$\int_0^{\pi}\sin\theta d\theta = \int_{-1}^{1}dv \tag{4.12}$$

and

$$\int_0^{\pi}\sin^2\beta d\beta = \int_{-1}^{1}\sqrt{1-u^2}du \tag{4.13}$$

to obtain

$$\lambda(P^2)A^i(p;P) = -\frac{2\pi}{(2\pi)^4}\sum_{j=1}^{N}\int_0^{\Lambda} q^3 dq \int_{-1}^{1} dv \int_{-1}^{1}\sqrt{1-u^2}\,du \times \frac{\mathcal{G}(k^2)}{k^2}T_{\mu\nu}(k)R^{ij}_{\mu\nu}(p,q;P)A^j(q;P). \tag{4.14}$$

To deal with the angular dependence of the amplitudes $A^i(p;P)$ we could in principle solve the integral equation in terms of two continuous variables q and u, but instead we take the simpler approach of expanding the angular dependence of the amplitudes in Chebyshev polynomials of the second kind. With $p\cdot P = pPw$ the expansion of $A^i(p;P)$ is

$$A^i(p;P) = A^i(p^2,P^2,w) = \sum_{m=0}^{\infty} U_m(w)\tilde{A}^i_m(p^2,P^2) \tag{4.15}$$

where a similar equation holds for $q\cdot P = qPu$. Using the orthogonality condition of Chebyshev polynomials in Eq. B.1, Eq. 4.14 becomes

$$\lambda(P^2)\tilde{A}^i_m(p^2,P^2) = -\frac{2}{\pi}\frac{2\pi}{(2\pi)^4}\sum_{n=0}^{\infty}\sum_{j=1}^{N}\int_0^{\Lambda} q^3 dq \times \int_{-1}^{1}\sqrt{1-w^2}dw\int_{-1}^{1} dv\int_{-1}^{1}\sqrt{1-u^2}\,du \times \frac{\mathcal{G}(k^2)}{k^2}T_{\mu\nu}(k)U_m(w)R^{ij}_{\mu\nu}(p,q;P)U_n(u)\tilde{A}^j_n(q^2,P^2). \tag{4.16}$$

Finally, we make one last substitution

$$\int_0^{\Lambda} q^3 dq \to \frac{1}{2}\int_0^{\Lambda^2} q^2 d(q^2) \tag{4.17}$$

and we get

$$\lambda(P^2)\tilde{A}^i_m(p^2,P^2) = -\frac{1}{2}\frac{2}{\pi}\frac{2\pi}{(2\pi)^4}\sum_{n=0}^{\infty}\sum_{j=1}^{N}\int_0^{\Lambda^2} q^2 d(q^2) \times \int_{-1}^{1}\sqrt{1-w^2}dw\int_{-1}^{1} dv\int_{-1}^{1}\sqrt{1-u^2}\,du \times \frac{\mathcal{G}(k^2)}{k^2}T_{\mu\nu}(k)U_m(w)R^{ij}_{\mu\nu}(p,q;P)U_n(u)\tilde{A}^j_n(q^2,P^2). \tag{4.18}$$

which can be simplified to

$$\lambda(P^2)\tilde{A}^i_m(p^2,P^2) = \sum_{n=0}^{\infty}\sum_{j=1}^{N}\int_0^{\Lambda^2} d(q^2)B^{ij}_{mn}(p^2,q^2,P^2)\tilde{A}^j_n(q^2,P^2) \tag{4.19}$$

where

$$\begin{aligned} B^{ij}_{mn}(p^2,q^2,P^2) &= -q^2\frac{1}{2}\frac{2}{\pi}\frac{2\pi}{(2\pi)^4}\int_{-1}^{1}\sqrt{1-w^2}dw\int_{-1}^{1}dv\int_{-1}^{1}\sqrt{1-u^2}\,du \\ &\times \frac{\mathcal{G}(k^2)}{k^2}T_{\mu\nu}(k)U_m(w)R^{ij}_{\mu\nu}(p,q;P)U_n(u). \end{aligned} \tag{4.20}$$

Figure 4.2: Using $\lambda(P^2)$ to find solutions to Eq 4.7.

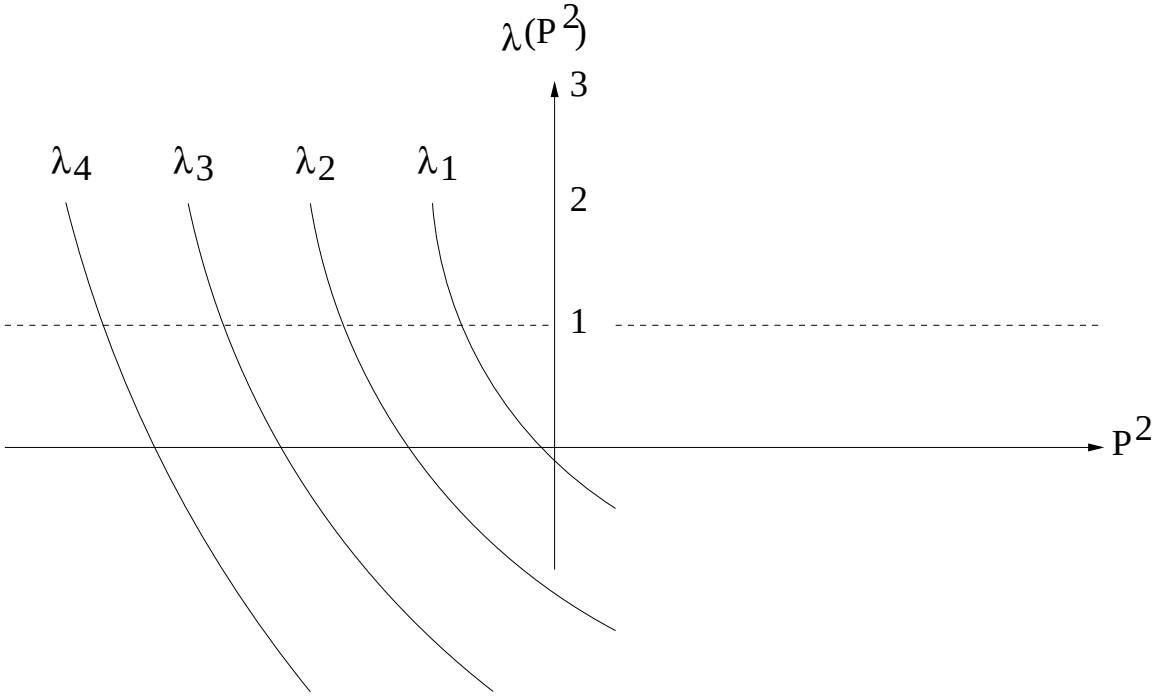

When the momentum integration is discretized for the computer and a finite number of Chebyshev polynomials are calculated, we then have a typical eigenvalue problem given by

$$\lambda(P^2)\tilde{A}^i_m(p^2_r,P^2) = \sum_{j=1}^{N}\sum_{n=0}^{N'}\sum_{s=1}^{N''}\triangle(q^2_s)B^{ij}_{mn}(p^2_r,q^2_s,P^2)\tilde{A}^j_n(q^2_s,P^2) \tag{4.21}$$

where $N'+1$ and N'' are the number of Chebyshev polynomials and number of quadrature points, respectively, and q^2_s and $\triangle(q^2_s)$ are the momentum quadrature points and weights,

respectively. In principle there are $N \cdot (N'+1) \cdot N''$ eigenvalues. In this work we only want the lowest $-P_i^2$ that satisfies Eq. 4.3. From Fig. 4.2 we see that we want to know the value of P^2 when the largest eigenvalue crosses $\lambda(P^2) = 1$. Since we want only the largest eigenvalue and its eigenfunction, we use the power method to obtain both [61].

4.2 Taylor Expansion of Quark Propagators

Because the quark propagators,

$$S(q_\pm) = -i\gamma \cdot q_\pm \sigma_v(q_\pm^2) + \sigma_s(q_\pm^2), \tag{4.22}$$

in $B_{mn}^{ij}(p_r^2, q_s^2, P^2)$ have the arguments $q_\pm^2 = (q \pm P/2)^2$ we need to know the value of $\sigma_s(q_\pm^2)$ and $\sigma_v(q_\pm^2)$ in the complex plane. To see this, write

$$q_\pm^2 = q^2 + \frac{1}{4}P^2 \pm q \cdot P \tag{4.23}$$

and

$$P^2 = -m^2 \tag{4.24}$$

then

$$q_\pm^2 = q^2 - \frac{1}{4}m^2 \pm iqmu \tag{4.25}$$

where the direction cosine, u, is defined by $q \cdot P = qPu$. For each u, Eq. 4.25 defines a parabola in the complex plane with vertex at $(-\frac{1}{4}m^2, 0)$. From Figure 4.3 we see that the greater the mass of the meson we want to calculate, the greater the area in the complex plane that we need to analytically continue the value of the quark propagators.

To calculate the quark propagators in the complex plane we will use the Momentum Expansion Method [27] of expanding σ_v and σ_s in a Taylor series around tabulated points along the positive real axis. If p_i^2 is the tabulated point closest to $\mathrm{Re}[q_\pm^2]$ then the vector and scalar parts of the quark propagator will be

$$\sigma_{s/v}(q_\pm^2) = \sigma_{s/v}^{(0)}|_{p_i^2} + \Delta\sigma_{s/v}^{(1)}|_{p_i^2} + \frac{1}{2}\Delta^2\sigma_{s/v}^{(2)}|_{p_i^2} + \cdots \tag{4.26}$$

Figure 4.3: Parabolic region of the complex plane needed by the Bethe-Salpeter equation for the argument of the quark propagators.

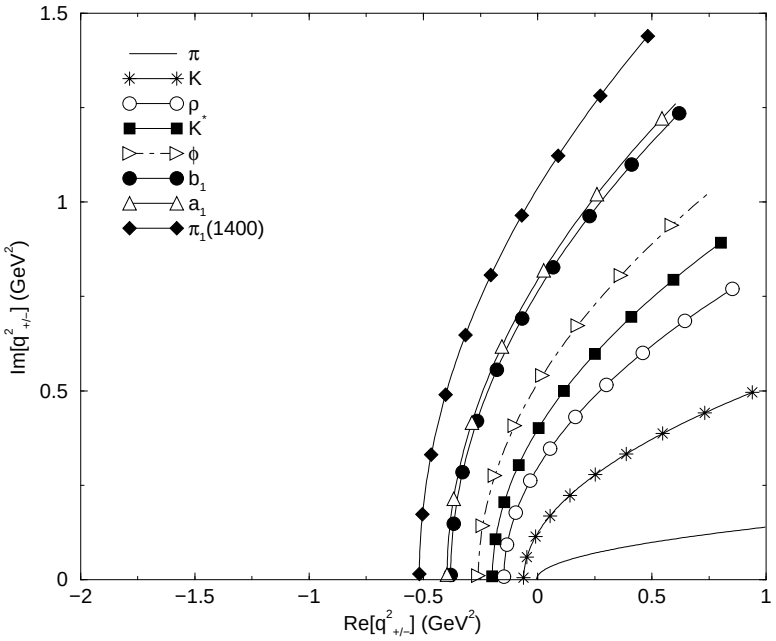

where $\Delta = q_{\pm}^2 - p_i^2$. Figures 4.4, 4.5, 4.6, and 4.7 show the scalar and vector parts for both the up and strange quark propagators with $\mathcal{F}(k^2)$ in Eq. 3.2 given by Eq. 3.51. All the graphs indicate a clear convergence to the exact model calculations.

The value of P^2 for which the quark propagator singularities enter into the domain of integration of the Bethe-Salpeter Equation can be calculated from Eq. 4.25 with $u = 1$. The masses 1092 MeV and 1474 MeV are, respectively, the values of P^2 for which the up and strange quark singularities at an (r, θ) of (0.39 GeV^2,122°) and (0.71 GeV^2,122°) enter into the domain of integration and above which the Momentum Expansion Method becomes a mathematically invalid approximation to the quark propagators.

Figure 4.4: Comparisons of the exact model calculations with the first through third orders of the Taylor expansions of the scalar part of the up quark propagator.

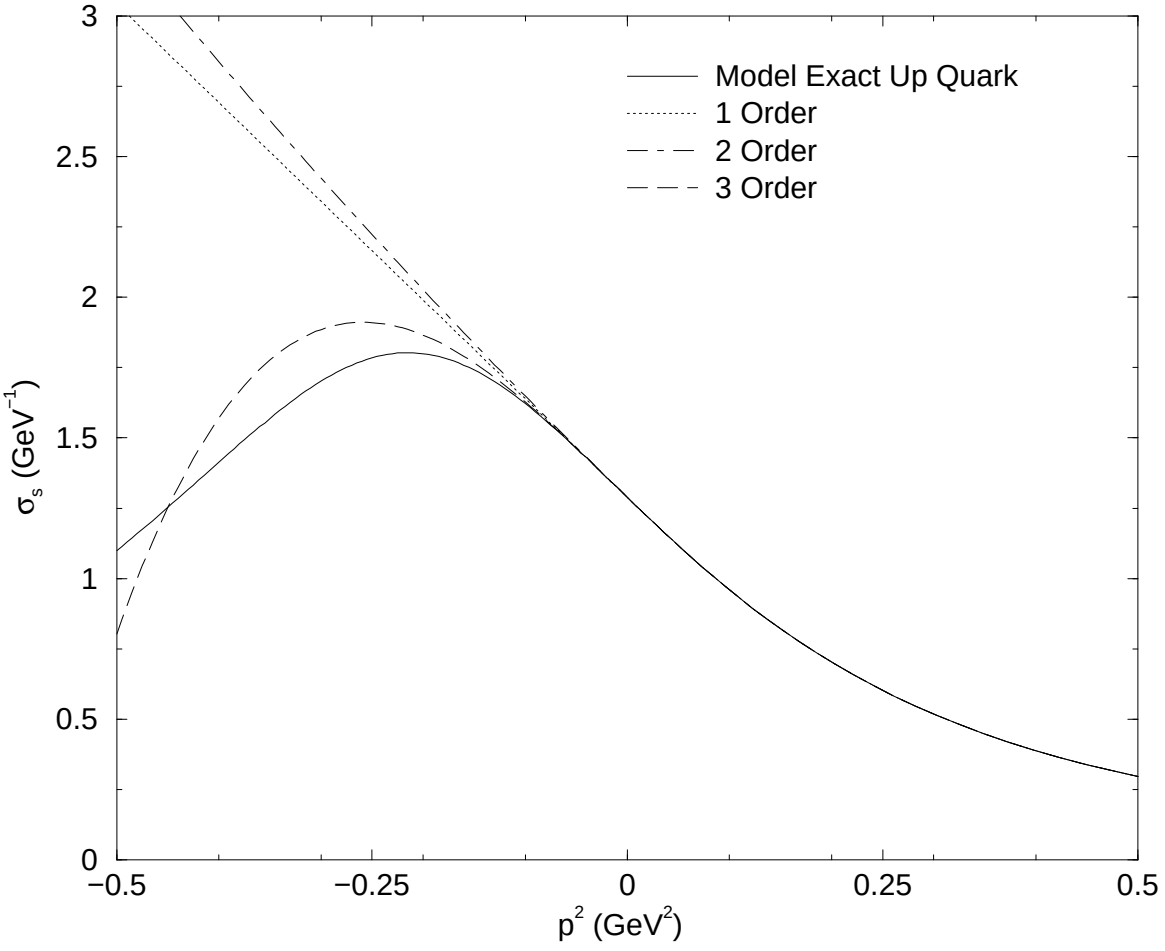

Figure 4.5: Comparisons of the exact model calculations with the first through third orders of the Taylor expansions of the vector part of the up quark propagator.

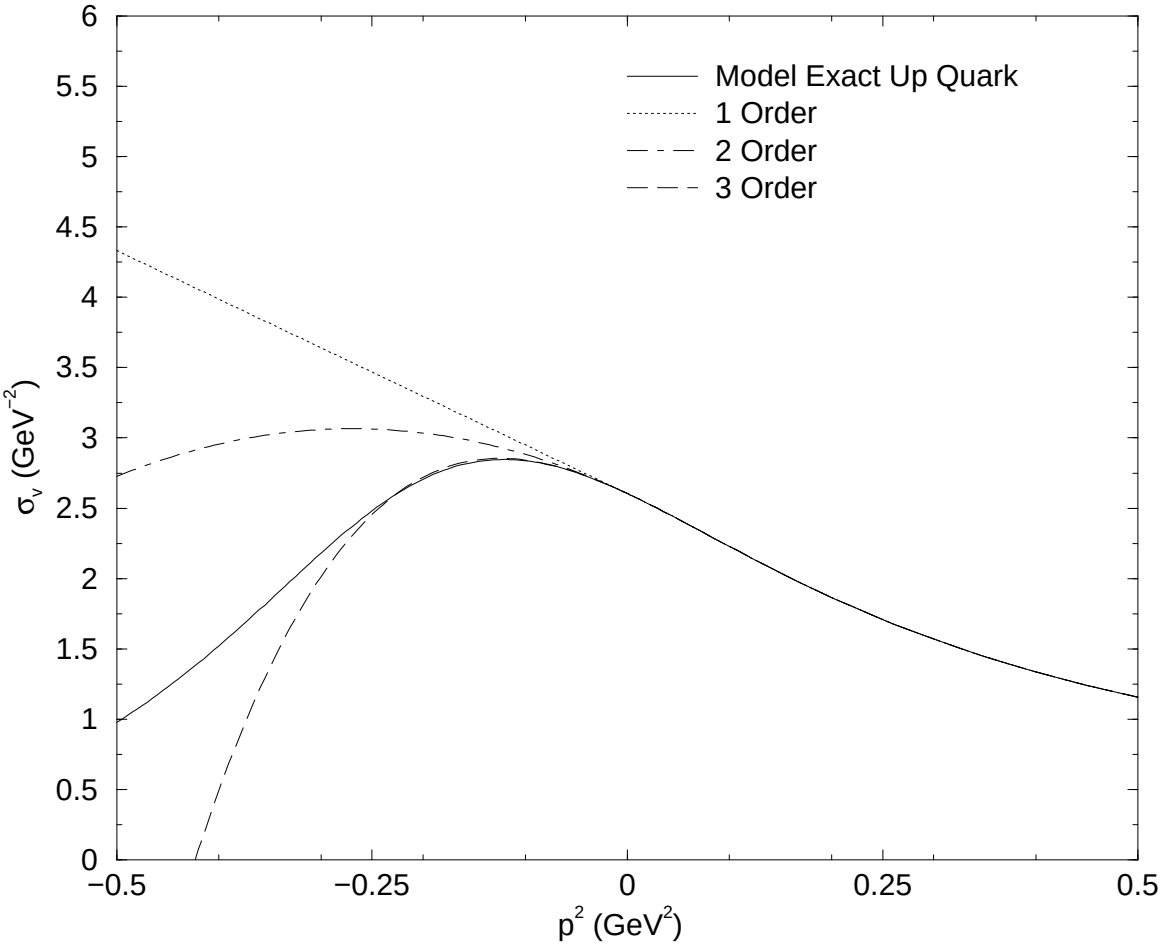

Figure 4.6: Comparisons of the exact model calculations with the first through third orders of the Taylor expansions of the scalar part of the strange quark propagator.

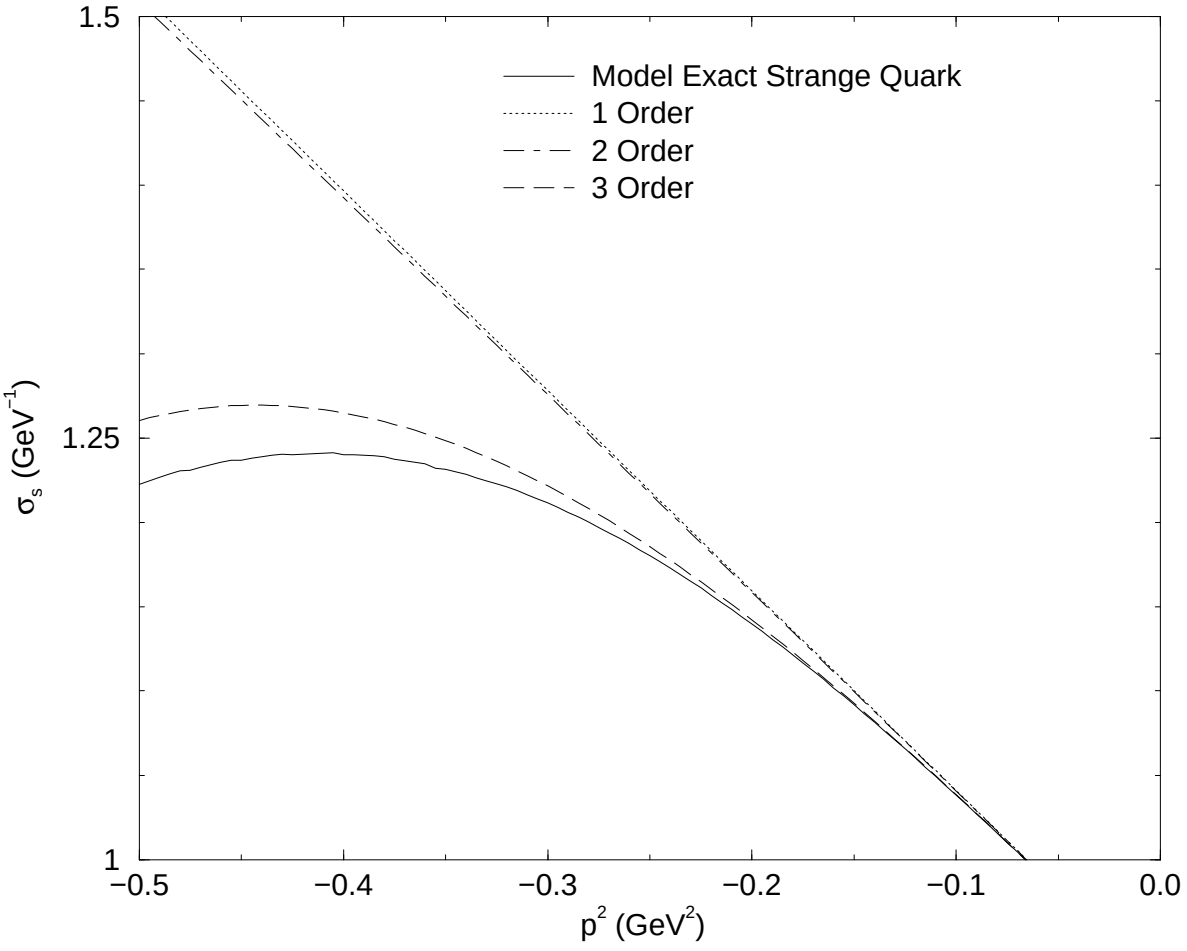

Figure 4.7: Comparisons of the exact model calculations with the first through third orders of the Taylor expansions of the vector part of the strange quark propagator.

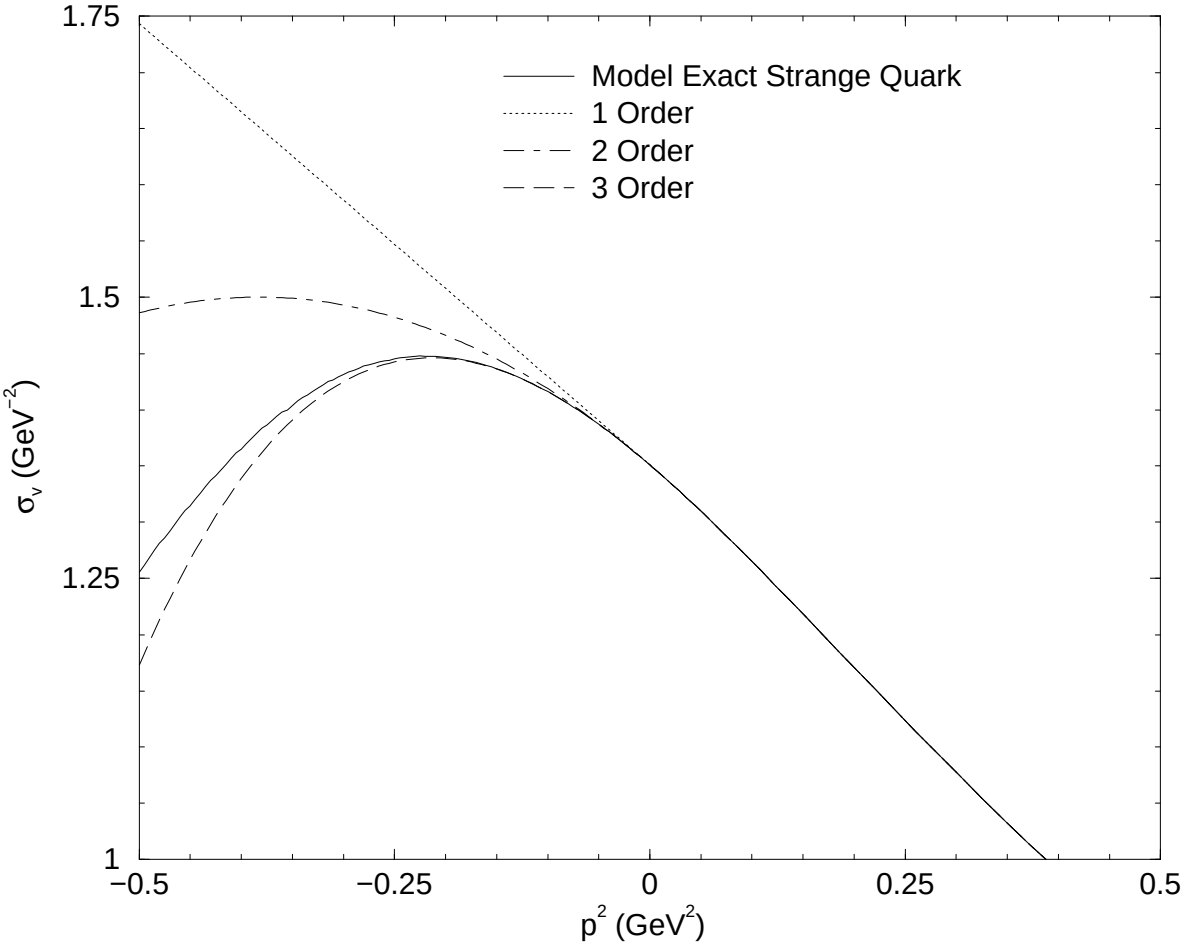

4.3 Pseudoscalar Mesons

The BSA for pseudoscalar mesons with $J^{PC} = 0^{-+}$ has the general form,

$$\begin{aligned}\Gamma^{uu}(q;P) &= i\gamma_5\, E_\pi(q;P) + \gamma_5\gamma\cdot P\, F_\pi(q;P) \\ &+ \gamma_5\gamma\cdot q\, q\cdot P\, G_\pi(q;P) + \gamma_5 q_\alpha\sigma_{\alpha\beta}P_\beta\, H_\pi(q;P),\end{aligned} \tag{4.27}$$

where q is the relative $q\bar{q}$ momentum and P is the four-momentum of the meson. Since the π^0 is a $C = +1$ charge eigenstate that obeys $C\,|\pi^0> = +|\pi^0>$, the BSA obeys

$$\bar{\Gamma}^{uu}(q;P) = +\Gamma^{uu}(q;P). \tag{4.28}$$

Table 4.1 lists the amplitudes for the anti-meson BSA defined by

$$\bar{\Gamma}^{du}(q;P) = [C^{-1}\Gamma^{ud}(-q;P)C]^T \tag{4.29}$$

by using the identities in Appendix A.4. Furthermore, because we work in the $m_u = m_d$ isospin limit, the $\pi^\pm$ mesons will have the same mass as the π^0 meson and thus have the same invariant amplitudes.

Table 4.1: Pseudoscalar Bethe-Salpeter amplitude with $J^{PC} = 0^{-+}$

$\Gamma^{ud}(q;P)$	$\bar{\Gamma}^{du}(q;P)$
$i\gamma_5\, E_\pi(q\cdot P)$	$i\gamma_5\, E_\pi(-q\cdot P)$
$\gamma_5\gamma\cdot P\, F_\pi(q\cdot P)$	$\gamma_5\gamma\cdot P\, F_\pi(-q\cdot P)$
$\gamma_5\gamma\cdot q\, q\cdot P\, G_\pi(q\cdot P)$	$\gamma_5\gamma\cdot q\, q\cdot P\, G_\pi(-q\cdot P)$
$\gamma_5 q_\alpha\sigma_{\alpha\beta}P_\beta\, H_\pi(q\cdot P)$	$\gamma_5 q_\alpha\sigma_{\alpha\beta}P_\beta\, H_\pi(-q\cdot P)$

The general method used to solve the BSE given at the beginning of this chapter needs to be modified in only two ways. First, the amplitudes do not need to be expanded over both even and odd Chebyshev polynomials. With our choice of pseudoscalar covariants, Eq. 4.28 requires the amplitudes E_π, F_π, G_π, and H_π to be even functions of $q\cdot P$ if and only if $\eta = \beta = 1/2$ in Eq. 4.1. We choose the convention $\eta = \beta = 1/2$ for all meson

calculations in this dissertation. Since E_π, F_π, G_π, and H_π are functions of $(q \cdot P)^2$, the coefficients of the odd Chebyshev polynomials are guaranteed to be zero.

Second, the covariants in Eq. 4.27 are not orthogonal to one another. This may be seen by forming the trace of each covariant with $\Gamma^{ud}(p;P)$:

$$Tr_D\left\{i\gamma_5\,\Gamma^{ud}(p;P)\right\} = -4E_\pi(p;P), \tag{4.30}$$

$$Tr_D\left\{\gamma_5\gamma\cdot P\,\Gamma^{ud}(p;P)\right\} = -4P^2F_\pi(p;P) - 4(p\cdot P)^2G_\pi(p;P), \tag{4.31}$$

$$Tr_D\left\{\gamma_5\gamma\cdot p\,p\cdot P\,\Gamma^{ud}(p;P)\right\} = -4(p\cdot P)^2\,F_\pi(p;P) \tag{4.32}$$

$$-4p^2(p\cdot P)^2\,G_\pi(p;P), \tag{4.33}$$

and

$$Tr_D\left\{\gamma_5 p_\alpha\sigma_{\alpha\beta}P_\beta\,\Gamma^{ud}(p;P)\right\} = 4N(p,P)^2\,H_\pi(p;P) \tag{4.34}$$

where

$$N(p,P)^2 = p^2P^2 - (p\cdot P)^2. \tag{4.35}$$

The first and fourth covariants are orthogonal to every other covariant, but covariants two and three are not orthogonal to each other. Eqs. 4.31 and 4.32 can be written in the matrix form,

$$\left\{\begin{array}{c} T_2 \\ T_3 \end{array}\right\} = \left\{\begin{array}{cc} -4P^2 & -4(p\cdot P)^2 \\ -4(p\cdot P)^2 & -4p^2(p\cdot P)^2 \end{array}\right\}\left\{\begin{array}{c} F_\pi(p;P) \\ G_\pi(p;P) \end{array}\right\}, \tag{4.36}$$

where T_2 and T_3 are the projections of Γ onto the second and third covariants. Eq. 4.36 is inverted by taking the transpose of the cofactor matrix and dividing by the determinant to obtain

$$\left\{\begin{array}{c} F_\pi(p;P) \\ G_\pi(p;P) \end{array}\right\} = \left\{\begin{array}{cc} -p^2/4N(p,P)^2 & 1/4N(p,P)^2 \\ 1/4N(p,P)^2 & -P^2/4(p\cdot P)^2N(p,P)^2 \end{array}\right\}\left\{\begin{array}{c} T_2 \\ T_3 \end{array}\right\}. \tag{4.37}$$

Eq. 4.37 shows what mixture of the projections T_2 and T_3 is needed to produce linear integral equations in standard form for the amplitudes F_π and G_π. Using Eqs. 4.3 and

4.37, $F_\pi(p;P)$ is found to be

$$
\begin{aligned}
(4.38) \qquad F_\pi(p;P) &= \frac{p^2}{4N(p,P)^2}\frac{4}{3}\int^{\Lambda}\frac{d^4q}{(2\pi)^4}\frac{\mathcal{G}(k^2)}{k^2}T_{\mu\nu}(k) \\
&\times \; Tr_D\left\{\gamma_5\gamma\cdot P\,\gamma_\mu\,S^u(q+\eta P)\Gamma^{ud}_M(q;P)S^d(q-\beta P)\gamma_\nu\right\} \\
&- \frac{1}{4N(p,P)^2}\frac{4}{3}\int^{\Lambda}\frac{d^4q}{(2\pi)^4}\frac{\mathcal{G}(k^2)}{k^2}T_{\mu\nu}(k) \\
&\times \; Tr_D\left\{\gamma_5\gamma\cdot p\,p\cdot P\,\gamma_\mu\,S^u(q+\eta P)\Gamma^{ud}_M(q;P)S^d(q-\beta P)\gamma_\nu\right\}
\end{aligned}
$$

and $G_\pi(p;P)$ is

$$
\begin{aligned}
(4.39) \qquad G_\pi(p;P) &= -\frac{1}{4N(p,P)^2}\frac{4}{3}\int^{\Lambda}\frac{d^4q}{(2\pi)^4}\frac{\mathcal{G}(k^2)}{k^2}T_{\mu\nu}(k) \\
&\times \; Tr_D\left\{\gamma_5\gamma\cdot P\,\gamma_\mu\,S^u(q+\eta P)\Gamma^{ud}_M(q;P)S^d(q-\beta P)\gamma_\nu\right\} \\
&+ \frac{P^2}{4(p\cdot P)^2N(p,P)^2}\frac{4}{3}\int^{\Lambda}\frac{d^4q}{(2\pi)^4}\frac{\mathcal{G}(k^2)}{k^2}T_{\mu\nu}(k) \\
&\times \; Tr_D\left\{\gamma_5\gamma\cdot p\,p\cdot P\,\gamma_\mu\,S^u(q+\eta P)\Gamma^{ud}_M(q;P)S^d(q-\beta P)\gamma_\nu\right\}.
\end{aligned}
$$

Finally, using Eqs. 4.3, 4.30, and 4.34

$$
\begin{aligned}
(4.40) \qquad E_\pi(p;P) &= \frac{1}{4}\frac{4}{3}\int^{\Lambda}\frac{d^4q}{(2\pi)^4}\frac{\mathcal{G}(k^2)}{k^2}T_{\mu\nu}(k) \\
&\times \; Tr_D\left\{i\gamma_5\,\gamma_\mu\,S^u(q+\eta P)\Gamma^{ud}_M(q;P)S^d(q-\beta P)\gamma_\nu\right\}
\end{aligned}
$$

and

$$
\begin{aligned}
(4.41) \qquad H_\pi(p;P) &= -\frac{1}{4N(p,P)^2}\frac{4}{3}\int^{\Lambda}\frac{d^4q}{(2\pi)^4}\frac{\mathcal{G}(k^2)}{k^2}T_{\mu\nu}(k) \\
&\times \; Tr_D\left\{\gamma_5 p_\alpha\sigma_{\alpha\beta}P_\beta\,\gamma_\mu\,S^u(q+\eta P)\Gamma^{ud}_M(q;P)S^d(q-\beta P)\gamma_\nu\right\}.
\end{aligned}
$$

Eqs. 4.40, 4.38, 4.39, and 4.41 are solved iteratively with the power method.

The general form of the BSA for pseudoscalar mesons that are not charge eigenstates, such as the kaon, is

$$
\begin{aligned}
(4.42) \qquad \Gamma^{us}(q;P) &= i\gamma_5\,E_K(q;P) + \gamma_5\gamma\cdot P\,F_K(q;P) \\
&+ \gamma_5\gamma\cdot q\,G_K(q;P) + \gamma_5 q_\alpha\sigma_{\alpha\beta}P_\beta\,H_K(q;P).
\end{aligned}
$$

The main difference between the kaon BSA and the pion BSA is the absence of $q \cdot P$ in the third covariant. Because of the difference between the s-quark and the d-quark propagators, $\Gamma^{us}(q;P)$ and $\bar{\Gamma}^{su}(q;P)$ are not related as $\Gamma^{ud}(q;P)$ and $\bar{\Gamma}^{ud}(q;P)$ are in Eq. 4.28.

Expressions for the kaon BSE are obtained from the corresponding pion BSE with the substitutions $\Gamma^{ud} \to \Gamma^{us}$, $S^d \to S^s$, and $q \cdot P\, G_\pi(q;P) \to G_K(q;P)$. Due to $S^d \neq S^s$ the amplitudes E_K, F_K, G_K, and H_K will have both even and odd Chebyshev moments. In the limit as $S^s \to S^d$, $m_K \to m_\pi$ and the odd Chebyshev moments in E_K, F_K, and H_K will decrease and vanish. For G_K the even moment will vanish and $G_K \to q \cdot P G_\pi$.

As with the pion there is some overlap between the second and third covariants of the kaon. With

$$T_2 = Tr_D\left\{\gamma_5 \gamma \cdot P\, \Gamma^{us}(p;P)\right\} = -4P^2\, F_K(p;P) - 4p \cdot P\, G_K(p;P) \tag{4.43}$$

and

$$\begin{aligned} T_3 &= Tr_D\left\{\gamma_5 \gamma \cdot p\, \Gamma^{us}(p;P)\right\} \\ &= -4p \cdot P\, F_K(p;P) - 4p^2\, G_K(p;P) \end{aligned} \tag{4.44}$$

we again have a matrix equation

$$\left\{ \begin{array}{c} T_2 \\ T_3 \end{array} \right\} = \left\{ \begin{array}{cc} -4P^2 & -4p \cdot P \\ -4p \cdot P & -4p^2 \end{array} \right\} \left\{ \begin{array}{c} F_K(p;P) \\ G_K(p;P) \end{array} \right\}, \tag{4.45}$$

which can be inverted to give

$$\left\{ \begin{array}{c} F_K(p;P) \\ G_K(p;P) \end{array} \right\} = \left\{ \begin{array}{cc} -p^2/4N(p,P)^2 & p \cdot P/4N(p,P)^2 \\ p \cdot P/4N(p,P)^2 & -P^2/4N(p,P)^2 \end{array} \right\} \left\{ \begin{array}{c} T_2 \\ T_3 \end{array} \right\}. \tag{4.46}$$

Now F and G for the kaon are

$$\begin{aligned} F_K(p;P) &= \frac{p^2}{4N(p,P)^2} \frac{4}{3} \int^{\Lambda} \frac{d^4q}{(2\pi)^4} \frac{\mathcal{G}(k^2)}{k^2} T_{\mu\nu}(k) \\ &\times\ Tr_D\left\{\gamma_5 \gamma \cdot P\, \gamma_\mu\, S^u(q+\eta P) \Gamma^{us}_M(q;P) S^s(q-\beta P) \gamma_\nu\right\} \end{aligned} \tag{4.47}$$

$$
\begin{aligned}
&- \quad \frac{p\cdot P}{4N(p,P)^2}\frac{4}{3}\int^{\Lambda}\frac{d^4q}{(2\pi)^4}\frac{\mathcal{G}(k^2)}{k^2}T_{\mu\nu}(k) \\
&\times \quad Tr_D\left\{\gamma_5\gamma\cdot p\,\gamma_\mu\, S^u(q+\eta P)\Gamma^{us}_M(q;P)S^s(q-\beta P)\gamma_\nu\right\}
\end{aligned}
$$

and

$$
\begin{aligned}
G_K(p;P) \quad &= \quad -\frac{p\cdot P}{4N(p,P)^2}\frac{4}{3}\int^{\Lambda}\frac{d^4q}{(2\pi)^4}\frac{\mathcal{G}(k^2)}{k^2}T_{\mu\nu}(k) \\
&\times \quad Tr_D\left\{\gamma_5\gamma\cdot P\,\gamma_\mu\, S^u(q+\eta P)\Gamma^{us}_M(q;P)S^s(q-\beta P)\gamma_\nu\right\} \\
&+ \quad \frac{P^2}{4N(p,P)^2}\frac{4}{3}\int^{\Lambda}\frac{d^4q}{(2\pi)^4}\frac{\mathcal{G}(k^2)}{k^2}T_{\mu\nu}(k) \\
&\times \quad Tr_D\left\{\gamma_5\gamma\cdot p\,\gamma_\mu\, S^u(q+\eta P)\Gamma^{us}_M(q;P)S^s(q-\beta P)\gamma_\nu\right\}.
\end{aligned} \tag{4.48}
$$

In the Ladder Approximation the $q\bar{q}$ scattering kernel, Eq. 4.2, is independent of the center-of-mass momentum, P_μ, reducing the Bethe-Salpeter normalization condition, Eq. 2.37, to

$$
\begin{aligned}
2P_\mu \quad &= \quad \frac{\partial}{\partial P_\mu}\left\{\int^{\Lambda}\frac{d^4q}{(2\pi)^4}Tr_{CD}\Big[\bar{\Gamma}^{ba}_M(q;-K)\right. \\
&\times \quad \left. S^a(q+\eta P)\Gamma^{ab}_M(q;K)S^b(q-\beta P)\Big]\right\}\Bigg|_{P^2=K^2=-m^2}.
\end{aligned} \tag{4.49}
$$

With

$$
\frac{\partial}{\partial P_\mu} = 2P_\mu\frac{\partial}{\partial P^2} \tag{4.50}
$$

Eq. 4.49 becomes

$$
\begin{aligned}
1 \quad &= \quad \frac{\partial}{\partial P^2}\left\{\int^{\Lambda}\frac{d^4q}{(2\pi)^4}Tr_{CD}\Big[\bar{\Gamma}^{ba}_M(q;-K)\right. \\
&\times \quad \left. S^a(q+\eta P)\Gamma^{ab}_M(q;K)S^b(q-\beta P)\Big]\right\}\Bigg|_{P^2=K^2=-m^2}.
\end{aligned} \tag{4.51}
$$

The Bethe-Salpeter normalization condition simplifies to a quark loop in the ladder approximation. See Figure 4.8. For multiflavor mesons like the π°, Eq. 4.51 needs to be modified by including a trace over flavor space:

$$
Tr_{CDF}\left[\begin{Bmatrix} \Gamma^{uu}(q;-K)/\sqrt{2} & 0 \\ 0 & -\Gamma^{dd}(q;-K)/\sqrt{2} \end{Bmatrix}\begin{Bmatrix} S^u(q+\eta P) & 0 \\ 0 & S^d(q+\eta P) \end{Bmatrix}\right. \tag{4.52}
$$

$$\times \left\{ \begin{array}{cc} \Gamma^{uu}(q;K)/\sqrt{2} & 0 \\ 0 & -\Gamma^{dd}(q;K)/\sqrt{2} \end{array} \right\} \left\{ \begin{array}{cc} S^u(q-\beta P) & 0 \\ 0 & S^d(q-\beta P) \end{array} \right\} \Big] .$$

Since we are dealing with the $m_u = m_d$ isospin limit, the normalization for π° will be equivalent to that for π^+ and π^-, up to a factor of $\sqrt{2}$.

Figure 4.8: Ladder Bethe-Salpeter Amplitude Normalization.

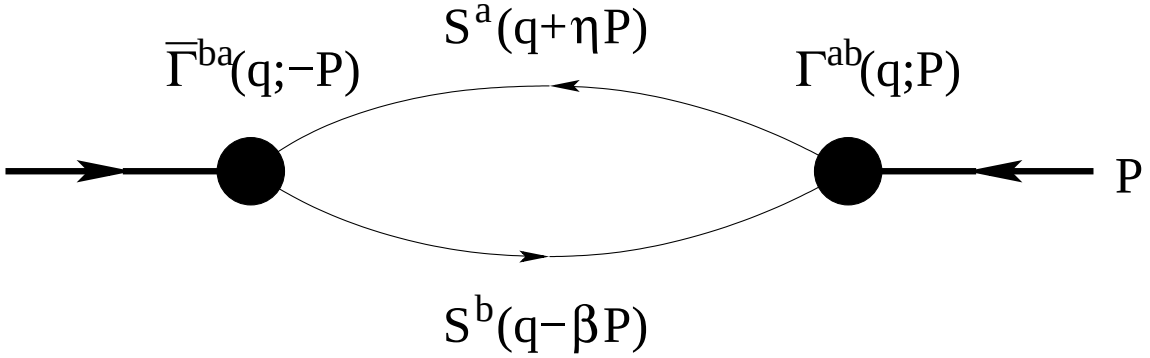

The normalization condition, Eq. 4.51, must be imposed by rescaling the Bethe-Salpeter amplitude. If the Pseudoscalar eigenstates are found to give

$$(4.53) \qquad \begin{aligned} N^2 &= \frac{\partial}{\partial P^2}\Big\{ \int^{\Lambda} \frac{d^4q}{(2\pi)^4} Tr_{CD}\Big[\bar{\Gamma}^{ba}_M(q;-K) \\ &\times S^a(q+\eta P)\Gamma^{ab}_M(q;K)S^b(q-\beta P)\Big]\Big\}\Big|_{P^2=K^2=-m^2} , \end{aligned}$$

then division of Γ by N will insure that the numerical solution to the pseudoscalar Bethe-Salpeter amplitude describes exactly one meson coupling to quarks a and b.

Since our mesons are made up of $q\bar{q}$ bound states, they can decay into a lepton pair via the electroweak interaction. For example, the decay $\pi^- \to \mu^+ + \nu_\mu$ is characterized by the pion decay constant given by [25]

$$(4.54) \qquad f_\pi = -\frac{Z_2 N_C}{m_\pi^2} \int^{\Lambda} \frac{d^4q}{(2\pi)^4} P_\mu Tr_D \left\{ \Gamma^{du}(q;P) S^u(q_-)\gamma_\mu\gamma_5 S^d(q_+) \right\} .$$

The BSA, $\Gamma^{du}(q;P)$, must be normalized according to Eq. 4.51.

In the following section we refer to a four-covariant pion and a one-covariant pion. A four-covariant pion refers to a pion Bethe-Salpeter amplitude with all four of the covariants

given in Eq. 4.27 and a one-covariant pion refers to a pion Bethe-Salpeter amplitude with only the canonical γ_5 term given in Eq. 4.27. Similar language will be used in the following sections when we deal with the vector mesons and their strong decays. In general, a full-covariant meson will refer to a meson being modeled with a Bethe-Salpeter amplitude that contains all possible covariants with the quantum numbers of the meson. A one-covariant or canonical-covariant meson will refer to a meson modeled with a Bethe-Salpeter amplitude that contains only the single gamma matrix with the quantum number of that particular meson. For the pion and kaon this is the γ_5 term and for vector mesons this will be the γ_μ^T term given in Eq. 4.60.

Table 4.2: The π and K masses and decay constants obtained from the Taylor expansion method. We include results for both the full covariant solution and for the dominant γ_5 solution.

	m_π	f_π	m_K	f_K
1^{st} order Taylor				
All 4 ampls	0.117	0.111	0.420	0.134
γ_5 ampl only	0.106	0.086	0.382	0.103
2^{nd} order Taylor				
All 4 ampls	0.138	0.131	0.497	0.157
γ_5 ampl only	0.121	0.098	0.437	0.116
3^{rd} order Taylor				
All 4 ampls	0.138	0.131	0.495	0.154
γ_5 ampl only	0.121	0.098	0.436	0.114
Model exact [1]	0.138	0.131	0.497	0.155
Experiment (GeV)	0.1385	0.131	0.496	0.160

Table 4.2 shows the results for the pion and kaon at different orders in the Taylor expansion. For the four-covariant pion, the masses and electroweak decay constants for all orders in the Taylor expansion are converged to within 1%. At all orders in the Taylor expansion the four-covariant pion requires only the first Chebyshev moment for convergence. At first order in the Taylor expansion, the pion mass and decay constant are within 16% of the experimental values and within 1% for both second and third orders. For the one-covariant

pion with only the canonical covariant γ_5, the mass is converged to within 1% and the electroweak decay constant to within 2.8%, 6.2%, and 1% for the first order, second order, and third order taylor expanded results, respectively. Again only one Chebyshev moment is needed for convergence of the pion mass and decay constant at all orders in the Taylor expansion. At first order, the pion mass is within 24% and the decay constant is within 34% of the experimental results. At second and third orders, the mass is within 13% and the decay constant within 25% of the experimental values.

The kaon requires at least three Chebyshev moments at all orders in the Taylor expansion. For the four-covariant kaon, the mass and decay constant is converged to within 1% for all orders in the Taylor expansion. At second order, the mass is within 0.497 GeV - 0.498 GeV and the decay constant is within 0.157 GeV -0.158 GeV. At first order, the mass is within 15% and the decay constant to within 16% of their experimental values, respectively. At second order in the Taylor expansion, we see convergence but not as strongly as we do for the pion. This is due to the larger region of the complex plane needed by the kaon BSE as well as the kaon being made up of both up and strange quark propagators whose complex plane contributions to the kaon Bethe-Salpeter amplitude do not cancel to the amount that they do for charge conjugation eigenstates that are made up of only up or strange quark propagators. The mass is within 1% of the experimental result for both second and third orders. The decay constant is within 2% and 4% of the experimental value for the second and third order Taylor expansions, respectively. While the model exact decay constant is 3.13% lower than the experimental value, the second and third order results are within 1.3% and 1% of the model exact results. The mass and decay constant for the one-covariant kaon is good to within 1% for all orders and Chebyshev moments. At second order in the Taylor expansion, the decay constant is between 0.115 GeV and 0.116 GeV. The mass is within 23% of the experimental value for first order and within 12% for

second and third orders. The decay constant is within 36% for first order and within 29% for second and third orders when compared to the experimental value. Finally, the kaon decay constant is within 34% for first order and within 27% for the second and third order when compared to the model exact kaon decay constant.

Figures 4.9, 4.10, 4.11, and 4.12 show the projection of the 0 Chebyshev moment of the pion and kaon amplitudes, respectively. The amplitudes graphed are obtained by rescaling the covariants and amplitudes such that they are both dimensionless. For example,

$$\gamma_5 q_\alpha \sigma_{\alpha\beta} P_\beta H_\pi(q;P) \to \frac{\gamma_5 q_\alpha \sigma_{\alpha\beta} P_\beta}{m_\pi \sqrt{q^2}} \cdot m_\pi \sqrt{q^2} H_\pi(q;P) \tag{4.55}$$

and $m_\pi \sqrt{q^2} H_\pi(q;P)$ is the amplitude graphed. Figures 4.9, 4.10, 4.11, and 4.12 show that the canonical covariant, γ_5, dominates the π and K Bethe-Salpeter amplitudes while $\gamma_5 \gamma \cdot P$ is the next dominant covariant.

Figure 4.9: Pion Bethe-Salpeter Amplitudes.

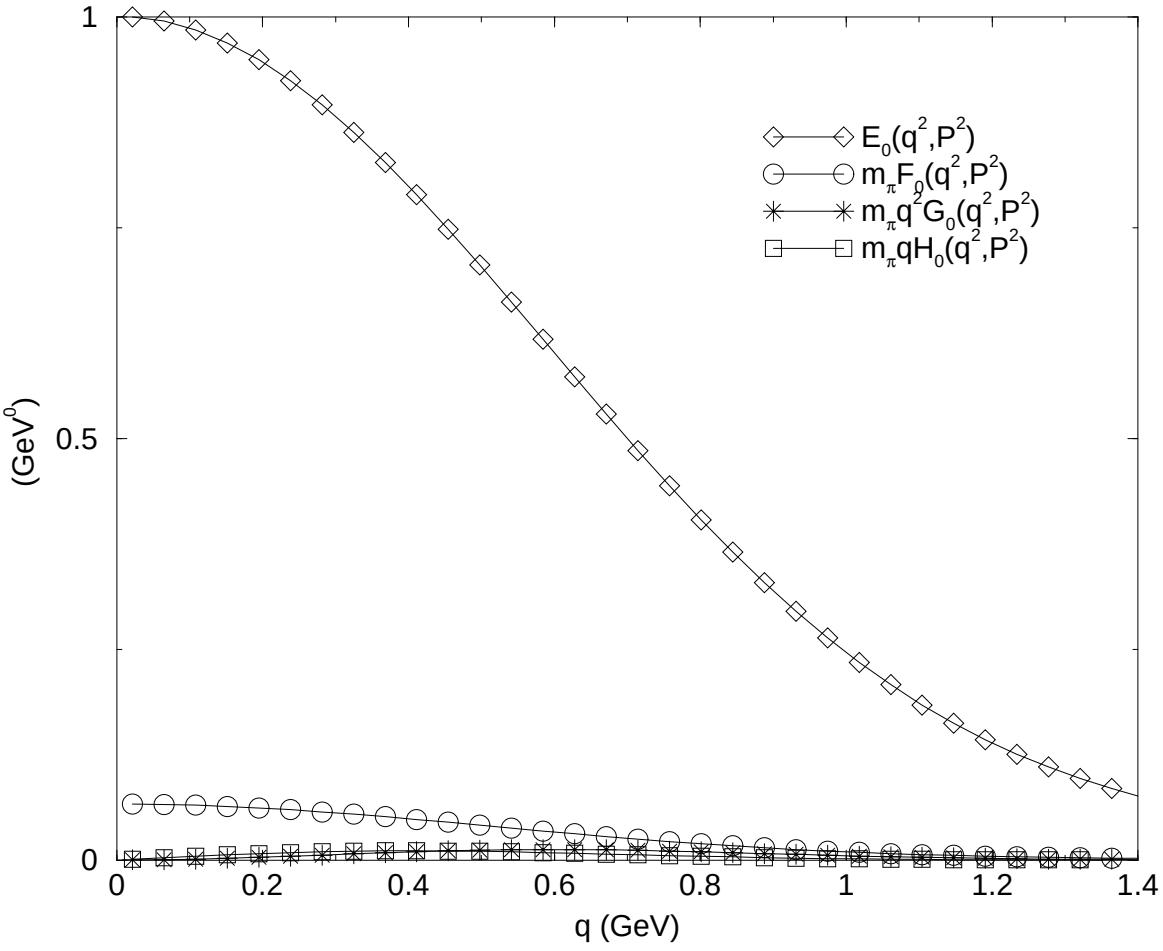

Figure 4.10: A magnified view of Pion amplitudes F, G, and H from Figure 4.9.

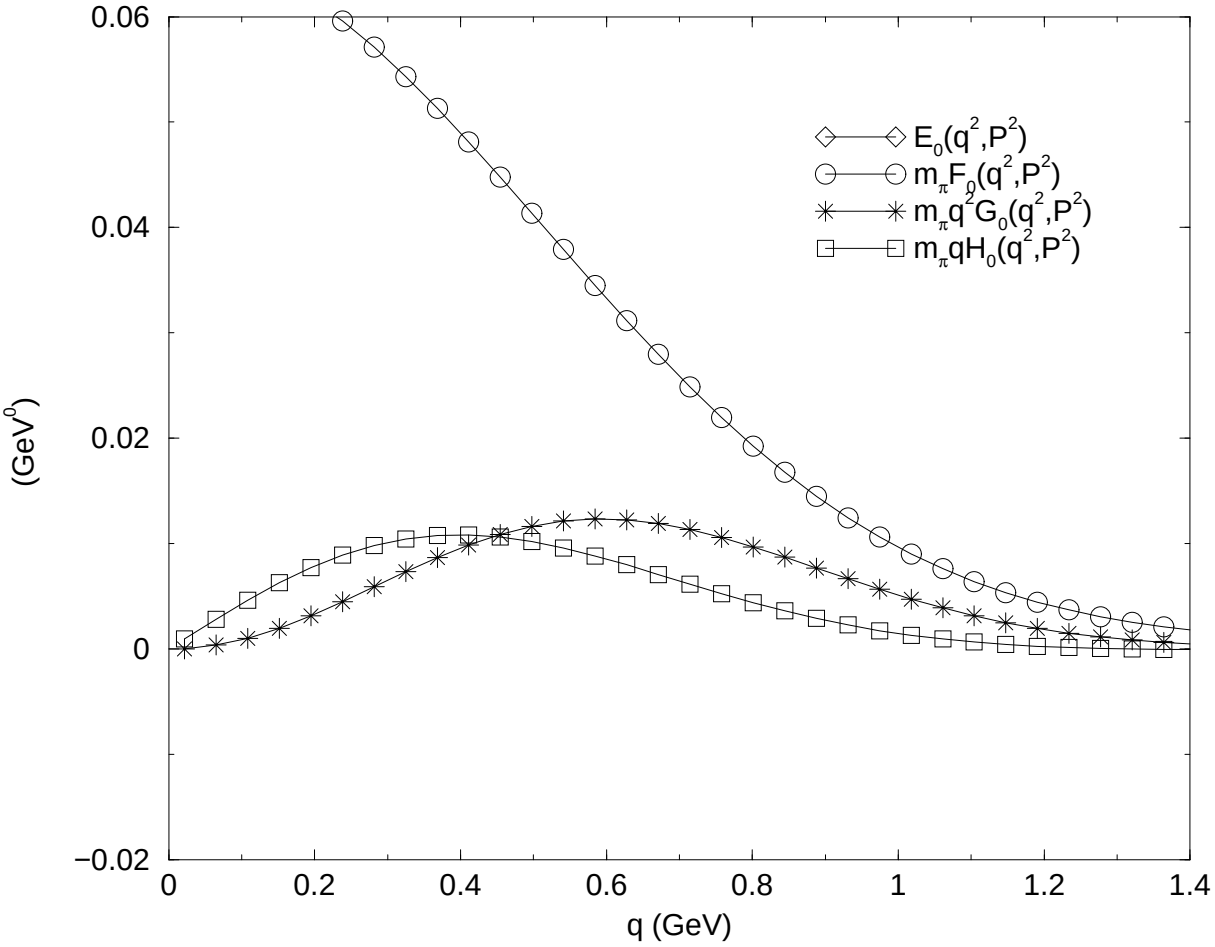

Figure 4.11: Kaon Bethe-Salpeter Amplitudes.

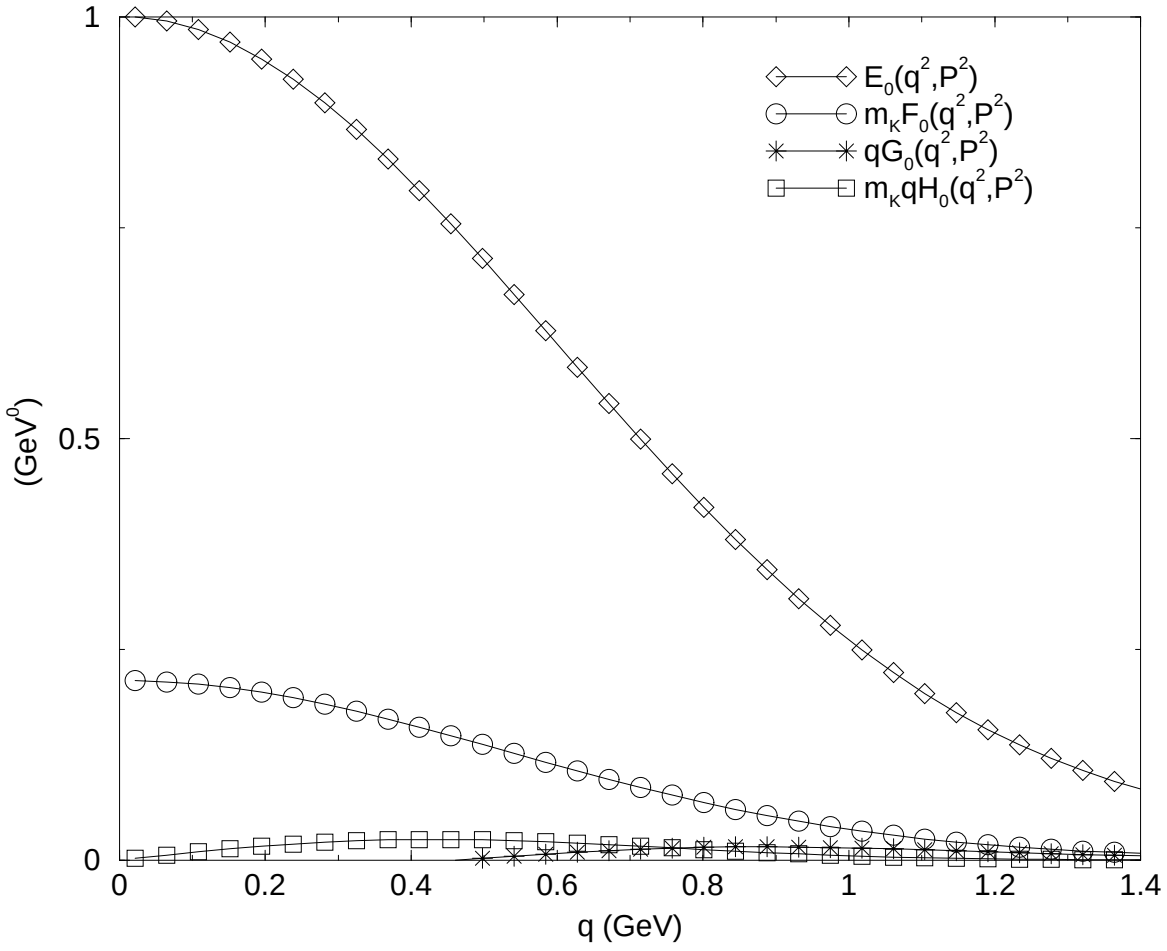

Figure 4.12: A magnified view of Kaon amplitudes F, G, and H from Figure 4.11.

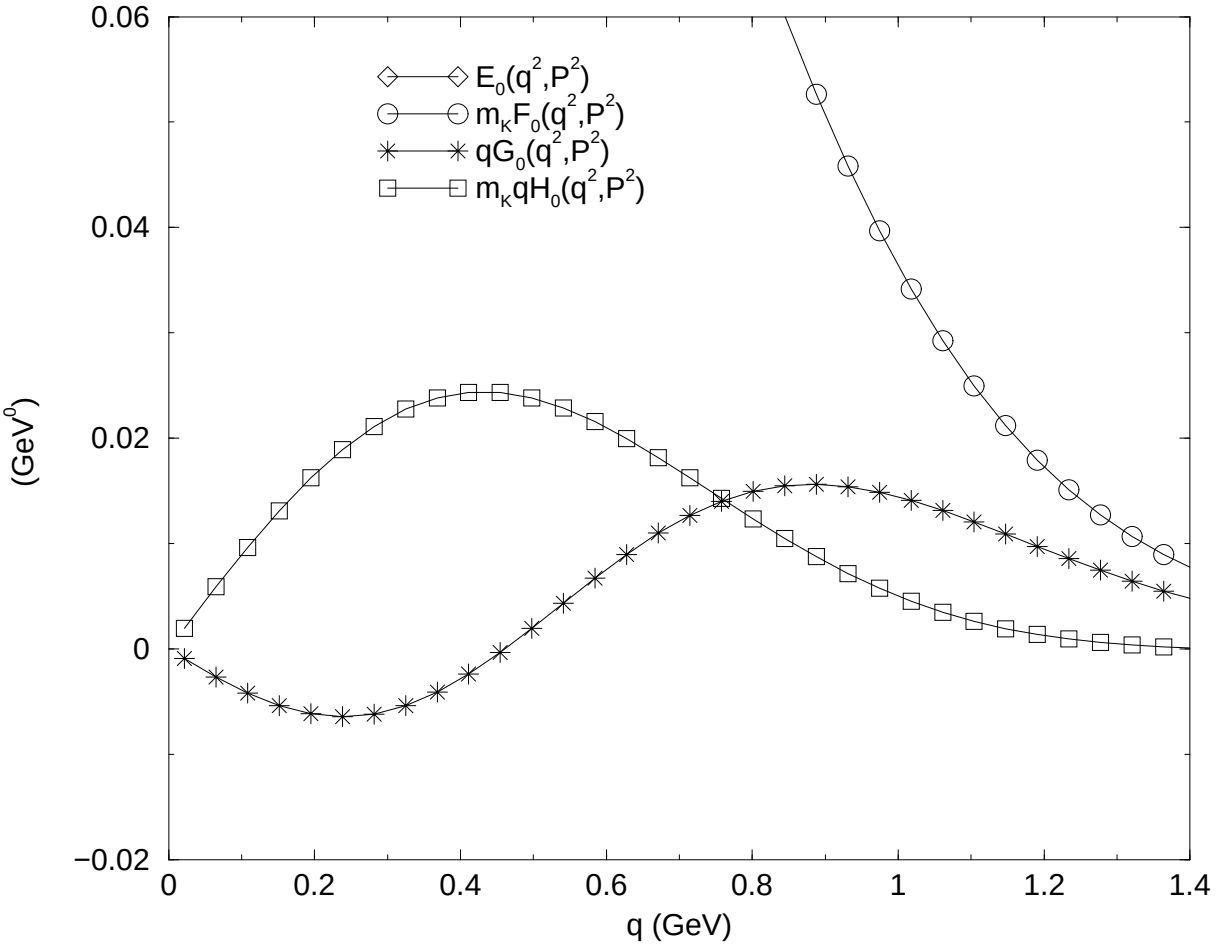

4.4 Vector Mesons

The general form of the BSA for vector mesons is

$$\Gamma^{ab(s)}(q;P) = \Gamma^{ab}_{\mu}(q;P)\epsilon^{(s)}_{\mu}(P) \tag{4.56}$$

where $\epsilon^{(s)}_{\mu}(P)$ is one of three spin polarization vectors and $\Gamma^{ab}_{\mu}(q;P)$ is the Lorentz BSA. Linear combinations of the three spin polarization vectors correspond to the three $m_s = \pm 1, 0$ spin states of the meson [62, 63]. The spin polarization vectors are transverse,

$$\epsilon^{(s)}_{\mu}(P)P_{\mu} = 0, \tag{4.57}$$

and have the property

$$\sum_{s=1}^{3} \epsilon^{(s)}_{\mu}(P)^{*}\epsilon^{(s)}_{\nu}(P) = T_{\mu\nu}(P) \tag{4.58}$$

where $T_{\mu\nu}(P)$ is the transverse projector defined in Chapter 3.

The general form of $\Gamma^{uu}_{\mu}(q;P)$ with $J^{PC} = 1^{--}$, such as the ρ^0 and the ϕ, is

$$\begin{aligned}
\Gamma^{uu}_{\mu}(q;P) &= \gamma_{\mu}\, V_1(q;P) + q_{\mu}\gamma\cdot q\, V_2(q;P) + q_{\mu}\gamma\cdot Pq\cdot P\, V_3(q;P) \\
&+ \gamma_5\epsilon_{\mu\alpha\nu\beta}\gamma_{\alpha}q_{\nu}P_{\beta}\, V_4(q;P) + q_{\mu}\, V_5(q;P) \\
&+ \sigma_{\mu\nu}q_{\nu}q\cdot P\, V_6(q;P) + \sigma_{\mu\nu}P_{\nu}\, V_7(q;P) + q_{\mu}q_{\alpha}\sigma_{\alpha\beta}P_{\beta}\, V_8(q;P) \\
&+ P_{\mu}q\cdot P V_9(q;P) + P_{\mu}\gamma\cdot P V_{10}(q;P) + P_{\mu}\gamma\cdot qq\cdot P V_{11}(q;P) \\
&+ P_{\mu}q_{\alpha}\sigma_{\alpha\beta}P_{\beta}\, q\cdot P V_{12}(q;P).
\end{aligned} \tag{4.59}$$

Because the spin polarization vectors are transverse, the BSE for physical vector mesons requires only the components of Γ_{μ} that are transverse to P_{μ}. Covariants nine through twelve are purely longitudinal to P_{μ} so they are not needed in the calculation of physical vector meson BSAs. Our vector meson BSA now takes on the form

$$\begin{aligned}
\Gamma^{uu}_{\mu}(q;P)^{T} &= \gamma^{T}_{\mu}\, V_1(q;P) + q^{T}_{\mu}\gamma\cdot q\, V_2(q;P) + q^{T}_{\mu}\gamma\cdot Pq\cdot P\, V_3(q;P) \\
&+ \gamma_5\epsilon^{T}_{\mu\alpha\nu\beta}\gamma_{\alpha}q_{\nu}P_{\beta}\, V_4(q;P) + q^{T}_{\mu}\, V_5(q;P) \\
&+ \sigma^{T}_{\mu\nu}q_{\nu}q\cdot P\, V_6(q;P) + \sigma^{T}_{\mu\nu}P_{\nu}\, V_7(q;P) + q^{T}_{\mu}q_{\alpha}\sigma_{\alpha\beta}P_{\beta}\, V_8(q;P)
\end{aligned} \tag{4.60}$$

where $\Gamma^{uu}_\mu(q;P)^T = T_{\mu\nu}(P)\Gamma^{uu}_\nu(q;P)$.

Just as in the pseudoscalar case we can calculate the anti-meson BSA, $\bar{\Gamma}^{du}_\mu(q;P) = [C^{-1}\Gamma^{ud}_\mu(-q;P)C]^{T\,1}$, by again using the identities in Appendix A.4. For the vector mesons $\bar{\Gamma}^{uu}_\mu(q;P) = -\Gamma^{uu}_\mu(q;P)$ where the minus sign comes from the charge conjugation quantum number, C, in $J^{PC} = 1^{--}$.

Table 4.3: Vector meson covariants with $J^{PC} = 1^{--}$

$\Gamma_\mu(q;P)$	$\bar{\Gamma}_\mu(q;P)$
$\gamma_\mu\, V(q\cdot P)$	$-\gamma_\mu\, V(-q\cdot P)$
$q_\mu \gamma\cdot q\, V(q\cdot P)$	$-q_\mu \gamma\cdot q\, V(-q\cdot P)$
$q_\mu \gamma\cdot P q\cdot P\, V(q\cdot P)$	$-q_\mu \gamma\cdot P q\cdot P\, V(-q\cdot P)$
$\gamma_5\epsilon_{\mu\alpha\nu\beta}\gamma_\alpha q_\nu P_\beta\, V(q\cdot P)$	$-\gamma_5\epsilon_{\mu\alpha\nu\beta}\gamma_\alpha q_\nu P_\beta\, V(-q\cdot P)$
$q_\mu\, V(q\cdot P)$	$-q_\mu\, V(-q\cdot P)$
$\sigma_{\mu\nu} q_\nu q\cdot P\, V(q\cdot P)$	$-\sigma_{\mu\nu} q_\nu q\cdot P\, V(-q\cdot P)$
$\sigma_{\mu\nu} P_\nu\, V(q\cdot P)$	$-\sigma_{\mu\nu} P_\nu\, V(-q\cdot P)$
$q_\mu q_\alpha \sigma_{\alpha\beta} P_\beta\, V(q\cdot P)$	$-q_\mu q_\alpha \sigma_{\alpha\beta} P_\beta\, V(-q\cdot P)$

Eq. 4.60 shows that covariants one through four have an odd number of γ matrices and covariants five through eight have an even number of γ matrices. Because the trace of an odd number of γ matrices is zero, we know covariants one through four are orthogonal to covariants five through eight.

From Eq. A.17 we know that covariant four is orthogonal to all other covariants. Furthermore, it is transverse to P_μ without being operated on by $T_{\mu\nu}(P)$. With

$$Tr\{\gamma_5\epsilon_{\mu\nu\alpha\beta}\gamma_\nu p_\alpha P_\beta \gamma_5\epsilon_{\mu\omega\theta\phi}\gamma_\omega p_\theta P_\phi\} = -8N(p,P)^2 \tag{4.61}$$

and $N(p,P)^2$ as defined in Eq. 4.35, we have

$$\begin{aligned} V_4(p;P) &= \frac{1}{8N(p,P)^2}\int^\Lambda \frac{d^4q}{(2\pi)^4}\frac{\mathcal{G}(k^2)}{k^2}T_{\mu\nu}(k) \\ &\times\ Tr\left\{\gamma_5\epsilon_{\alpha\beta\omega\rho}\gamma_\beta p_\omega P_\rho \frac{\lambda^c}{2}\gamma_\mu S^u(q_+)\Gamma^{ud}_\alpha(q;P)^T S^d(q_-)\frac{\lambda^c}{2}\gamma_\nu\right\}. \end{aligned} \tag{4.62}$$

[1] T denotes transpose in $\bar{\Gamma}^{du}_\mu(q;P) = [C^{-1}\Gamma^{ud}_\mu(-q;P)C]^T$ as opposed to denoting a transverse Bethe-Salpeter amplitude in $\Gamma^{ud}_\mu(q;P)^T$.

As was done for the pseudoscalars, we define T_i as the projection of Γ_μ onto covariant i. The projections of covariants one, two, and three onto Γ_μ can then be written in the matrix form

$$\left\{\begin{array}{c} T_1 \\ T_2 \\ T_3 \end{array}\right\} = \left\{\begin{array}{ccc} 12 & 4(p^T)^2 & 0 \\ 4(p^T)^2 & 4(p^T)^2p^2 & 4(p^T)^2(p\cdot P)^2 \\ 0 & 4(p^T)^2(p\cdot P)^2 & 4(p^T)^2P^2(p\cdot P)^2 \end{array}\right\} \left\{\begin{array}{c} V_1 \\ V_2 \\ V_3 \end{array}\right\} \tag{4.63}$$

and inverted to give

$$\left\{\begin{array}{c} V_1 \\ V_2 \\ V_3 \end{array}\right\} = \frac{1}{8(p^T)^4P^2} \left\{\begin{array}{ccc} (p^T)^4P^2 & -(p^T)^2P^2 & (p^T)^2 \\ -(p^T)^2P^2 & 3P^2 & -3 \\ (p^T)^2 & -3 & \psi/(p\cdot P)^2 \end{array}\right\} \left\{\begin{array}{c} T_1 \\ T_2 \\ T_3 \end{array}\right\} \tag{4.64}$$

where $\psi = 3p^2 - (p^T)^2$. So now the amplitudes may be read directly off of Eq. 4.64. For example,

$$\begin{aligned} V_2(p;P) &= \frac{(p^T)^2P^2}{8(p^T)^4P^2}\int\cdots Tr\{\gamma_\alpha^T\cdots\Gamma_\alpha^{ud}(q;P)^T\cdots\} \\ &- \frac{3P^2}{8(p^T)^4P^2}\int\cdots Tr\{p_\alpha^T\gamma\cdot p\cdots\Gamma_\alpha^{ud}(q;P)^T\cdots\} \\ &+ \frac{3}{8(p^T)^4P^2}\int\cdots Tr\{p_\alpha^T\gamma\cdot Pp\cdot P\cdots\Gamma_\alpha^{ud}(q;P)^T\cdots\}. \end{aligned} \tag{4.65}$$

Covariant five is orthogonal to covariants six, seven, and eight and is given by

$$\begin{aligned} V_5(p;P) &= -\frac{1}{4(p^T)^2}\int^\Lambda \frac{d^4q}{(2\pi)^4}\frac{\mathcal{G}(k^2)}{k^2}T_{\mu\nu}(k) \\ &\times\ Tr\{p_\alpha^T\frac{\lambda^c}{2}\gamma_\mu S^u(q_+)\Gamma_\alpha^{ud}(q;P)^T S^d(q_-)\frac{\lambda^c}{2}\gamma_\nu\}. \end{aligned} \tag{4.66}$$

Similarly, covariants six, seven, and eight have the projection matrix

$$\left\{\begin{array}{c} T_6 \\ T_7 \\ T_8 \end{array}\right\} = \left\{\begin{array}{ccc} 4\psi(p\cdot P)^2 & 12(p\cdot P)^2 & 4(p^T)^2(p\cdot P)^2 \\ 12(p\cdot P)^2 & 12P^2 & 4(p^T)^2P^2 \\ 4(p^T)^2(p\cdot P)^2 & 4(p^T)^2P^2 & 4(p^T)^4P^2 \end{array}\right\} \left\{\begin{array}{c} V_6 \\ V_7 \\ V_8 \end{array}\right\} \tag{4.67}$$

which is inverted to give

$$\left\{\begin{array}{c} V_6 \\ V_7 \\ V_8 \end{array}\right\} = \frac{1}{8(p^T)^2P^2}\left\{\begin{array}{ccc} P^2/(p\cdot P)^2 & -1 & 0 \\ -1 & p^2 & -1 \\ 0 & -1 & 3/(p^T)^2 \end{array}\right\}\left\{\begin{array}{c} T_6 \\ T_7 \\ T_8 \end{array}\right\}. \tag{4.68}$$

The K^* vector meson has a strangeness quantum number and therefore has no charge conjugation quantum number. Because of this it has a $J^P = 1^-$ and we use

$$\begin{aligned} \Gamma^{us}_\mu(q;P)^T &= \gamma^T_\mu\, V_1(q;P) + q^T_\mu \gamma\cdot q\, V_2(q;P) + q^T_\mu \gamma\cdot P\, V_3(q;P) \\ &+ \gamma_5 \epsilon^T_{\mu\alpha\nu\beta}\gamma_\alpha q_\nu P_\beta\, V_4(q;P) + q^T_\mu\, V_5(q;P) \\ &+ \sigma^T_{\mu\nu} q_\nu\, V_6(q;P) + \sigma^T_{\mu\nu} P_\nu\, V_7(q;P) + q^T_\mu q_\alpha \sigma_{\alpha\beta} P_\beta\, V_8(q;P) \end{aligned} \tag{4.69}$$

for its BSA. These covariants differ from those of the ρ and ϕ by only the third and sixth covariants where $q\cdot P$ is absorbed into the amplitude. The projection matrices and their inverses for the K^* are given in Appendix C.1.

For pseudoscalar mesons the normalization condition Eq. 4.51 is sufficient, but for vector mesons the three spin polarizations need to be averaged over giving

$$\begin{aligned} 1 &= \frac{1}{3}\frac{\partial}{\partial P^2}\left\{ \int^\Lambda \frac{d^4q}{(2\pi)^4} Tr_{CD}\left[\bar{\Gamma}^{ba}_\mu(q;-K)^T \right.\right. \\ &\times \left.\left. S^a(q+\eta P)\Gamma^{ab}_\mu(q;K)^T S^b(q-\beta P)\right]\right\}\Bigg|_{P^2=K^2=-m^2}. \end{aligned} \tag{4.70}$$

Vector mesons can also decay via the electroweak interaction with a decay constant given by [1]

$$f_V m_V \epsilon^{(s)}_\mu(P) = Z_2 N_C \int^\Lambda \frac{d^4q}{(2\pi)^4} Tr_D\left\{\Gamma^{ab(s)}(q;P) S^b(q_-)\gamma_\mu S^a(q_+)\right\}. \tag{4.71}$$

We know from Eq. 4.58 that

$$\sum_{s=1}^{s} \epsilon^{(s)}_\mu(P)^* \epsilon^{(s)}_\mu(P) = T_{\mu\mu}(P) = 3. \tag{4.72}$$

By contracting both sides of Eq. 4.71 with $\epsilon_\mu^{(s)}(P)^*$ we have

$$f_V = \frac{Z_2 N_C}{3m_V} \int^{\Lambda} \frac{d^4q}{(2\pi)^4} Tr_D \left\{ \Gamma_\mu^{ab}(q;P)^T S^b(q_-) \gamma_\mu S^a(q_+) \right\} \tag{4.73}$$

where $\Gamma_\mu^{ab}(q;P)$ must be normalized according to Eq. 4.70.

Figure 4.13: Taylor series order comparison of lowest ρ BSE eigenvalue.

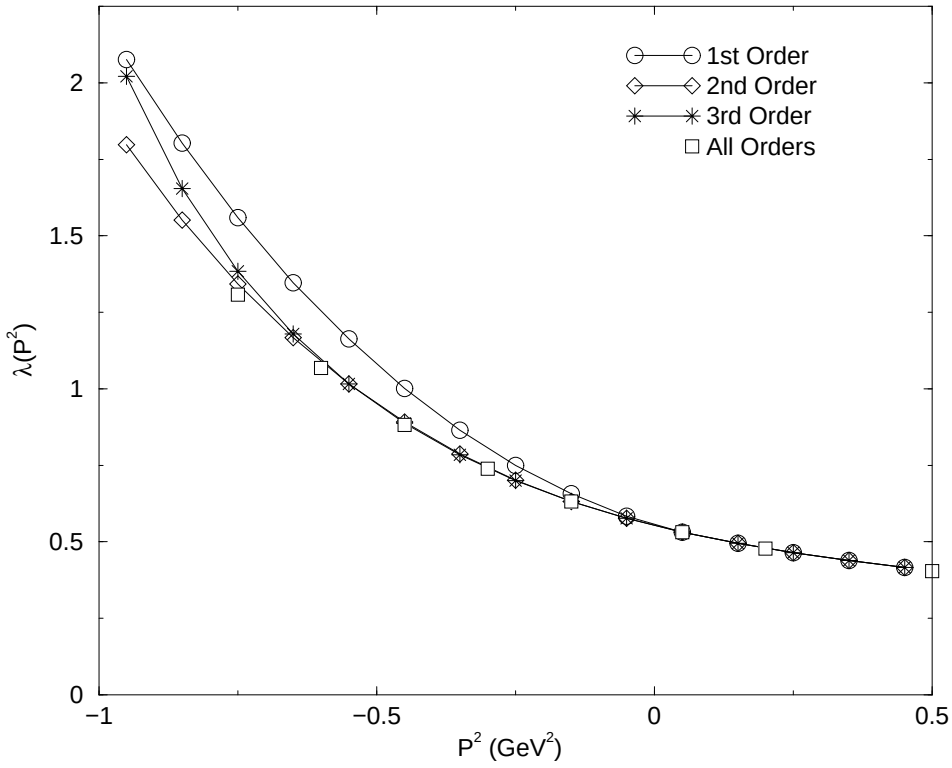

In calculating the vector meson BSAs we want to get an idea of how good the Momentum Expansion Method works. In Figure 4.13 we show the single Chebyshev expansion for the ρ $\lambda(P^2)$ for the first three orders of the Taylor expansion as well as the exact solution given in [1]. When $\lambda(P^2) = 1$ we see convergence at second order, but when P^2 approaches -1GeV^2 we see that second order is insufficient for convergence. This weak convergence is due to the complex conjugate singularities in the region of -1GeV^2 influencing the Taylor series expansion of the quark propagators.

Figure 4.14: A comparison of the zero Chebyshev ρ amplitudes. The amplitudes are rescaled in the same way as the pseudoscalars such that the covariants and amplitudes are dimensionless.

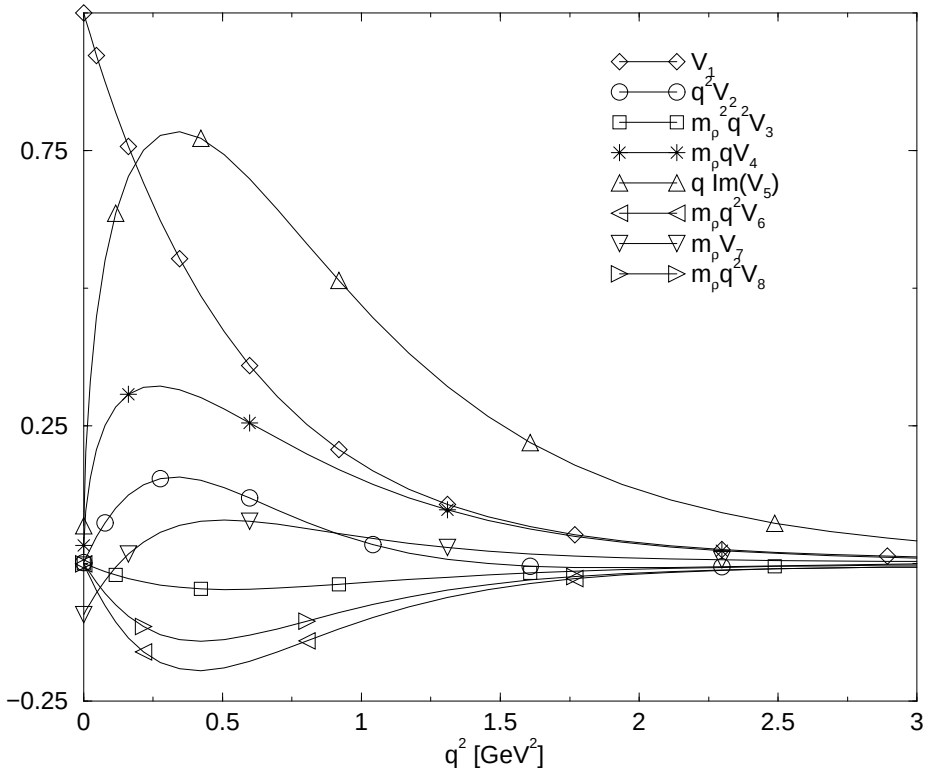

Figure 4.14 is the zero Chebyshev moment for the rescaled ρ amplitudes. This graph suggests that covariants one, four, and five are the dominant covariants. However, from Eq.A.28 we see that

$$\gamma_5 \epsilon^T_{\mu\nu\alpha\beta}\gamma_\beta q_\alpha P_\beta = \gamma^T_\mu \gamma\cdot q\gamma\cdot P - q^T_\mu \gamma\cdot P - \gamma^T_\mu q\cdot P \tag{4.74}$$

contains terms proportional to covariants one and three. The mixing of covariants one through three and the reduction of covariant four into covariants one, three, and a term proportional to $\gamma_\mu\gamma\cdot q\gamma\cdot P$ suggest that a five covariant solution with covariants one through five will contain the dominant physics.

Table 4.4 shows the masses and electroweak decay constants for the first through third

Table 4.4: The vector meson masses and electroweak decay constants (in GeV) through several orders in the Taylor expansion method of treating the complex argument of the quark propagator amplitudes. The values quoted give the masses and decay constants converged in the Chebyshev expansion. Comparison is made to the exact results of this ladder-rainbow model from Ref. [1] The consequences from truncation of the complete set of eight covariants to five and one (canonical/Dirac matrix) covariants is indicated.

	ρ		$K^\star$		ϕ	
	m_ρ	f_ρ	$m_{K^\star}$	$f_{K^\star}$	m_ϕ	f_ϕ
1^{st} order Taylor						
All 8 amplitudes	0.669	0.223	0.854	0.276	1.009	0.300
V_1-V_5	0.656	0.213	0.836	0.259	0.997	0.290
V_1 only	0.811	0.255	-	-	1.202	0.329
2^{nd} order Taylor						
All 8 amplitudes	0.732	0.208	0.949	0.253	1.064	0.266
V_1-V_5	0.717	0.200	0.924	0.238	1.052	0.257
V_1 only	0.856	0.214	-	-	1.235	0.269
3^{rd} order Taylor						
All 8 amplitudes	0.732	0.200	0.934	0.253	1.054	0.252
V_1-V_5	0.719	0.192	0.911	0.227	1.043	0.242
V_1 only	0.844	0.189	-	-	1.180	0.213
Model exact [1]	0.742	0.207	0.936	0.241	1.072	0.259
Experiment	0.770	0.216	0.892	0.225	1.020	0.237

orders of the Taylor expansion. The ρ and ϕ mesons are $C = -1$ charge conjugation eigenstates that require only the even Chebyshev moments in Eq. 4.15. The values quoted in Table 4.4 give the masses and decay constants converged in the Chebyshev expansion. For the ρ and ϕ mesons only the 0^{th} and 2^{nd} Chebyshev moments are needed for convergence. However, the K^* is not a charge conjugation eigenstate and requires both even and odd Chebyshev moments. The eight and five covariant K^* masses and decay constants are converged by four Chebyshev moments while the one-covariant K^* has no solution (see below). The results for the ρ meson are converged to within 1% for both the masses and electroweak decay constants. For the K^* the masses are converged to within 1.1% and the decay constances within 2%. The ϕ mass results are within 0.1% except for the first order $V_1 - V_5$ which is within 1% and the canonical third order results which is within 0.26%.

Table 4.5: The percent deviation of the vector meson masses and electroweak decay constants given in Table 4.4 with respect to the experimental values and with respect to the model exact results. Percent deviations from the model exact results are given in parentheses. The model exact results for the five and single covariant solutions are given in Table III of [1].

	ρ		$K^\star$		ϕ	
	m_ρ	f_ρ	$m_{K^\star}$	$f_{K^\star}$	m_ϕ	f_ϕ
1^{st} order Taylor						
All 8 amplitudes	13.1 (9.8)	3.2 (7.7)	4.3 (8.8)	22.7 (14.5)	1.1 (5.9)	26.6 (15.9)
V_1-V_5	14.8 (10.1)	1.4 (7.1)	6.3 (9.1)	15.1 (12.7)	2.3 (6.2)	22.4 (16.0)
V_1 only	5.3 (7.9)	18.1 (27.5)	-	-	17.8 (3.1)	38.8 (64.5)
2^{nd} order Taylor						
All 8 amplitudes	5.0 (1.4)	3.7 (0.5)	6.4 (1.4)	12.4 (5.0)	4.3 (0.7)	12.2 (2.7)
V_1-V_5	6.9 (1.7)	7.5 (0.6)	3.6 (0.6)	5.8 (3.5)	3.1 (1.0)	8.5 (2.8)
V_1 only	11.2 (2.8)	1.9 (7.0)	-	-	21.0 (1.0)	13.6 (34.5)
3^{rd} order Taylor						
All 8 amplitudes	4.9 (1.3)	7.4 (3.4)	4.7 (0.2)	12.4 (5.0)	3.3 (1.7)	6.4 (2.8)
V_1-V_5	6.6 (1.4)	11.2 (3.6)	2.1 (1.0)	0.9 (1.4)	2.3 (1.8)	2.1 (3.2)
V_1 only	9.6 (4.1)	12.5 (5.5)	-	-	15.7 (4.9)	10.1 (6.5)

The ϕ electroweak decay constants are converged to within 2% except for the canonical third order result which is within 9%.

Table 4.5 summarizes the percent deviations of the values in Table 4.4 with both the experimental results and the model exact results. Only the model exact results for the full covariant solutions are given here. Model exact results for the five covariant and single covariant solutions are given in Table III of [1].

At second order, the full covariant meson masses and decay constant are within 2% of the exact model calculations except for f_ϕ which is within 3% and f_{K^*} which is within 5%. At third order, the masses are within 2% and the decay constants f_ρ, f_{K^*}, and f_ϕ are 4%, 5%, and 3% off of their model exact results, respectively. The increased error in the electroweak decay constants compared to the error in the mass is not surprising. While errors in the masses come from the Taylor expansion of the quark propagators in the BSE only, the decay constants have a greater error due to errors in the quark propagator being

propagated through the normalization and electroweak quark loops.

Table 4.4 also shows that the first five covariants contains the dominant physics in the mass and electroweak decays. Here we compare the second order results to the experimental results. Comparison of experimental results to the other orders is given in Table 4.5. For the ρ meson mass, the canonical covariant γ_μ is 11.2% too high, while covariants one through five and all eight covariants produce meson masses that are 6.9% and 5.0% too low, respectively. The ρ meson electroweak decay constant is 1.9%, 7.5%, and 3.7% too low for the canonical, five, and eight covariant solutions, respectively. The K^* mass solutions are 3.6% and 6.4% too low for the five and eight covariant solutions while the electroweak decay constant was 5.8% and 12.4% too high for the five and eight covariant solutions, respectively. The ϕ meson mass canonical solution was 21% too high while the five and eight covariant solutions were 3.1% and 4.3% too low. The ϕ electroweak decay constant was 13.6%, 8.5%, and 12.2% too high for the canonical, five, and eight covariant solutions, respectively. These results verify our conclusions drawn from Figure 4.14 of the ρ meson amplitudes and indicate that for this particular model covariants one through five contain the dominant vector meson physics.

The calculation of the K^* mass and decay constant with only the canonical covariant does not have a converged solution most likely due to the complex conjugate singularities of the up and strange quark propagators. Our search algorithm for the ground-state K^* mass uses the power method to determine when the largest real eigenvalue is equal to one. Because the power method is insufficient in determining complex eigenvalues we instead use [64] in our search algorithm. Unlike the power method, this search algorithm will filter out the complex eigenvalues and only look for when the largest real eigenvalue is equal to one. This more robust calculation of the canonical covariant K^* eigenvalues shows that many, but not all, of the real eigenvalues portrayed in Fig. 4.2 sequentially become

complex conjugate pairs just before $\lambda(P^2) = 1$. The largest real eigenvalue will equal one for P^2 equal to 1323 MeV, 1646 MeV, and 1356 MeV for the first through third orders in the momentum expansion, respectively. The results are converged by the fifth Chebyshev moment but unconverged in the Taylor expansion. For the first-order and third-order results, the integration domain of the BSE encompasses the up quark singularities only while the second-order result encompasses both the up and strange quark singularities. Because the Taylor expansions are unconverged near the singularities, the above results do not represent converged physical solutions.

CHAPTER 5

Strong Decays of Vector Mesons

5.1 General Technique

The amplitude for the decay of a vector meson with spin polarization i into two pseudoscalars is given by

$$\mathcal{M}^{(i)}(P,Q) = \epsilon_\mu^{(i)}(Q)\Lambda_\mu(P,Q) \tag{5.1}$$

where Q is the vector meson momentum, P is the relative pseudoscalar momentum, and

$$\Lambda_\mu(P,Q) = 2P_\mu \tilde{F}(P^2,Q^2,(P\cdot Q)^2) + Q_\mu P\cdot Q\, H(P^2,Q^2,(P\cdot Q)^2). \tag{5.2}$$

If the vector meson decays into two pseudoscalars with the same mass, then $P\cdot Q$ is zero and Eq. 5.2 simplifies to $2P_\mu\tilde{F}(P^2,Q^2)$. However, if the vector meson decays into two different mass pseudoscalars, then the second term in Eq. 5.2 is still not needed for the calculation of the decay rate and coupling constant. To see this we average over the spin polarization of the vector meson to get the decay rate

$$\Gamma = \frac{\hat{\rho}}{2M_A}\frac{1}{3}\sum_{i=1}^{3}|\mathcal{M}^{(i)}|^2 \tag{5.3}$$

where M_A is the mass of the decaying vector meson. The two-body phase space factor, $\hat{\rho}$, is given in Appendix D. Using Eqs. 4.58 and 5.1 we can simplify the decay rate to

$$\Gamma = \frac{\hat{\rho}}{2M_A}\frac{1}{3}\Lambda_\mu(P,Q)^T\Lambda_\mu(P,Q)^T \tag{5.4}$$

where

$$\Lambda_\mu(P,Q)^T = T_{\mu\nu}(Q)\Lambda_\nu(P,Q). \tag{5.5}$$

Since

$$T_{\mu\alpha}(Q)\Lambda_\alpha(P,Q) = 2P_\mu^T\tilde{F}(P^2,Q^2,(P\cdot Q)^2), \tag{5.6}$$

we see that the decay rate does not depend on the longitudinal piece of $\Lambda_\mu(P,Q)$. If the mesons are on their mass-shell then

$$g_{ABC} = \tilde{F}(P^2, Q^2, (P\cdot Q)^2) \tag{5.7}$$

where g_{ABC} is the coupling constant associated with the decay of vector meson, A, decaying into the pseudoscalar mesons B and C. The decay rate then simplifies to

$$\Gamma = \frac{\hat{\rho}}{2M_A}\frac{4(P^T)^2}{3}g_{ABC}^2 \tag{5.8}$$

where $(P^T)^2 = P_\mu^T P_\mu^T = P_\mu T_{\mu\nu}(Q) P_\nu$.

To calculate the decay rates and coupling constants we need to find a way to calculate Λ_μ. For photon momentum in the vicinity of the ρ and ϕ mesons, we know that the charge form factors for the pion and kaon will exhibit a resonant pole behavior due to the propagation of an intermediate state ρ or ϕ meson. The form factors can be calculated from the $\gamma\pi\pi$ and γKK vertex functions and $g_{\rho\pi\pi}$ and $g_{\phi KK}$ extracted from them. Thus, the quality of $g_{\rho\pi\pi}$ and $g_{\phi KK}$ depend directly on the quality of the $\gamma\pi\pi$ and γKK vertex functions. In [65] it has been shown that the impulse approximation of meson charge form factors conserves the electromagnetic current and provides the correct charge in a model independent way so long as the quark propagators, photon-quark vertex, and meson BSAs are calculated in the rainbow-ladder approximation. Furthermore, [66] extends these arguments to the $K^* \to K\pi$ decay where the K^{*-} appears as a pole in the W^- vertex. Therefore, we will use the impulse approximation to calculate the decay amplitude, Λ_μ.

In the impulse approximation, irreducible three-body interactions are neglected and Λ_μ takes on the form

$$\begin{aligned}\Lambda_\mu^{bac}(P,Q) &= \int \frac{d^4k}{(2\pi)^4} Tr_{DC}\Big\{\Gamma_5^{ba}(k_2; P-Q/2) S^a(k+Q/2) \\ &\times \Gamma_\mu^{ac}(k;Q) S^c(k-Q/2)\bar{\Gamma}_5^{cb}(k_3; -P-Q/2) S^b(k+P)\Big\},\end{aligned} \tag{5.9}$$

Figure 5.1: Impulse approximation of the $A \to BC$ decay amplitude.

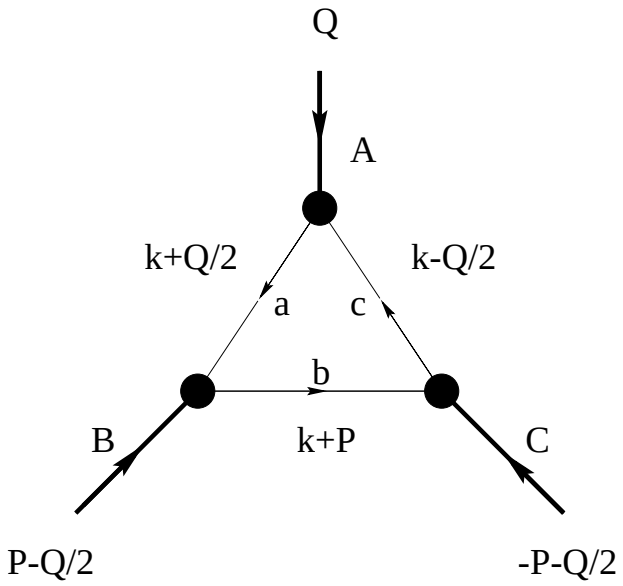

where $k_2 = k+P/2+Q/4$, $k_3 = k+P/2-Q/4$, and internal quark labels have been added to $\Lambda_\mu(P,Q)$ in an obvious way. The Feynman diagram of Λ_μ in the impulse approximation (Fig. 5.1) takes on the simple form of a triangle diagram. Because the calculation of the coupling constants requires the mesons be on their mass shells, the relative $q\bar{q}$ momenta of the mesons is complex. However, we are integrating over the internal quark momenta and are free to choose the integration variable. We have chosen the symmetric representation such that the a quark momentum is $k + Q/2$ and that the c quark momentum is $k - Q/2$. This representation is advantageous because it eliminates the need to go into the complex plane with the vector meson relative $q\bar{q}$ momentum. In principle we could solve the Bethe-Salpeter equations for the pseudoscalar mesons at complex momenta, but we use the simpler approach of Taylor expanding the BSAs into the complex plane. As was done for the quark propagators in the BSE, we expand the pseudoscalar BSAs in a Taylor series about the closest point on the positive real axis.

Figure 5.2: Impulse approximation of the $\rho^\circ \to \pi^+\pi^-$ decay amplitude.

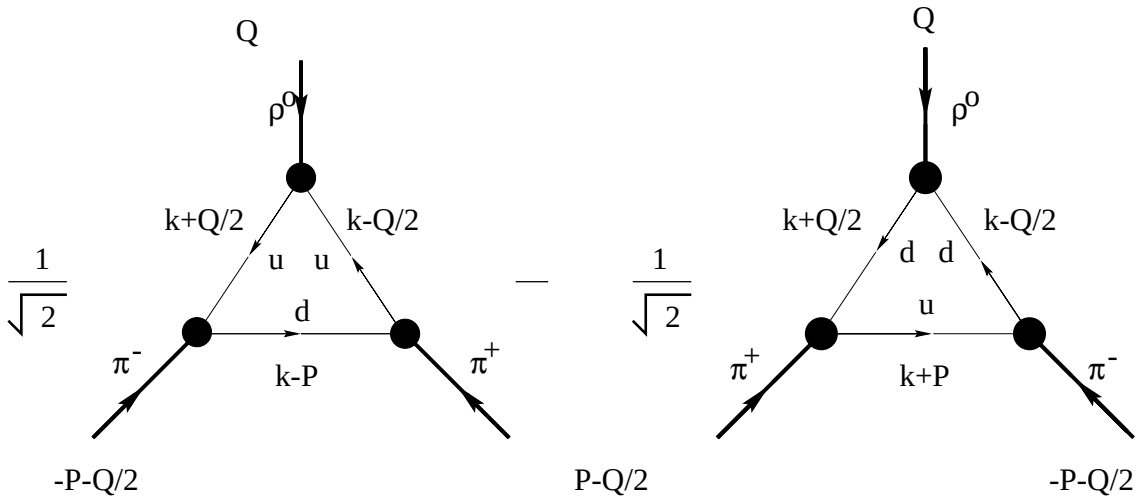

5.2 Two Pseudoscalar Strong Decays

The amplitude for the decay of a ρ° into a π^+ and π^- is given by

$$\begin{aligned}(5.10)\qquad \Lambda_\mu(\rho^\circ\pi^+\pi^- : P;Q)^T &= \frac{1}{\sqrt{2}}\int \frac{d^4k}{(2\pi)^4}\mathrm{Tr}_{DC}\Big\{\bar{\Gamma}_5^{du}(k_2';-P-Q/2)\\ &\times\ S^u(k+Q/2)\Gamma_\mu^{uu}(k;Q)^T S^u(k-Q/2)\Gamma_5^{ud}(k_3';P-Q/2)S^d(k-P)\Big\}\\ &-\ \frac{1}{\sqrt{2}}\int \frac{d^4k}{(2\pi)^4}\mathrm{Tr}_{DC}\Big\{\Gamma_5^{ud}(k_2;P-Q/2)S^d(k+Q/2)\Gamma_\mu^{dd}(k;Q)^T\\ &\times\ S^d(k-Q/2)\bar{\Gamma}_5^{du}(k_3;-P-Q/2)S^u(k+P)\Big\}\end{aligned}$$

where $k_2' = k - P/2 + Q/4$, and $k_3' = k - P/2 - Q/4$. See Figure 5.2. This can be simplified as

$$(5.11)\qquad \Lambda_\mu(\rho^\circ\pi^+\pi^- : P;Q)^T = \frac{1}{\sqrt{2}}\tilde{\Lambda}_\mu^{duu}(P;Q)^T - \frac{1}{\sqrt{2}}\Lambda_\mu^{udd}(P;Q)^T.$$

Since we are working in the isospin symmetric limit, $m_u = m_d$, and because $\Gamma^{uu}(q;P) = \bar{\Gamma}^{uu}(q;P)$ for the pion, we have

$$(5.12)\qquad \tilde{\Lambda}_\mu^{duu}(P;Q) = \Lambda_\mu^{udd}(-P;Q)$$

and Eq. 5.11 becomes

$$(5.13)\qquad \Lambda_\mu(\rho^\circ\pi^+\pi^- : P;Q)^T = \frac{1}{\sqrt{2}}\Lambda_\mu^{udd}(-P;Q)^T - \frac{1}{\sqrt{2}}\Lambda_\mu^{udd}(P;Q)^T.$$

Next, we want to show that $\Lambda_\mu^{udd}(-P;Q) = -\Lambda_\mu^{udd}(P;Q)$ [67]. Starting with

$$\begin{aligned}(5.14)\qquad \Lambda_\mu^{udd}(P;Q) &= \int_k \mathrm{Tr}_{DC}\Big\{\Gamma_5^{ud}(k+P/2+Q/4;P-Q/2)\\ &\times\ S^d(k+Q/2)\Gamma_\mu^{dd}(k;Q)S^d(k-Q/2)\\ &\times\ \bar{\Gamma}_5^{du}(k+P/2-Q/4;-P-Q/2)S^u(k+P)\Big\}\end{aligned}$$

and the charge conjugation operators in Appendix A.4, we have

$$\begin{aligned}(5.15)\qquad \Lambda_\mu^{udd}(P;Q) &= \int_k \mathrm{Tr}_{DC}\Big\{C\Gamma_5^{ud}C^{-1}CS^dC^{-1}C\Gamma_\mu^{dd}C^{-1}CS^dC^{-1}\\ &\times\ C\bar{\Gamma}_5^{du}C^{-1}CS^uC^{-1}\Big\}\end{aligned}$$

$$\begin{aligned}(5.16)\qquad &= \int_k \mathrm{Tr}_{DC}\Big\{\bar{\Gamma}_5^{du}(-k-P/2-Q/4;P-Q/2)^T\\ &\times\ S^d(-k-Q/2)^T\bar{\Gamma}_\mu^{dd}(-k;Q)^TS^d(-k+Q/2)^T\\ &\times\ \Gamma_5^{ud}(-k-P/2+Q/4;-P-Q/2)^TS^u(-k-P)^T\Big\}.\end{aligned}$$

Using the trace property $\mathrm{Tr}\{A^TB^TC^T\} = \mathrm{Tr}\{CBA\}$ and changing the integration variable from k to $-k$ we obtain

$$\begin{aligned}(5.17)\qquad \Lambda_\mu^{udd}(P;Q) &= \int_k \mathrm{Tr}_{DC}\Big\{\Gamma_5^{ud}(k-P/2+Q/4;-P-Q/2)\\ &\times\ S^d(k+Q/2)\bar{\Gamma}_\mu^{dd}(k;Q)S^d(k-Q/2)\\ &\times\ \bar{\Gamma}_5^{du}(k-P/2-Q/4;P-Q/2)S^u(k-P)\Big\}.\end{aligned}$$

Finally, because $\bar{\Gamma}_\mu(k;Q) = -\Gamma_\mu(k;Q)$ for the ρ°, Eq. 5.17 becomes $-\Lambda_\mu^{udd}(-P;Q)$. Therefore,

$$(5.18)\qquad \Lambda_\mu^{udd}(P;Q) = -\Lambda_\mu^{udd}(-P;Q).$$

and

$$(5.19)\qquad \Lambda_\mu(\rho^\circ\pi^+\pi^- : P;Q)^T = -\sqrt{2}\Lambda_\mu^{udd}(P;Q)^T.$$

By equating Eq. 5.19 with $g_{\rho\pi\pi}2P_\mu$ we find the decay constant to be

$$(5.20)\qquad g_{\rho\pi\pi} = -\frac{1}{\sqrt{2}}\frac{P_\mu\Lambda_\mu^{udd}(P;Q)^T}{P^2}.$$

Although we have calculated this specifically for the $\rho^\circ \to \pi^+\pi^-$ decay, we are working in the $m_u = m_d$ isospin limit so all of the $\rho \to \pi\pi$ decays will have the same value of $g_{\rho\pi\pi}$.

The amplitude for the decay of a ϕ meson into a K^+ and a K^- is given by

$$\Lambda_\mu(\phi\, K^+\, K^- : P;Q)^T = \Lambda_\mu^{uss}(P;Q)^T \tag{5.21}$$

and the decay amplitude, $g_{\phi KK}$, is

$$g_{\phi KK} = \frac{1}{2}\frac{P_\mu \Lambda_\mu^{ssu}(P;Q)^T}{P^2}. \tag{5.22}$$

The K^* decays one hundred percent of the time into a kaon and a pion. However, the isospin of the K^* allows for two different sets of $K\pi$ decay products. For example, the decay amplitude of a K^{*o} into a K^+ and a π^- is given by

$$\Lambda_\mu(K^{*o}\, K^+\, \pi^- : P;Q)^T = \Lambda_\mu^{uds}(P;Q)^T \tag{5.23}$$

and its decay into a K° and a π° is given by

$$\Lambda_\mu(K^{*\circ}\, K^\circ\, \pi^\circ : P;Q)^T = -\frac{1}{\sqrt{2}}\Lambda_\mu^{dds}(P;Q)^T. \tag{5.24}$$

From Eqs. 5.23 and 5.24 we find that the coupling constants

$$g_{K^{*o}K^+\pi^-} = \frac{P_\mu \Lambda_\mu^{uds}(P;Q)^T}{2(P^T)^2} \tag{5.25}$$

and

$$g_{K^{*\circ}K^\circ\pi^\circ} = -\frac{P_\mu \Lambda_\mu^{dds}(P;Q)^T}{2\sqrt{2}(P^T)^2} \tag{5.26}$$

differ by only a constant of $\sqrt{2}$ due to the isospin symmetric limit.

Because the pion and kaon masses are different $P \cdot Q \neq 0$ in our calculation of $\Lambda_\mu^{uds}(P;Q)^T$ and we must determine the angle β such that

$$P_\mu = |P|(0, 0, \sin\beta, \cos\beta). \tag{5.27}$$

With

$$(P - \frac{Q}{2})^2 = P^2 + \frac{1}{4}Q^2 - P \cdot Q = -M_\pi^2 \tag{5.28}$$

and

$$(-P - \frac{Q}{2})^2 = P^2 + \frac{1}{4}Q^2 + P \cdot Q = -M_K^2 \tag{5.29}$$

we find that

$$P \cdot Q = \frac{m_K^2 - m_\pi^2}{2} \tag{5.30}$$

and that

$$P^2 = \frac{1}{4}(m_{K^*}^2 - 2m_\pi^2 - 2m_K^2). \tag{5.31}$$

With $Q_\mu = iM_{K^*}(0,0,0,1)$ we find that

$$P \cdot Q = iM_{K^*}|P|\cos\beta. \tag{5.32}$$

Because $|P|$ and $P \cdot Q$ are real $\cos\beta$ must be purely imaginary, and therefore β must be complex. Since $\beta = a + ib$ and

$$\cos\beta = \cos(a)\cosh(b) - i\sin(a)\sinh(b) \tag{5.33}$$

we know that $\cos(a) = 0$ and that $\sin(a) = 1$. This reduces β to $\beta = \pi/2 + ib$. Finally we know that

$$\cos\beta = -i\sinh(b) = \frac{-iP \cdot Q}{M_{K^*}|P|} \tag{5.34}$$

so

$$b = \sinh^{-1}\left\{\frac{P \cdot Q}{M_{K^*}|P|}\right\}. \tag{5.35}$$

In the $m_s \to m_u$ or $m_u \to m_s$ limit $b \to 0$ and P_μ reduce to $P_\mu = |P|(0,0,1,0)$ and $P \cdot Q = 0$.

Table 5.1 gives our results for the vector meson strong decays. Because of the functional form of our internal quark momentum, Eq. 5.9 requires the values of the pseudoscalar Bethe-Salpeter amplitudes in the complex plane. The complex plane behavior of the

Table 5.1: Vector meson strong decay coupling constants calculated with the second-order momentum expansion results of both the vector and pseudoscalar Bethe-Salpeter amplitudes. The complex plane behavior of the pseudoscalar Bethe-Salpeter amplitudes is calculated with a Taylor expansion into the complex plane with the first-order through third-order results given. The dependence on the number of invariant amplitudes employed is indicated. The $K^\star$ decay process shown in brackets is related by isospin symmetry to the former process by a factor $1/\sqrt{2}$. The notation (v,p) indicates the number of invariant amplitudes used for the vector and pseudoscalar mesons, respectively.

$g_{v\to pp}$	(v,p)=(8,4)	(v,p)=(5,4)	(v,p)=(1,4)	(v,p)=(1,1)	Expt
1^{st} Order Taylor					
$g_{\rho\to\pi\pi}$	5.16	4.96	6.5	9.0	6.02
$g_{\phi\to KK}$	4.39	4.22	6.35	7.38	4.64
$g_{K^{*+}\to K^0\pi^+}$	4.86	4.48	-	-	4.60
$(g_{K^{*+}\to K^+\pi^0})$	(3.44)	(3.17)	-	-	(3.26)
2^{nd} Order Taylor					
$g_{\rho\to\pi\pi}$	5.10	4.90	6.4	8.8	6.02
$g_{\phi\to KK}$	4.26	4.10	6.12	6.93	4.64
$g_{K^{*+}\to K^0\pi^+}$	4.84	4.44	-	-	4.60
$(g_{K^{*+}\to K^+\pi^0})$	(3.42)	(3.14)	-	-	(3.26)
3^{rd} Order Taylor					
$g_{\rho\to\pi\pi}$	5.10	4.90	6.4	8.8	6.02
$g_{\phi\to KK}$	4.25	4.09	6.10	6.91	4.64
$g_{K^{*+}\to K^0\pi^+}$	4.83	4.44	-	-	4.60
$(g_{K^{*+}\to K^+\pi^0})$	(3.42)	(3.14)	-	-	(3.26)

pseudoscalar Bethe-Salpeter amplitudes is calculated with a Taylor expansion centered around the spacelike part of the complex relative $q\bar{q}$ momentum. The pseudoscalar Bethe-Salpeter amplitudes with spacelike relative $q\bar{q}$ momentum were calculated in Chapter 4 and for the coupling constants calculated here we use the Bethe-Salpeter amplitudes obtained from the second order Taylor expanded quark propagators. The results show a clear convergence in the order of the Taylor expansion at second order for all of the strong decays at different covariant representations of the vector and pseudoscalar mesons. With only the canonical γ_5 and γ_μ covariants, the ρ and ϕ coupling constants are approximately 50% larger than their experimental values. The introduction of the full pseudoscalar covariant representation lowers the ρ and ϕ strong decays to 6% and 32%, respectively. Although

both decays are larger than the experimental results, the ρ meson is significantly close to the experimental value. Table 4.5 shows that, when compared to experimental values, our ρ mass calculations improve with added covariants. However, when compared to experiment the electroweak decay constant has a relative error of less than 2% for the canonical covariant and less than 4% for the full covariant solution. Furthermore, the table shows that the ϕ electroweak decay constant improves when going from the canonical covariant solution to the full covariant solution. Because both the electroweak and strong decay constants are dependent on the Bethe-Salpeter amplitudes, the errors in the strong decays from the Bethe-Salpeter amplitudes follow the trend of increasing or decreasing when going from the canonical covariant to the full covariant solution just as the errors in the electroweak decays increase or decrease when going from the canonical-covariant to the full-covariant solution.

The ρ eight-covariant and five-covariant strong decays are 15% and 19% lower than the experimental results while the ϕ eight-covariant and five-covariant solutions are 8% and 12% lower than the experimental results. The relative errors in the strong decay results follow the relative errors in the electroweak decays given in Table 4.5. The K^* eight-covariant and five-covariant strong decays are 5% higher and 4% lower, respectively. Comparison with the eight-covariant and five-covariant solutions for all the strong decays are consistent with the previous chapter in that the five-covariant solution captures the dominant physics.

The Bethe-Salpeter kernel in Eq. 4.2 allows for the $\pi\pi$, KK, and $K\pi$ strong decay channels. Because of this the ρ width is 20% of its mass while the widths of the ϕ and K^* are significantly less. We believe that this accounts for the large relative error in the ρ strong decay as compared to the ϕ and K^*.

CHAPTER 6

Axial-Vector and Exotic Mesons

6.1 Real Argument Projection

The complex conjugate singularities mention in Chapter 3 hinder the calculation of mesons above the ϕ mass. Because the eigenvalue of the BSE is real we naively expect that the complex plane contribution of the quark propagators to be a minimal effect in the solution of the ground-state mesons. This viewpoint is further supported by our Taylor series expansion of the quark propagators given in Tables 4.2 and 4.4. In order to avoid the numerical difficulties in solving the BSE with singularities in the region of integration, we explore estimates of the ground-state mesons using only the real part of the argument of the quark propagators. This technique replaces Eq. 4.26 by

$$\sigma_{s/v}(q_{\pm}^2) \approx \sigma_{s/v}(q^2 - M^2/4) \tag{6.1}$$

and requires knowledge of the quark propagators along the negative real axis.

Knowledge of the quark propagator in the interval $[-M^2/4, 0]$ requires an analytic continuation of the Dyson-Schwinger equation. The current model characterized by Eq. 3.2 with $\mathcal{F}(k^2)$ given by Eq. 3.3 will contain the numerical instabilities discussed in Chapter 3 and needs to be modified so that the gluon propagator is zero at $k^2 = 0$. With $\mathcal{F}(k^2)$ replaced by Eq. 3.51, numerically stable solutions of σ_s and σ_v can be obtained and the ground-state pseudoscalar and vector mesons solutions compared to the Taylor expanded solutions.

Table 6.1 shows that the real axis approximation differs from the Taylor expanded solutions, exact model calculations, and the experimental masses by 11% for both the full

Table 6.1: The pseudoscalar masses and decay constants (in GeV) obtained from the real part of the argument of the quark propagators for all four Dirac covariants and the dominant E amplitude for γ_5.

	π		K	
	m_π	f_π	m_K	f_K
All 4 ampls	0.123	0.099	0.440	0.127
E only	0.116	0.075	0.404	0.098
Model in [1]	0.138	0.131	0.497	0.155
Experiment	0.1385	0.131	0.496	0.160

covariant pion and kaon masses. The full covariant pion and kaon electroweak decay constants differ from the experimental results by 24% and 21%, respectively. Table 6.2 shows that the full covariant masses in the real axis approximation differ from the experimental results by 8%, 2%, and 5% for ρ, K^*, and ϕ respectively. The vector decay constants are 1%, 7%, and 21% for the ρ, K^*, and ϕ respectively. The real axis results have errors comparable to that of the Taylor-expanded solutions and are further evidence that the meson's masses are dominated by the real axis values of the quark propagators. Furthermore, this is consistent with the cancellation of imaginary parts of the quark propagators in the Bethe-Salpeter Equation to produce real eigenvalues. Therefore, we naively expect errors of 10% for bound state masses in the 1-2 GeV range.

Table 6.2: The vector meson masses and electroweak decay constants (in GeV) using only the real part of the argument of the quark propagators.

	ρ		$K^\star$		ϕ	
	m_ρ	f_ρ	$m_{K^\star}$	$f_{K^\star}$	m_ϕ	f_ϕ
All 8 amplitudes	0.711	0.217	0.872	0.241	1.066	0.288
V_1 only	0.894	0.249	1.086	0.278	1.330	0.334
Model in [1]	0.742	0.207	0.936	0.241	1.072	0.259
Experiment	0.770	0.216	0.892	0.225	1.020	0.237

6.2 Axial-Vector Mesons

The $a_1(1260)$ and $b_1(1235)$ mesons are the lowest lying orbital excitations in the meson spectrum. The a_1 axial-vector meson has $J^{PC} = 1^{++}$ and has

$$\begin{aligned}
\Gamma^{uu}_{\mu}(q;P)^T &= \gamma_5\gamma^T_\mu\, A_1(q;P) + \gamma_5 q^T_\mu \gamma\cdot q\, A_2(q;P) \\
&+ \gamma_5 q^T_\mu \gamma\cdot P q\cdot P\, A_3(q;P) \\
&+ \epsilon^T_{\mu\nu\omega\rho}\gamma_\nu q_\omega P_\rho\, A_4(q;P) + \gamma_5 q^T_\mu q\cdot P\, A_5(q;P) \\
&+ \gamma_5\sigma^T_{\mu\nu} q_\nu\, A_6(q;P) + \gamma_5\sigma^T_{\mu\nu} P_\nu q\cdot P\, A_7(q;P) \\
&+ \gamma_5 q^T_\mu q_\alpha\sigma_{\alpha\beta}P_\beta q\cdot P\, A_8(q;P)
\end{aligned} \tag{6.2}$$

for its Bethe-Salpeter amplitude. The b_1 axial-vector meson has $J^{PC} = 1^{+-}$ and we use

$$\begin{aligned}
\Gamma^{uu}_{\mu}(q;P)^T &= \gamma_5\gamma^T_\mu q\cdot P\, A_1(q;P) + \gamma_5 q^T_\mu \gamma\cdot q q\cdot P\, A_2(q;P) \\
&+ \gamma_5 q^T_\mu \gamma\cdot P\, A_3(q;P) \\
&+ \epsilon^T_{\mu\nu\omega\rho}\gamma_\nu q_\omega P_\rho q\cdot P\, A_4(q;P) + \gamma_5 q^T_\mu\, A_5(q;P) \\
&+ \gamma_5\sigma^T_{\mu\nu} q_\nu q\cdot P\, A_6(q;P) + \gamma_5\sigma^T_{\mu\nu} P_\nu\, A_7(q;P) \\
&+ \gamma_5 q^T_\mu q_\alpha\sigma_{\alpha\beta}P_\beta\, A_8(q;P)
\end{aligned} \tag{6.3}$$

for its Bethe-Salpeter amplitude. Because of their opposite C-parity, Eqs. 6.2 and 6.3 differ by only the inclusion or removal of $q\cdot P$ in each covariant.

The real-axis approximation for both the a_1 and b_1 mesons is converged at two Chebyshev moments. The a_1 mass is 30% too low at 884 MeV and the b_1 mass is 37% too low at 776 MeV. Comparison of the ρ and a_1 masses indicates that the orbital excitation energy $m_{a1} - m_\rho$ is 153 MeV and thus a factor of three too small in this model. Because the masses lie below the singularities in the quark propagators, exact complex-plane calculations of the a_1 and b_1 masses can be computed yielding similar results in this model and in a related study [68]. These axial-vector results indicate that our current model is too attractive to describe the lowest energy orbital excitations properly.

6.3 Exotic Mesons

Mesons whose quantum numbers cannot be produced by $\bar{q}q$ bound states are called exotic states. In the static quark model the parity is given by $P = (-1)^{L+1}$ and the charge conjugation quantum number for neutral states is given by $C = (-1)^{L+S}$ where L is the orbital angular momentum and S is the total spin. Thus, resonances with $J^{PC} = 0^{--}$, 0^{+-}, 1^{-+}, 2^{+-}, ... represent exotic states. These exotic states can come from a gluonic excitation such as a hybrid $\bar{q}qg$, a glueball, or a multiquark state. In the covariant bound state Bethe-Salpeter equation, an extra degree of freedom from the relative time (relative energy) modifies the charge conjugation quantum number to

$$C = (-1)^{L+S+\kappa} \tag{6.4}$$

and thus becomes useful in describing the gluonic excitation $\bar{q}qg$. The case when κ is odd has no analog in the static quark model.

We examine the pseudoscalar exotic meson with $J^{PC} = 0^{--}$ and vector $\pi_1(1400)$ exotic meson with $J^{PC} = 1^{-+}$. While there is no evidence for the 0^{--} exotic meson, there is evidence for the $\pi_1(1400)$. Evidence for the $\pi_1(1400)$ is supported by πd scattering and $\bar{p}d$ annihilation [32]. Furthermore, the reaction $\pi^- p \to \eta\pi^- p$ is a candidate for the hybrid $\bar{q}qg$ state and yields a resonance of mass 1370 MeV and width 385 MeV [69, 70].

The general form of the 0^{--} and $\pi_1(1400)$ Bethe-Salpeter amplitudes is given by

$$\begin{aligned} \Gamma^{uu}(q;P) &= i\gamma_5 q\cdot PE(q;P) + \gamma_5\gamma\cdot Pq\cdot PF(q;P) \\ &+ \gamma_5\gamma\cdot qG(q;P) + \gamma_5 q_\alpha\sigma_{\alpha\beta}P_\beta q\cdot PH(q;P) \end{aligned} \tag{6.5}$$

and

$$\begin{aligned} \Gamma^{uu}_\mu(q;P)^T &= \gamma^T_\mu q\cdot P\,V_1(q;P) + q^T_\mu\gamma\cdot qq\cdot P\,V_2(q;P) \\ &+ q^T_\mu\gamma\cdot P\,V_3(q;P) + \gamma_5\epsilon^T_{\mu\alpha\nu\beta}\gamma_\alpha q_\nu P_\beta q\cdot P\,V_4(q;P) \end{aligned} \tag{6.6}$$

$$+ \quad q_\mu^T q \cdot P\, V_5(q;P) + \sigma_{\mu\nu}^T q_\nu\, V_6(q;P) + \sigma_{\mu\nu}^T P_\nu q \cdot P\, V_7(q;P)$$

$$+ \quad q_\mu^T q_\alpha \sigma_{\alpha\beta} P_\beta q \cdot P\, V_8(q;P),$$

respectively. Eqs. 6.5 and 6.6 differ from the π and ρ amplitudes by appropriate factors of $q \cdot P$ in order to create the opposite C-parity of the hybrid states. Both exotic states converge at two Chebyshev moments. The 0^{--} state yields a mass of 741 MeV. We obtain a mass of 1020 MeV for the $\pi_1(1400)$ that is 26% too low. The fact that the $\pi_1(1400)$ lies 136 MeV above the a_1 is consistent with the study [71]. Because the ground-state orbital excitations are approximately 400 MeV too low, we expect that a model which accurately reproduces the a_1 and b_1 will result in a $\pi_1(1400)$ around 1400 MeV.

CHAPTER 7

Conclusions

In this work we studied the properties of mesons from Bethe-Salpeter amplitudes. We used a Euclidean model of the gluon propagator in the rainbow-ladder truncation of the Dyson-Schwinger equations to compare alternatives to direct analytic continuations of the quark propagators into the complex plane.

In Chapter 3 we obtained numerical solutions for the quark propagators along the positive real-axis of the complex plane. These spacelike solutions arose from iterative solutions of the Dyson-Schwinger equations for the quark self-energy in the rainbow approximation where the quark-gluon vertex is a bare vertex and the running coupling constant reproduces the 1-loop renormalization group behavior in the ultraviolet. An infrared enhancement is used to produce dynamical chiral symmetry breaking. Comparison of these results to lattice QCD showed good agreement with $M(p^2)$ while comparison of $Z(p^2)$ show deficiencies in the bare quark-gluon vertex.

For practical reasons, studies in the Dyson-Schwinger approach take advantage of the freedom in modeling the infrared behavior of the gluon to allow for the analytic continuation of the quark propagators to be made with a contour integration along the real axis. Our complex plane calculations showed that a nontrivial contour integration was required to calculate the values of the quark propagators in the complex plane resulting in the integration over nonintegrable singularities when using this expedient approach. A physically insignificant modification to $\mathcal{F}(k^2)$ allows for small k^2 behavior that results in properly defined contour integration along the real axis. Our numerical solutions confirm the presence of complex conjugate singularities in the timelike region of the complex plane. All

but one of these singularities remains when the pQCD tail term of the model is removed. The singularities are not present in the self-energy amplitudes and thus are not generated by the self-energy integrals. These singularities limit the calculation of meson observables calculated with the momentum expansion method to the ϕ meson and below.

In Chapter 4 we calculated the mass and electroweak decay constants of the light pseudoscalar and vector mesons. The meson Bethe-Salpeter amplitudes were calculated in the ladder truncation to provide self-consistent solutions that satisfy the vector and axial-vector Ward-Takahashi identities. Our numerical procedure consisted of discretizing the relative $q\bar{q}$ momentum, reducing the integral equation to an eigenvalue problem and solving for the meson mass that gives the largest eigenvalue equal to one. The angular dependence between the center of mass and relative $q\bar{q}$ momentum of the meson Bethe-Salpeter amplitudes is approximated by an expansion in Chebyshev polynomials. The mass-shell condition of meson bound states required that the quark propagators be analytically continued into a parabolic region of the complex plane. This parabolic region increases exponentially with increasing meson mass and becomes numerically intractable for all but the lightest pseudoscalar and vector mesons. Here we compare masses and electroweak decay constants calculated with the first through third orders of Taylor expanded vector and scalar parts of the quark propagator with their direct analytic continuations into the complex plane. At second and third orders, the momentum expansion method provides meson masses and electroweak decay constants that are all within 5% of the direct analytically continued solutions.

The main goal of this project was to calculate the vector meson strong decays in the impulse approximation. The $g_{\rho\pi\pi}$ and $g_{\phi KK}$ coupling constants can be indirectly extracted from the pion and kaon electromagnetic form factors in the impulse approximation. Our results verify that a direct calculation in the impulse approximation yield high quality

solutions when the quark propagators and meson Bethe-Salpeter amplitudes are calculated in the rainbow-ladder approximation. In the impulse approximation, we ignore three-body interactions and reduce the vector-pseudoscalar vertex to a simple triangle diagram. We choose a symmetric functional form of the internal quark momentum such that the vector meson's relative $q\bar{q}$ momentum is spacelike while the two pseudoscalar relative $q\bar{q}$ momenta extend into the complex plane. To obtain the necessary complex plane behavior we Taylor expanded the pseudoscalar Bethe-Salpeter amplitudes from the positive real-axis. As in the case of the quark propagators, the expansion of the meson relative $q\bar{q}$ momentum converges at second order.

In general, the relative errors of the strong decays increase or decrease as the relative errors in the electroweak decays increase or decrease indicating sensitivity to the form of the Bethe-Salpeter amplitudes. Single covariant solutions to the ρ and ϕ strong decays are 50% larger than experimental results. The introduction of all pseudoscalar covariants lowers this number to 6% and 32% for the ρ and ϕ, respectively. Full covariant solutions to the ρ and ϕ strong decays are 15% and 8% lower than experimental values, respectively. The K^* eight-covariant and five-covariant strong decays were 5% higher and 4% lower, respectively.

Finally, we calculated axial-vector and exotic meson masses. The axial-vector mesons a_1 and b_1 are the lightest orbital excitations in the meson spectrum. Exotic mesons have J^{PC} quantum numbers that cannot be obtained from the static quark model. However, in the Bethe-Salpeter formalism such observables exist due to the relative time degree of freedom. Experimental predictions of axial-vector masses and empirical evidence for exotic meson masses require an analtyic continuation into a region of the complex plane encompassing the singularities found in this model. Our meson mass results from Taylor expanded quark propagators motivates a new approximation to circumvent the singularities

in the region of integration and provide numerically tractable solutions to Bethe-Salpeter calculations of these heavier mesons. We studied the approximation in which the argument of the quark propagators in the Bethe-Salpeter equation is replaced by its real part only. This approximation required knowledge of the quark propagators along the real timelike axis which was determined in Chapter 3. Light pseudoscalar and vector meson masses were within 11% of the exact model calculations with the errors decreasing with increasing meson mass. Our a_1 and b_1 meson masses were too low by 30% and 37%, respectively. The orbital excitation energy was a factor of three too small indicating that our model is too attractive to describe these orbital excitations properly. Comparison of our calculation with empirical evidence of the exotic vector meson $\pi_1(1400)$ yielded a mass that was 26% too low. We feel that a model that accurately produces the axial-vector mesons will accurately produce a $\pi_1(1400)$ around 1400 MeV.

In conclusion, a direct comparison of analytically continued quark propagators and Taylor expanded ones in the solution of meson observables showed that the complex plane behavior of the propagators largely cancels in the solution of meson observables. The value of the mass is particularly insensitive to the complex plane behavior of the quark propagators. The electroweak and strong decay constants are sensitive to the functional form of the Bethe-Salpeter amplitudes. The most surprising result was the relative insenstivity of the calculations to the complex plane behavior in general. The real-axis approximation employed in Chapter 6 emphasizes this point with meson masses within 11% of their experimental values.

APPENDIX A

Euclidean Metric

A.1 Integration

Integrations over a 4-momentum, k, can be accomplished using four dimensional spherical coordinates. We write

$$k_\mu = (k_1, k_2, k_3, k_4) \tag{A.1}$$

as

$$k_\mu = |k|(\cos\phi \sin\theta \sin\beta, \sin\phi \sin\theta \sin\beta, \cos\theta \sin\beta, \cos\beta) \tag{A.2}$$

and

$$\int_{-\infty}^{\infty} d^4k = \int_{-\infty}^{\infty} dk_1 dk_2 dk_3 dk_4 \tag{A.3}$$

as

$$\int_{-\infty}^{\infty} d^4k = \int_0^{\infty} k^3 dk \int_0^{2\pi} d\phi \int_0^{\pi} \sin\theta d\theta \int_0^{\pi} \sin^2\beta d\beta. \tag{A.4}$$

A.2 Euclidean Dirac Matrices

From the Weyl or chiral Minkowski representation of γ^o and γ^i the Euclidean Dirac matrices are the following:

$$\gamma_4 = \begin{pmatrix} 0 & 1 \\ 1 & 0 \end{pmatrix} \tag{A.5}$$

$$\gamma_i = \begin{pmatrix} 0 & -i\sigma_i \\ i\sigma_i & 0 \end{pmatrix} \tag{A.6}$$

$$\gamma_5 = \gamma_4\gamma_1\gamma_2\gamma_3 = \begin{pmatrix} -1 & 0 \\ 0 & 1 \end{pmatrix} \tag{A.7}$$

$$\sigma_{\mu\nu} = \frac{i}{2}\gamma_\mu\gamma_\nu - \frac{i}{2}\gamma_\nu\gamma_\mu \tag{A.8}$$

where the σ_i refer to the three 2x2 Pauli spin matrices. With no contractions among repeated indices, the Euclidean Dirac matrices have the following properties:

$$\gamma_\mu\gamma_\mu = I \tag{A.9}$$

$$\gamma_5\gamma_5 = I \tag{A.10}$$

$$\{\gamma_\mu, \gamma_\nu\} = \gamma_\mu\gamma_\nu + \gamma_\nu\gamma_\mu = 2\delta_{\mu\nu} \tag{A.11}$$

$$\{\gamma_5, \gamma_5\} = \gamma_5\gamma_\mu + \gamma_\mu\gamma_5 = 0. \tag{A.12}$$

A.3 Trace Theorems

$$Tr(\gamma_\mu\gamma_\nu) = 4\delta_{\mu\nu} \tag{A.13}$$

$$Tr(\text{Odd Number Of } \gamma\text{'s}) = 0 \tag{A.14}$$

$$Tr(\gamma_\mu\gamma_\nu\gamma_\alpha\gamma_\beta) = 4\delta_{\mu\nu}\delta_{\alpha\beta} - 4\delta_{\mu\alpha}\delta_{\nu\beta} + 4\delta_{\mu\beta}\delta_{\nu\alpha} \tag{A.15}$$

$$Tr(\sigma_{\mu\nu}\sigma_{\alpha\beta}) = 4\delta_{\mu\alpha}\delta_{\nu\beta} - 4\delta_{\mu\beta}\delta_{\nu\alpha} \tag{A.16}$$

$$Tr(\gamma_5\gamma_\mu\gamma_\nu) = 0 \tag{A.17}$$

$$Tr(\gamma_5\gamma_\mu\gamma_\nu\gamma_\alpha\gamma_\beta) = 4\epsilon_{\mu\nu\alpha\beta} \tag{A.18}$$

$$\epsilon_{4123} = +1 \tag{A.19}$$

A.4 Charge Conjugation Properties

The charge conjugation operator ($C = \gamma_2\gamma_4$) has the following properties

$$C = -C^{-1} \tag{A.20}$$

$$C^T = C^{-1} \tag{A.21}$$

where T refers to the transpose of that matrix. The charge conjugation operator acts on the Dirac matrices in the following way:

$$\left[C^{-1}\gamma_\mu C\right]^T = -\gamma_\mu \tag{A.22}$$

$$\left[C^{-1}\sigma_{\mu\nu}C\right]^T = = -\sigma_{\mu\nu} \tag{A.23}$$

$$\left[C^{-1}\gamma_5 C\right]^T = = \gamma_5 \tag{A.24}$$

$$\left[C^{-1}\gamma_5\gamma_\mu C\right]^T = = \gamma_5\gamma_\mu \tag{A.25}$$

$$\left[C^{-1}\gamma_5\gamma_\mu\gamma_\nu C\right]^T = = \gamma_5\gamma_\nu\gamma_\mu \tag{A.26}$$

$$\left[C^{-1}\gamma_5\sigma_{\mu\nu} C\right]^T = = -\gamma_5\sigma_{\mu\nu} \tag{A.27}$$

A.5 Other Useful Properties

An important relation for the vector and axial-vector covariants is

$$\gamma_5\epsilon_{\mu\nu\alpha\beta}\gamma_\beta q_\alpha P_\beta = \gamma_\mu\gamma\cdot q\gamma\cdot P - (q_\mu\gamma\cdot P - P_\mu\gamma\cdot q + \gamma_\mu q\cdot P). \tag{A.28}$$

The transpose of the Dirac matrices is also useful:

$$\gamma_0^T = \gamma_4 \tag{A.29}$$

$$\gamma_1^T = -\gamma_1 \tag{A.30}$$

$$\gamma_2^T = \gamma_2 \tag{A.31}$$

$$\gamma_3^T = -\gamma_3 \tag{A.32}$$

$$\gamma_5^T = \gamma_5 \tag{A.33}$$

APPENDIX B

Chebyshev Polynomials of Type II

The orthogonality condition for Type II Chebyshev polynomials is

$$\int_{-1}^{1} U_m(x)U_n(x)\sqrt{1-x^2}dx = \frac{\pi}{2}\delta_{mn}. \tag{B.1}$$

Odd indexed U's are odd functions in x and even indexed U's are even in x. A partial list of these functions is as follows:

$$U_0(x) = 1 \tag{B.2}$$

$$U_1(x) = 2x \tag{B.3}$$

$$U_2(x) = 4x^2 - 1 \tag{B.4}$$

$$U_3(x) = 8x^3 - 4x \tag{B.5}$$

$$U_4(x) = 16x^4 - 12x^2 + 1 \tag{B.6}$$

$$U_5(x) = 32x^5 - 32x^3 + 6x \tag{B.7}$$

APPENDIX C

Additional Covariant Projection Matrices and their Inverses

In the following M_{ijk} is defined as

$$\left\{ \begin{array}{c} T_i \\ T_j \\ T_k \end{array} \right\} = M_{(ijk)} \left\{ \begin{array}{c} V_i \\ V_j \\ V_k \end{array} \right\}$$

and $N^2 = (q^T)^2 P^2 = q^2 P^2 - (q \cdot P)^2$ and $\psi = 3q^2 - (q^T)^2$.

C.1 K^* Vector Meson

$$M_{(123)} = \left\{ \begin{array}{ccc} 12 & 4(q^T)^2 & 0 \\ 4(q^T)^2 & 4(q^T)^2 q^2 & 4(q^T)^2\, q \cdot P \\ 0 & 4(q^T)^2\, q \cdot P & 4(q^T)^2 P^2 \end{array} \right\} \tag{C.1}$$

$$M^{-1}_{(123)} = \frac{1}{8N^4} \left\{ \begin{array}{ccc} N^4 & -P^2 N^2 & q \cdot P\, N^2 \\ -P^2 N^2 & 3P^4 & -3\, q \cdot P\, P^2 \\ q \cdot P\, N^2 & -3\, q \cdot P\, P^2 & 3q^2 P^2 - N^2 \end{array} \right\} \tag{C.2}$$

$$M_{(678)} = \left\{ \begin{array}{ccc} 4\psi & 12 q \cdot P & 4(q^T)^2 q \cdot P \\ 12 q \cdot P & 12 P^2 & 4(q^T)^2 P^2 \\ 4(q^T)^2 q \cdot P & 4(q^T)^2 P^2 & 4(q^T)^4 P^2 \end{array} \right\} \tag{C.3}$$

$$M^{-1}_{(678)} = \frac{1}{8(q^T)^2 P^2} \left\{ \begin{array}{ccc} P^2 & -q \cdot P & 0 \\ -q \cdot P & q^2 & -1 \\ 0 & -1 & 3/(q^T)^2 \end{array} \right\} \tag{C.4}$$

C.2 a_1 Axial-Vector Meson

$$M_{(123)} = \begin{Bmatrix} -12 & -4(q^T)^2 & 0 \\ -4(q^T)^2 & -4(q^T)^2 q^2 & -4(q^T)^2(q\cdot P)^2 \\ 0 & -4(q^T)^2(q\cdot P)^2 & -4(q^T)^2 P^2(q\cdot P)^2 \end{Bmatrix} \tag{C.5}$$

$$M^{-1}_{(123)} = \frac{1}{8(q^T)^4 P^2} \begin{Bmatrix} -(q^T)^4 P^2 & (q^T)^2 P^2 & -(q^T)^2 \\ (q^T)^2 P^2 & -3P^2 & 3 \\ -(q^T)^2 & 3 & -\psi/(q\cdot P)^2 \end{Bmatrix} \tag{C.6}$$

$$M_{(678)} = \begin{Bmatrix} 4\psi & 12(q\cdot P)^2 & 4(q^T)^2(q\cdot P)^2 \\ 12(q\cdot P)^2 & 12P^2(q\cdot P)^2 & 4(q^T)^2 P^2(q\cdot P)^2 \\ 4(q^T)^2(q\cdot P)^2 & 4(q^T)^2 P^2(q\cdot P)^2 & 4(q^T)^4 P^2(q\cdot P)^2 \end{Bmatrix} \tag{C.7}$$

$$M^{-1}_{(678)} = \frac{1}{8(q^T)^2 P^2(q\cdot P)^2} \begin{Bmatrix} P^2(q\cdot P)^2 & -(q\cdot P)^2 & 0 \\ -(q\cdot P)^2 & q^2 & -1 \\ 0 & -1 & 3/(q^T)^2 \end{Bmatrix} \tag{C.8}$$

C.3 b_1 Axial-Vector Meson

$$M_{(123)} = \begin{Bmatrix} -12(q\cdot P)^2 & -4(q^T)^2(q\cdot P)^2 & 0 \\ -4(q^T)^2(q\cdot P)^2 & -4(q^T)^2 q^2(q\cdot P)^2 & -4(q^T)^2(q\cdot P)^2 \\ 0 & -4(q^T)^2(q\cdot P)^2 & -4(q^T)^2 P^2 \end{Bmatrix} \tag{C.9}$$

$$M^{-1}_{(123)} = \frac{1}{8(q^T)^4 P^2(q\cdot P)^2} \times \begin{Bmatrix} -(q^T)^4 P^2 & (q^T)^2 P^2 & -(q^T)^2(q\cdot P)^2 \\ (q^T)^2 P^2 & -3P^2 & 3(q\cdot P)^2 \\ -(q^T)^2(q\cdot P)^2 & 3(q\cdot P)^2 & -\psi(q\cdot P)^2 \end{Bmatrix} \tag{C.10}$$

$$(C.11) \quad M_{(678)} = \left\{ \begin{array}{ccc} 4\psi(q\cdot P)^2 & 12(q\cdot P)^2 & 4(q^T)^2(q\cdot P)^2 \\ 12(q\cdot P)^2 & 12P^2 & 4(q^T)^2P^2 \\ 4(q^T)^2(q\cdot P)^2 & 4(q^T)^2P^2 & 4(q^T)^4P^2 \end{array} \right\}$$

$$(C.12) \quad M^{-1}_{(678)} = \frac{1}{8(q^T)^2P^2} \left\{ \begin{array}{ccc} P^2/(q\cdot P)^2 & -1 & 0 \\ -1 & q^2 & -1 \\ 0 & -1 & 3/(q^T)^2 \end{array} \right\}$$

C.4 $\hat{\pi}$ Pseudoscalar Meson

$$(C.13) \quad M_{(23)} = \left\{ \begin{array}{cc} -4P^2(q\cdot P)^2 & -4(q\cdot P)^2 \\ -4(q\cdot P)^2 & -4q^2 \end{array} \right\}$$

$$(C.14) \quad M^{-1}_{(23)} = \frac{1}{16(q\cdot P)^2N^2} \left\{ \begin{array}{cc} -4q^2 & 4(q\cdot P)^2 \\ 4(q\cdot P)^2 & -4P^2(q\cdot P)^2 \end{array} \right\}$$

C.5 $\hat{\rho}$ Vector Meson

$$(C.15) \quad M_{(123)} = \left\{ \begin{array}{ccc} 12(q\cdot P)^2 & 4(q^T)^2(q\cdot P)^2 & 0 \\ 4(q^T)^2(q\cdot P)^2 & 4(q^T)^2q^2(q\cdot P)^2 & 4(q^T)^2(q\cdot P)^2 \\ 0 & 4(q^T)^2(q\cdot P)^2 & 4(q^T)^2P^2 \end{array} \right\}$$

$$(C.16) \quad M^{-1}_{(123)} = \frac{1}{8(q^T)^2} \left\{ \begin{array}{ccc} (q^T)^2/(q\cdot P)^2 & -1/(q\cdot P)^2 & 1/P^2 \\ -1/(q\cdot P)^2 & 3/(q^T)^2(q\cdot P)^2 & -3/(q^T)^2P^2 \\ 1/P^2 & -3/(q^T)^2P^2 & \psi/(q^T)^2(q\cdot P)^2 \end{array} \right\}$$

$$(C.17) \quad M_{(678)} = \left\{ \begin{array}{ccc} 4\psi & 12(q\cdot P)^2 & 4(q^T)^2(q\cdot P)^2 \\ 12(q\cdot P)^2 & 12P^2(q\cdot P)^2 & 4(q^T)^2P^2(q\cdot P)^2 \\ 4(q^T)^2(q\cdot P)^2 & 4(q^T)^2P^2(q\cdot P)^2 & 4(q^T)^4P^2(q\cdot P)^2 \end{array} \right\}$$

$$\text{(C.18)} \quad M^{-1}_{(678)} = \frac{1}{8(q^T)^2P^2} \left\{ \begin{array}{ccc} P^2 & -1 & 0 \\ -1 & q^2/(q\cdot P)^2 & -1/(q\cdot P)^2 \\ 0 & -1/(q\cdot P)^2 & 3/(q^T)^2(q\cdot P)^2 \end{array} \right\}$$

APPENDIX D

Phase Space

The two-body phase space operator for a particle, A, decaying into particles B and C is

$$\hat{\rho} = \int_{-\infty}^{\infty} \frac{d^3p_B}{(2\pi)^3\, 2E_B} \int_{-\infty}^{\infty} \frac{d^3p_C}{(2\pi)^3\, 2E_C} (2\pi)^3 \delta^3(\vec{p}_B + \vec{p}_C - \vec{p}_A)\delta(E_B + E_C - E_A). \tag{D.1}$$

Doing the integration yields

$$\hat{\rho} = \frac{1}{8\pi M_A^2}\sqrt{\lambda(M_A^2, M_B^2, M_C^2)} \tag{D.2}$$

where

$$\lambda(u^2, v^2, w^2) = (u + v + w)(u + v - w)(u - v + w)(u - v - w). \tag{D.3}$$

For the special case when $v = w$

$$\lambda(u^2, v^2, v^2) = u^4(1 - \frac{4v^2}{u^2}). \tag{D.4}$$

If $M_B = M_C$ then the two-body phase space take on the simple form of

$$\hat{\rho} = \frac{1}{8\pi}\sqrt{1 - \frac{4M_B^2}{M_A^2}}. \tag{D.5}$$

BIBLIOGRAPHY

[1] Pieter Maris and Peter C. Tandy. Bethe-salpeter study of vector meson masses and decay constants. *Physical Review C*, 60(055214), 1999.

[2] M. Gell-Mann. *Phys. Lett.*, 8:214, 1964.

[3] G. Zweig. Cern preprints 8182/th.401 and 8419/th.412. Unpublished, 1964.

[4] W. Marciano and H. Pagels. *Phys. Rep.*, 36:137, 1977.

[5] N. Brown and M. R. Pennington. Sudies of confinement: How the gluon propagates. *Phys. Rev. D*, 39(9):2723, 1989.

[6] D. J. Gross and F. Wilczek. Ultraviolet behavior of non-abelian gauge theories. *Physical Review Letters*, 30(26):1343–1346, 1973.

[7] H. D. Politzer. Reliable perturbative results for strong interactions? *Physical Review Letters*, 30(26):1346–1349, 1973.

[8] J. Goldstone. *Nuovo Cimento*, 19:154, 1961.

[9] F. J. Dyson. The s matrix in quantum electrodynamics. *Phys. Rev.*, 75:1736, 1949.

[10] J. S. Schwinger. On the Green's functions of quantized fields I. *Proc. Nat. Acad. Sc.*, 37:452, 1951.

[11] J. S. Schwinger. On the Green's functions of quantized fields II. *Proc. Nat. Acad. Sc.*, 37:455, 1951.

[12] C. D. Roberts and A. G. Williams. Dyson-Schwinger equations and their application to hadronic physics. *Progress in Particle and Nuclear Physics*, 33:477, 1994.

[13] C. D. Roberts and S. M. Schmidt. Dyson-Schwinger equations: Density, temperature, and strong continuum qcd. *Prog. Part. Nucl. Phys.*, 45:S1–S103, 2000. nucl-th/0005064.

[14] C. J. Burden, C. D. Roberts, and A. G. Williams. *Phys. Lett. B*, 285:347, 1992.

[15] G. Krein, C. D. Roberts, and A. G. Williams. *Int. J. Mod. Phys. A*, 7:5607, 1992.

[16] P. Maris. Confinement and complex singularities in three-dimensional qed. *Phys. Rev. D*, 52(10):6087, 1995. hep-ph/9508323.

[17] D. Atkinson and P. W. Johnson. Chiral-symmetry breaking in qcd. II. running coupling constant. *Phys. Rev. D*, 37(8):2296, 1988.

[18] Craig D. Roberts and Bruce H. J. McKellar. Critical coupling for dynamical chiral-symmetry breaking. *Phys. Rev. D*, 41(2):672, 1990.

[19] Pieter Maris and Craig D. Roberts. π- and k-meson bethe-salpeter amplitudes. *Physical Review C*, 56(6):3369, 1997.

[20] D. Lurie, Y. Takahashi, and H. Umezawa. Generalized Ward identity and unified treatment of conservation laws. *Journal of Mathematical Physics*, 7(8):1478, 1966.

[21] Pieter Maris, Craig D. Roberts, and Peter Tandy. Pion mass and decay constant. *Phys. Lett. B*, 420:267, 1998. nucl-th/9707003.

[22] S. Mandelstam. Approximation scheme for quantum chromodynamics. 20(12):3223, 1979.

[23] U. Bar-Gadda. *Nucl. Phys. B*, 163:312, 1980.

[24] H. J. Munczek and A. M. Nemirovsky. Ground-state $q\bar{q}$ mass spectrum in quantum chromodynamics. *Phys. Rev. D*, 28(1):181, 1983.

[25] Pankaj Jain and Herman J. Munczek. Calculation of the pion decay constant in the framework of the Bethe-Salpeter equation. *Phys. Rev. D*, 44(6):1873, 1991.

[26] Herman J. Munczek and Pankaj Jain. Relativistic pseudoscalar $q\bar{q}$ bound states: Results on Bethe-Salpeter wave functions and decay constants. *Phys. Rev. D*, 46(1):438, 1992.

[27] Pankaj Jain and Herman J. Munczek. $q\bar{q}$ bound states in the Bethe-Salpeter formalism. *Physical Review D*, 48(11):5403, 1993.

[28] M. R. Frank and C. D. Roberts. Model gluon propagator and pion and *rho*-meson observables. *Phys. Rev. C*, 53(1):390, 1996.

[29] Pieter Maris and Peter C. Tandy. Quark-photon vertex and the pion charge radius. *Physical Review C*, 61(045202), 2000.

[30] Pieter Maris and Peter C. Tandy. π, k^+, and k^o electromagnetic form factors. *Physical Review C*, 62(055204), 2000.

[31] Pieter Maris and Peter C. Tandy. Electromagnetic transistion form factors of light mesons. *Physical Review C*, 65(045211), 2002.

[32] Groom et al. Review of particle physics. *The European Physical Journal C*, 15, 2000.

[33] Walter Greiner and Berndt Muller. *Quantum Mechanics Symmetries.* Springer-Verlag, New York, second edition, 1994.

[34] F. J. Yndurain. *The Theory of Quark and Gluon Interactions.* Spring-Verlag, New York, 1993.

[35] C. J. Burden et al. Ground state spectrum of light quark mesons. *Physical Review C*, 55(5), 1997.

[36] G. C. Wick. Properties of bethe-salpeter wave functions. *Physical Review*, 96(4):1124, 1954.

[37] Claude Itzykson and Jean-Bernard Zuber. *Quantum Field Theory*, chapter 6, pages 299–301. McGraw-Hill, Inc., New York, 1980.

[38] S. J. Stainsby and R. T. Cahill. Is space-time euclidean "inside" hadrons? *Physics Letters A*, 146(9):467, 1990.

[39] A. A. Slavnov. *Theoretical and Mathematical Physics*, 10:99, 1972.

[40] J. C. Taylor. *Nuclear Physics B*, 33:436, 1971.

[41] C. G. Callan. Broken scale invariance in scalar field theory. *Physical Review D*, 2(8):1541–1547.

[42] K. Symanzik. *Comm. Math. Phys.*, 18:227, 1970.

[43] D. J. Gross and F. Wilczek. Asymptotically free gauge theories I. *Physical Review D*, 8(10):3633–3652, 1973.

[44] Michael E. Peskin and Daniel V. Schroeder. *An Introduction to Quantum Field Theory*, chapter 17, pages 551–553. Addison-Wesley Publishing Co., New York, 1995.

[45] James S. Ball and Ting-Wai Chiu. Analytic properties of the vertex function in gauge theories. II. *Physical Review D*, 22(10):2550, 1980.

[46] S. K. Kim and M. Baker. *Nucl. Phys. B*, 164:152, 1980.

[47] E. E. Salpeter and H. A. Bethe. A relativistic equation for bound-state problems. *Physical Review*, 84(6):1232, 1951.

[48] Murray Gell-Mann and Francis Low. Bound states in quantum field theory. *Physical Review*, 84(2):350, 1951.

[49] C. H. Llewellyn Smith. A relativistic formulation of the quark model for mesons. *Annals of Physics*, 53:521–558, 1969.

[50] Rubin Landau. *Quantum Mechanics II: A second Course in Quantum Theory.* John Wiley and Sons, Inc., New York, 1990.

[51] Kerson Huang and H. Arthur Weldon. Bound-state wave functions and bound-state scattering in relativistic field theory. *Physical Review D*, 11(2):257, 1975.

[52] C. Itzykson and J. B. Zuber. *Quantum Field Theory.* McGraw-Hill Inc., 1980.

[53] V. A. Miransky. *Dynamical Symmetry Breaking in Quantum Field Theories.* World Scientific, Singapore, 1993.

[54] D. B. Leinweber. *Ann. Phys.*, 254:328, 1997.

[55] Jonivar Skullerud, Derek B. Leinweber, and Anthony G. Williams. Nonperturbative improvement and tree-level correction of the quark propagator. *hep-lat/0102013*, 2001.

[56] C. S. Fischer. PhD thesis, University of Tubingen. Unpublished.

[57] R. Alkofer. Private Communication.

[58] Milton Abramowitz and Irene A. Stegun, editors. *Handbook of Mathematical Functions with Formulas, Graphs, and Mathematical Functions.* Dover Publications, Inc., New York, 1972.

[59] Murray R. Spiegel. *Schaum's Outline of Theory and Problems of Complex Variables with an Introduction to Conformal Mapping and its Applications*, chapter 10, page 266. McGraw-Hill, Inc., New York, 1994.

[60] Masayasu Harada and Yuhsuke Yoshida. Solving the homogeneous Bethe-Salpeter equation. *Physical Review D*, 53(3):1482, 1996.

[61] Anthony Ralston and Philip Rabinowitz. *A First Course in Numerical Analysis*, chapter 10, pages 492–495. Dover Publications, Inc., Mineola, New York, 2001.

[62] David Griffiths. *Introduction to Elementary Particles*, chapter 7, page 228. John Wiley and Sons, Inc., New York, 1987. See the first footnote at the bottom of the page.

[63] Claude Itzykson and Jean-Bernard Zuber. *Quantum Field Theory*, chapter 3, pages 134–138. McGraw-Hill, Inc., New York, 1980.

[64] Eispack. www.netlib.org/eispack. Collection of Fortran subroutines that compute the eigenvalues and eigenvectors of matrices.

[65] J. C. R. Bloch et al. Nuclean form factors and a nonpointlike diquark. *Physical Review C*, 60(062201), 1999.

[66] A. Bender, C. D. Roberts, and L. von Smekal. *Physics Letters B*, 380(7), 1996.

[67] Pieter Maris. Private Communication.

[68] R. Alkofer, P. Watson, and H. Weigel. Mesons in a Poincaré covariant Bethe-Salpeter approach. *Physical Review D*, 65(094026), 2002.

[69] D. R. Thompson *et al.* Evidence for exotic meson production in the reaction $\pi^- p \to \eta\pi^- p$ at 18gev/c. *Physical Review Letters*, 79(9):1630, 1997.

[70] S. U. Chung *et al.* Evidence for exotic $j^{PC} = 1^{-+}$ meson production in the reaction $\pi^- p \to \eta\pi^- p$ at 18gev/c. *Physical Review D*, 60(9), 1999.

[71] C. J. Burden and M. A. Pichowsky. j^{PC} - exotic mesons from the Bethe-Salpeter equation. *Few Body Systems*, 32:119–126, 2002.